PACIFIC EARTHQUAKE ENGINEERING RESEARCH CENTER

Analysis of Cumulative Absolute Velocity (CAV) and JMA Instrumental Seismic Intensity (I_{JMA}) Using the PEER-NGA Strong Motion Database

Kenneth W. Campbell
EQECAT, Inc.

and

Yousef Bozorgnia
Pacific Earthquake Engineering Research Center
University of California, Berkeley

PEER 2010/102
FEBRUARY 2010

Analysis of Cumulative Absolute Velocity (CAV) and JMA Instrumental Seismic Intensity (I_{JMA}) Using the PEER-NGA Strong Motion Database

Kenneth W. Campbell
EQECAT, Inc.

Yousef Bozorgnia
Pacific Earthquake Engineering Research Center
University of California, Berkeley

PEER Report 2010/102
Pacific Earthquake Engineering Research Center
College of Engineering
University of California, Berkeley

February 2010

ABSTRACT

This report summarizes the results of a study of cumulative absolute velocity (CAV) and Japan Meteorological Agency instrumental seismic intensity (I_{JMA}) with the objectives of (1) analyzing the relationship between I_{JMA} and the standardized version of CAV (standardized CAV) and our variant of this parameter (CAV_S) that includes the operating basis earthquake (OBE) exceedance criteria proposed by the U.S. Nuclear Regulatory Commission for shutting down a nuclear power plant after an earthquake; (2) developing a ground motion prediction equation (GMPE) for CAV_S and the geometric mean horizontal component of CAV (CAV_{GM}), and (3) developing a GMPE for I_{JMA}. All of these analyses used the Pacific Earthquake Engineering Research Center Next Generation Attenuation (PEER-NGA) strong motion database. We explored the relationship between CAV_S and I_{JMA} using both the full PEER-NGA database and a subset of that database (the CB08 subset) that we previously used to develop GMPEs for peak ground motion and linear-elastic and inelastic response spectra. We used only the CB08 subset of the PEER-NGA database to develop GMPEs for CAV_{GM}, CAV_S and I_{JMA} in order to limit the analysis to those recordings that were considered to be most reliable. Thus far, we have found that CAV_{GM} has less aleatory uncertainty than any of the peak ground motion and response-spectral parameters we have studied and that the aleatory uncertainty associated with CAV_S is among the smallest.

ACKNOWLEDGMENTS

This project was partially funded by the International Atomic Energy Agency (IAEA) as part of the activities of Seismic Working Group 1 (WG1) of the Extra Budgetary Program (EPB). Dr. Bozorgnia's participation was partially sponsored by the Pacific Earthquake Engineering Research Center (PEER). Publication of this report was also supported by PEER. Any opinions, findings, and conclusions or recommendations expressed in this material are those of the authors and do not necessarily reflect those of the sponsors. We would like to thank Dr. Yoshimitsu Fukushima and Prof. Saburoh Midorikawa for providing us with a description of recently published ground motion prediction equations for JMA instrumental seismic intensity from the Japanese literature and Dr. Fumio Yamazaki for providing us with original line drawings demonstrating the calculation of JMA instrumental seismic intensity.

CONTENTS

LIST OF FIGURES

LIST OF TABLES

1 Introduction

One of the main objectives of this study was to use the Pacific Earthquake Engineering Research Center Next Generation Attenuation (PEER-NGA) Strong Motion Database of shallow crustal earthquakes in the western United States and other global active tectonic regions to develop ground motion prediction equations (GMPEs), also known as attenuation relationships, for several alternative, non-traditional ground motion parameters. These alternative ground motion parameters were selected because they were expected to better correlate with earthquake energy content and structural damage and to decrease the dispersion in the predicted value of ground motion as compared to the more common engineering ground motion parameters (e.g., peak ground motion and linear-elastic and inelastic response spectra). The alternative ground motion parameters that we analyzed for this report are the cumulative absolute velocity (CAV) (EPRI 1988; 1991) and the Japan Meteorological Agency (JMA) instrumental seismic intensity (I_{JMA}) (Japan Meteorological Agency 1996). Another main objective of this study was to use the PEER-NGA database to develop a relationship between CAV and I_{JMA} that can assist in establishing a relationship between CAV and the qualitative description of damage to well-engineered buildings provided by the vast amount of experience data contained within the JMA seismic intensity scale. Our study was performed in parallel to similar studies conducted by other investigators using different local and regional strong motion databases.

The acronym CAV is used in this study as a generic term for the cumulative absolute velocity and its filtered variants (see Section 2.1 for a description of these variants). The different variants are identified by adding a unique subscript to this acronym. The variant of interest in this study is standardized CAV (EPRI 1991), which is used in conjunction with response-spectral acceleration and velocity to determine whether a U.S. nuclear power plant should be shut down after an earthquake (U.S. Nuclear Regulatory Commission 1997). The empirical GMPEs for CAV and I_{JMA} developed in this study build on a five-year multidisciplinary study sponsored by the Pacific Earthquake Engineering Research Center (PEER) to develop next generation attenuation (NGA) relationships for shallow crustal earthquakes in active tectonic regions (Power et al. 2008). This study is currently referred to as the NGA-West project. The "West" has been added to the NGA acronym to distinguish it from another multi-year PEER study that is under way to develop NGA relationships for shallow crustal earthquakes in stable continental regions referred to as the NGA-East project. The CAV and I_{JMA} relationships developed in this study complement our existing NGA-West relationships for peak ground acceleration (PGA), peak ground velocity (PGV), peak ground displacement (PGD), 5%-damped linear-elastic pseudo-absolute response-spectral acceleration (PSA), and inelastic pseudo-absolute response-spectral acceleration (Campbell and Bozorgnia 2008; Bozorgnia et al. 2010a, 2010b).

Although the NGA-West relationships were intended originally for use in the western United States, several studies have shown that they are consistent with strong motion data from shallow crustal earthquakes in other active tectonic regions throughout the world, including Europe and the Mediterranean region (Campbell and Bozorgnia 2006; Stafford et al. 2008; Peruš and Fajfar 2009), Taiwan (Lin 2007), Italy (Scasserra et al. 2009), and Iran (Shoja-Taheri et al. 2010). Unpublished results from similar ongoing studies are finding similar results for shallow crustal earthquakes in New Zealand, Japan, and Latin America. Therefore, we suggest that the ground motion prediction equations for CAV and I_{JMA} developed in this study can be used in active tectonic regions worldwide.

Since its introduction in 1988, CAV and its filtered variants have generated a great deal of interest. This interest has taken the form of correlating CAV parameters with macroseismic intensity and instrumental ground motion parameters (Cabañas et al. 1997; Koliopoulos et al. 1998; EPRI 2006; Martinez-Rueda et al. 2008; Tselentis and Danciu 2008) and developing GMPEs that allow the estimation of CAV directly from physical parameters of an earthquake (Kostov 2005; Kramer and Mitchell 2006; Danciu and Tselentis 2007). Similarly, since its introduction in 1996, there has been a great deal of interest in I_{JMA}, although this has been mainly restricted to Japanese researchers. Most of the interest has been in correlating I_{JMA} with modified Mercalli intensity (MMI) and other instrumental ground motion parameters (Dong et al. 1996; Tong and Yamazaki 1996; Midorikawa et al. 1999; Sugawara et al. 1999; Davenport 2001, 2003; Shabestari and Yamazaki 2001; Karim and Yamazaki 2002; Fujimoto and Midorikawa 2005; Sokolov and Furumura 2008). Japanese colleagues have made us aware of four recently published GMPEs for I_{JMA} (Shabestari and Yamazaki 1998; Kataoka et al. 2006; Matsuzaki et al. 2006; Morikawa et al. 2007); however, there could be others in the Japanese literature that we are not aware of.

Chapter 2 presents a detailed definition of CAV and $I_{JMA,}$ followed by a description of the PEER-NGA Strong Motion Database in Chapter 3. The development of a relationship between CAV and I_{JMA} are discussed in Chapter 4, the development of GMPEs for CAV and I_{JMA} in Chapter 5, and the use of CAV in probabilistic seismic hazard analysis (PSHA) in Chapter 6. Chapter 7 is a discussion of results, followed by conclusions in Chapter 8. Additional documentation and justification of the database and the functional forms of the GMPEs used in this study can be found in Campbell and Bozorgnia (2007, 2008).

2 Parameter Definitions

2.1 CUMULATIVE ABSOLUTE VELOCITY (CAV)

Cumulative absolute velocity (CAV) is defined as the integral of the absolute value of an acceleration time series, which is represented mathematically by the following equation (EPRI 1988):

$$\mathrm{CAV} = \int_0^{t_{max}} |a(t)|\, dt \tag{2.1}$$

where $a(t)$ is the acceleration time series, t is time, and t_{max} is the total duration of the time series. Figure 2.1 shows a hypothetical acceleration time series and the corresponding value of CAV as it evolves over time. In this figure, CAV is the summation of the shaded areas. It is evident from the definition of CAV that its value increases with time until it reaches its maximum value at t_{max}. Therefore, CAV includes the cumulative effects of ground motion duration. This is a key advantage of CAV over other peak ground motion and response-spectral parameters and is one of the reasons that EPRI (1988) found it to be the ground motion parameter that best correlated with structural damage out of the many ground motion parameters that it investigated.

Although named the cumulative absolute velocity, CAV is not directly related to the ground motion velocity $v(t)$, although it does have units of velocity, typically g-sec. The name cumulative absolute velocity comes from the recognition that since $a(t) = dv(t)/dt$, the integral over acceleration in Equation (2.1) can be rewritten as the following summation of incremental velocities (i.e., peak-to-valley and valley-to-peak), regardless of sign, in the velocity time series (EPRI 1988):

$$\mathrm{CAV} = \sum_{i=1}^{N} |\Delta v_i| \tag{2.2}$$

where Δv_i is the ith value of incremental velocity in the time series and N is the total number of incremental velocities.

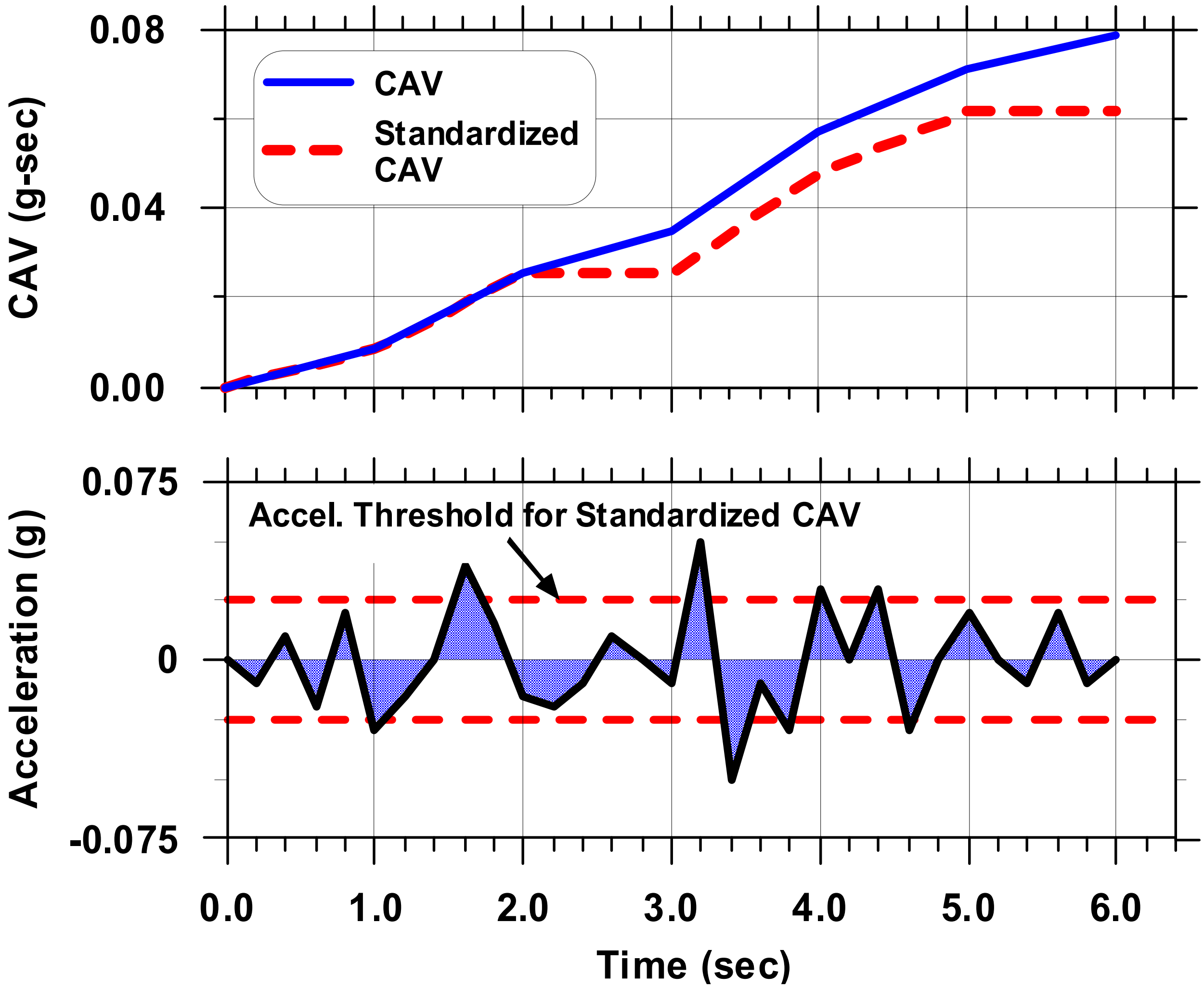

Fig. 2.1 Definitions of CAV and standardized CAV showing their evolution with time. Hypothetical acceleration time series is that given in EPRI (1991). Acceleration threshold for determining when the value of standardized CAV in any one-second interval is included in the summation is 0.025g. Modified from EPRI (1988).

In its review of the EPRI (1988) study, EPRI (1991) noted that the calculation of CAV could be overly influenced by a time series of long duration that contained small-amplitude (non-damaging) accelerations. Therefore, EPRI found it necessary to standardize the method of calculating CAV to account for record length. We refer to this version of CAV as standardized CAV. The recommended method to standardize the CAV calculation for a given time series was to window its calculation on a second-by-second basis. Only if the absolute value of acceleration exceeds 0.025g at any time during each non-overlapping one-second interval of an acceleration time series is the incremental value of CAV for that interval included in the summation. This calculation is mathematically represented by the following equation (EPRI 2006):

$$\mathrm{CAV} = \sum_{i=1}^{N}\left(H(\mathrm{PGA}_i - 0.025)\int_{t_{i-1}}^{t_i} |a(t)|\, dt \right) \tag{2.3}$$

where N is the number of one-second non-overlapping time intervals in the acceleration time series, PGA_i is the peak ground acceleration (g) in time interval i, t_i is the start time of time interval i, and $H(x)$ is the Heaviside step function, given by the equation:

$$H(x) = \begin{cases} 0 & x < 0 \\ 1 & x \geq 0 \end{cases} \tag{2.4}$$

Figure 2.1 shows the calculation of standardized CAV and its relationship to CAV for a hypothetical acceleration time series. Inspection of this figure and Equations (2.1) and (2.3) indicates that standardized CAV will always be equal to or less than CAV. This difference can be large for small-amplitude recordings.

Although many investigators have evaluated both CAV and standardized CAV as potential damage indices, their use has been limited. The USNRC (U.S. Nuclear Regulatory Commission 1997) uses standardized CAV as one of the ground motion measures to determine whether a nuclear power plant must be shut down after an earthquake when the operating basis earthquake (OBE) ground motion is exceeded. Kramer and Mitchell (2006) recommend the use of a filtered variant of CAV, which they call CAV_5, to replace PGA and magnitude in the assessment of liquefaction potential. EPRI (2006) and Watson-Lamprey and Abrahamson (2007) demonstrate how standardized CAV can be used to remove small-magnitude (non-damaging) earthquakes from contributing to a PSHA.

2.2 JMA INSTRUMENTAL SEISMIC INTENSITY ($\mathbf{I_{JMA}}$)

The JMA seismic intensity scale has been used in Japan as a measure of strong ground shaking effects for many years. It has traditionally been assessed after an earthquake based on the judgment of JMA officers. In 1996, the JMA seismic intensity scale was revised and became an instrumental seismic intensity measure (I_{JMA}) (Japan Meteorological Agency 1996; Earthquake Research Committee 1998).

I_{JMA} is computed by first taking the Fourier transform for a selected time window of each of the three components (i.e., two horizontal and one vertical) of an acceleration time series. Then, a band-pass filter is applied to these Fourier transforms in the frequency domain. This filter is composed of a period filter $F_1(f)$, a high-cut filter $F_2(f)$, and a low-cut filter $F_3(f)$, as given by the following equation (Fig. 2.2a):

$$F(f) = F_1(f)F_2(f)F_3(f) \tag{2.5}$$

where

$$F_1(f) = \sqrt{1/f} \tag{2.6}$$

$$F_2(f) = (1 + 0.694x^2 + 0.241x^4 + 0.0557x^6 + 0.009664x^8 + 0.00134x^{10} + 0.000155x^{12})^{-1/2} \tag{2.7}$$

$$x = \sqrt{1/f_c} \tag{2.8}$$

$$F_3(f) = \sqrt{1 - \exp(-f/f_0)^3} \tag{2.9}$$

In the above equations, f is frequency, f_c is the reference frequency of the high-cut filter, and f_0 is the reference frequency of the low-cut filter. After taking the inverse Fourier transforms of the filtered Fourier spectra, the absolute value of the geometric mean of the three transformed times series is computed at each time increment and the total duration τ of those pulses that exceed acceleration values ranging from zero to the maximum of the time series is calculated (Fig. 2.2b). An acceleration value a_0 having a total duration τ_0 satisfying the condition $\tau(a_0) \geq 0.3$ sec is defined (Fig. 2.2c) after which I_{JMA} is calculated from the following equation:

$$I_{JMA} = 2.0 \log a_0 + 0.94 \tag{2.10}$$

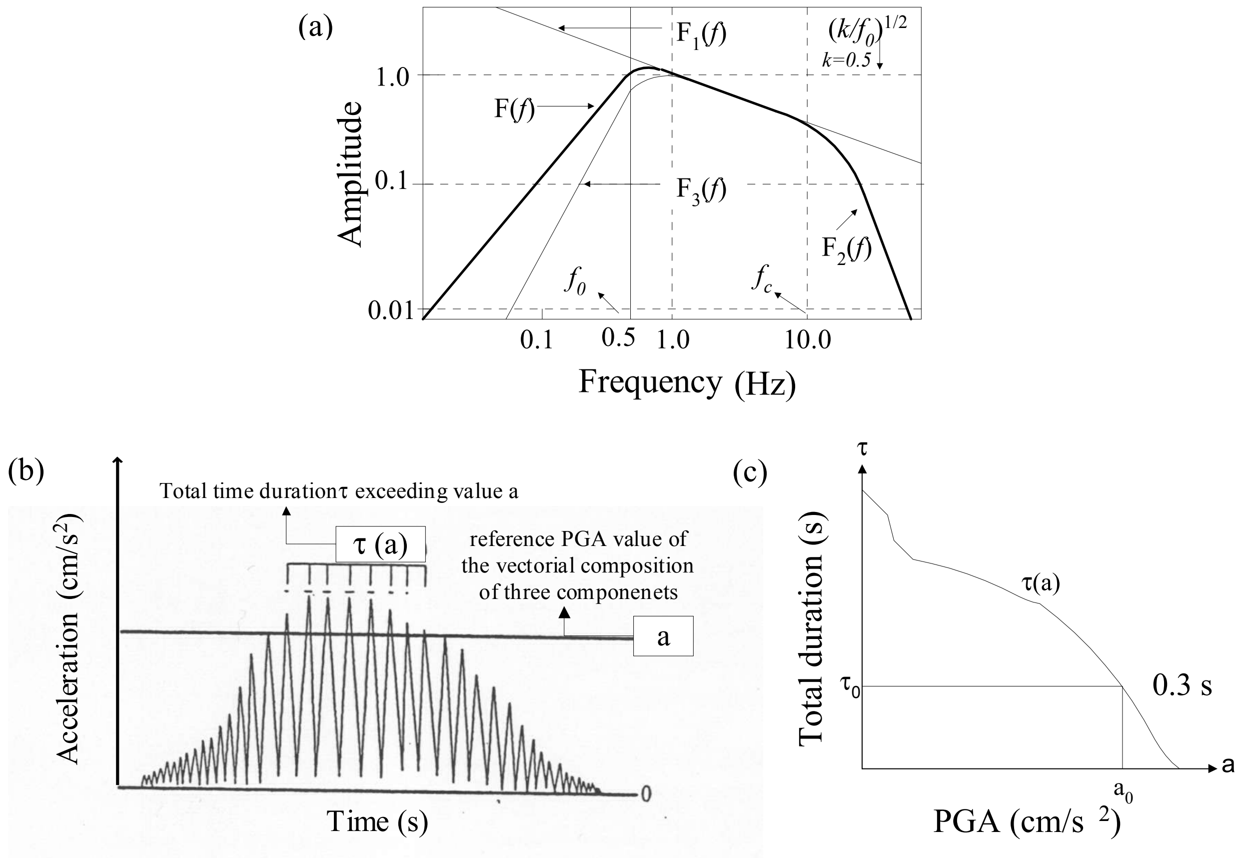

Fig. 2.2 Calculation of JMA instrumental seismic intensity: (a) applying a band-pass filter in the frequency domain, (b) summing time segments exceeding a reference PGA value of the absolute value of the geometric mean of the three components of the filtered acceleration time series, and (c) accounting for the effect of duration on PGA. Modified from Karim and Yamazaki (2002).

According to Karim and Yamazaki (2002), the JMA has deployed a large number of seismometers (574 in total) to measure I_{JMA} throughout Japan (Japan Meteorological Agency 1996), and the Fire and Disaster Management Agency (FDMA) has deployed one seismometer measuring I_{JMA} in each municipality (3255 in total). Using these seismometer networks, the distribution of JMA intensity can be determined rapidly after an earthquake even for a local event. The disaster management agencies in Japan use the JMA intensity as the most important index for estimating structural damage, identifying affected areas, and preparing for crisis management after an earthquake (Yamazaki 1996; Yamazaki et al. 1998).

3 Database

3.1 STRONG MOTION DATABASE

Two strong motion databases were used in this study: (1) the full PEER-NGA strong motion database (Chiou et al. 2008) and (2) a subset of this database used previously to develop NGA-West empirical GMPEs (Campbell and Bozorgnia 2007, 2008). The full PEER-NGA database consists of 3551 publicly available multi-component recordings from 173 shallow crustal earthquakes with moment magnitudes ranging from 4.2 to 7.9 and rupture distances ranging from 0.1 to 472 km. The subset of the PEER-NGA database that we used to develop the GMPEs for CAV and I_{JMA} (hereafter referred to as the CB08 subset) consists of 1561 recordings from 64 earthquakes with moment magnitudes ranging from 4.3 to 7.9 and rupture distances ranging from 0.1 to 199 km. The distribution of these databases with respect to magnitude and distance is shown in Figure 3.1.

The general criteria that we used to select the CB08 subset of the PEER-NGA database was intended to meet the following requirements: (1) the earthquake should be located within the shallow continental lithosphere (i.e., the earth's crust) in a region considered to be tectonically active, (2) the recording should be located at or near ground level and exhibit no known embedment or topographic effects, (3) the earthquake should have enough recordings to reliably represent the mean horizontal ground motion (especially for small-magnitude events), and (4) the earthquake or the recording should be considered reliable. Additional details are available in Campbell and Bozorgnia (2007, 2008). A complete list of the selected earthquakes and recording stations are given in Appendix A of Campbell and Bozorgnia (2007).

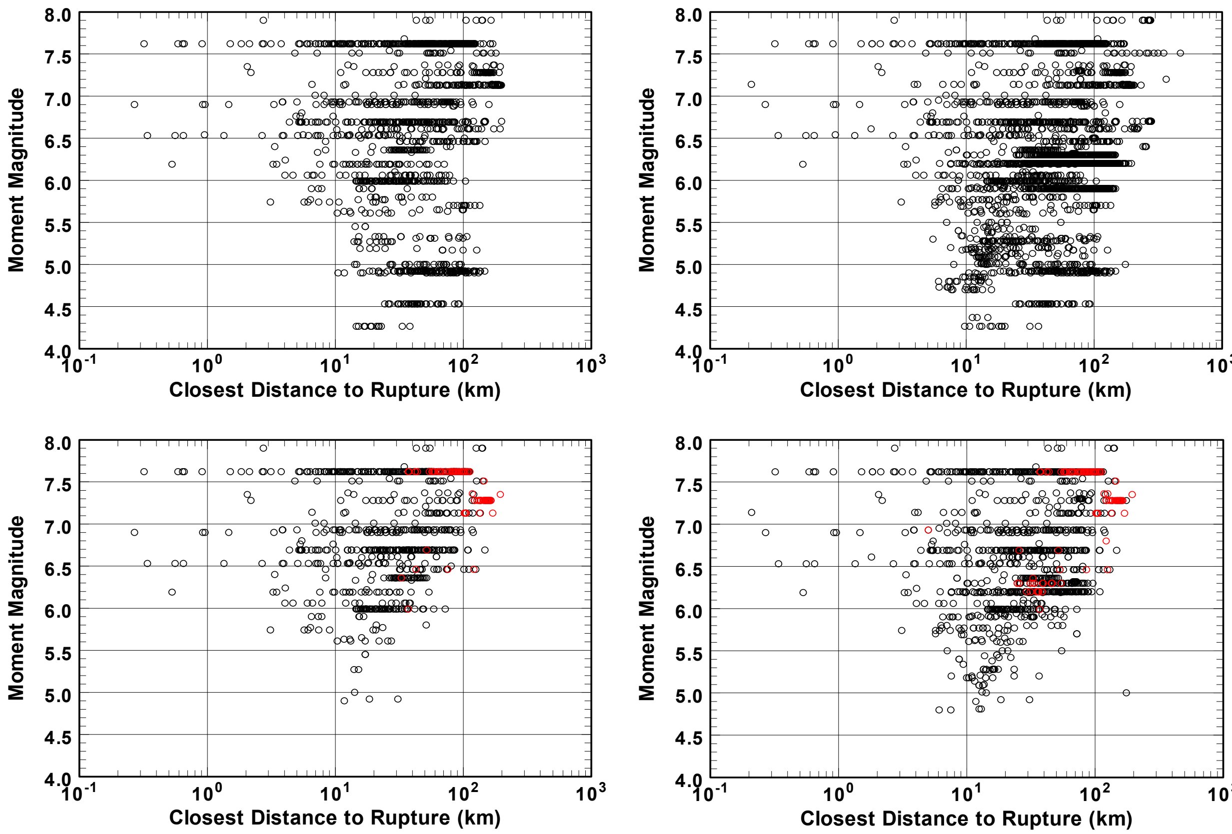

Fig. 3.1 **Distribution of recordings with respect to moment magnitude (M) and rupture distance (R_{RUP}) for the CB08 subset of the PEER-NGA database used in the analysis of CAV_{GM} and I_{JMA} (upper left) and CAV_S (lower left), and the full PEER-NGA database used in the analysis of CAV_{GM} and I_{JMA} (upper right) and CAV_S (lower right). Red circles are additional recordings that pass the spectral velocity check.**

3.2 GROUND MOTION COMPONENTS

3.2.1 Horizontal Geometric Mean of CAV (CAV_{GM})

The ground motion component used to define CAV is the geometric mean of the two as-recorded horizontal components of a recording (CAV_{GM}). Therefore, CAV_{GM} is undefined if any one of the horizontal components is missing. This definition of the horizontal geometric mean is different from the GMRotI50 component (Boore et al. 2006) used in the NGA-West relationships, which is a version of the horizontal geometric mean that is independent of sensor orientation. However, the two geometric means have been shown on average to be within a few percent of each other for peak ground motion and response-spectral parameters (Beyer and Bommer 2006; Boore et al. 2006; Bozorgnia et al. 2006, 2010a; Campbell and Bozorgnia 2007). Therefore, we consider the difference between these two definitions of the geometric mean to be negligible for purposes of this study. Since most of the recordings in the database have both horizontal components, we were able to use 3528 of the 3551 recordings (99.4%) from the full PEER-NGA database and all 1561 recordings from the CB08 subset of this database for the analysis of CAV_{GM} (Table 3.1).

Table 3.1 Ground motion components and databases used in the regression analyses.

Parameter	Database	Spectral Velocity Check	No. of Recordings	**M**	R_{RUP} (km)
CAV_S	CB08	Yes	903	4.9 – 7.9	0.1 – 195
CAV_S	CB08	No	819	4.9 – 7.9	0.1 – 161
CAV_S	Full	Yes	1281	4.8 – 7.9	0.1 – 195
CAV_S	Full	No	1182	4.8 – 7.9	0.1 – 176
CAV_{GM}	CB08	–	1561	4.3 – 7.9	0.1 – 199
I_{JMA}	CB08	–	1540	4.3 – 7.9	0.1 – 199

3.2.2 Maximum Standardized CAV (CAV_S)

The USNRC proposes the use of both the standardized CAV (the CAV check) and the response spectrum (the response spectrum check) in its post-event procedures to determine whether the OBE response spectrum is exceeded and a nuclear power plant must be shut down after an earthquake (U.S. Nuclear Regulatory Commission 1997). These shutdown criteria are consistent with those originally recommended by EPRI (1988) except as noted below. The response spectrum check is exceeded if any one of the three components (i.e., two horizontal and one vertical) of the 5%-damped response spectra generated using the recorded free-field ground motion is larger than:

1. The corresponding design spectral acceleration [OBE spectrum if used in the design; otherwise one third of the safe shutdown earthquake ground motion (SSE) spectrum] or 0.2g, whichever is greater, for frequencies between 2 to 10 Hz; or

2. The corresponding design spectral velocity [OBE spectrum if used in the design; otherwise one third of the SSE spectrum] or a spectral velocity of 6 in. per sec (15.24 cm/sec), whichever is greater, for frequencies between 1 and 2 Hz.

The CAV check is exceeded if any one of the three components of the standardized CAV from the free-field ground motion is greater than 0.16 g-sec. If both the response spectrum check and the CAV check are exceeded, the OBE is considered exceeded and plant shutdown is required. These criteria differ from those originally proposed by EPRI (1988), which used a CAV of 0.3 g-sec rather than a standardized CAV of 0.16 g-sec as later recommended by EPRI (1991) for the CAV check and which did not include a spectral velocity component in the response spectrum check.

In order to embody the USNRC shutdown criteria in a single ground motion parameter, we defined a new variant of standardized CAV that met all of these criteria. However, like EPRI (1988), we questioned whether the spectral velocity check was necessary in order to fulfill the objectives of this study. To explore this further, we performed an analysis of our PEER-NGA database and found that the spectral velocity check allows primarily large magnitude ground motions at long distances to initiate plant shutdown when the spectral acceleration and CAV checks would not otherwise be exceeded. The average moment magnitude and rupture distance of those additional recordings in the CB08 subset and full version of the PEER-NGA databases that exceed the spectral velocity check are greater than 7.0 and 90 km, respectively. The smallest magnitude is 6.0 and the smallest distance is 30 km. These recordings are generally not important to our primary objective of screening out high-acceleration near-source recordings from small-magnitude earthquakes. Nevertheless, in order to demonstrate the impact of including the spectral velocity check, we provide results with and without this check. Thus, we develop four relationships for CAV_S, one for each database and, for each database, one with and one without including the spectral velocity check.

The standardized CAV ground motion component that meets both the response spectrum and CAV checks described above can be defined as the value of standardized CAV for which both of the following criteria are met for a given free-field recording: (1) the maximum value of PSA in the period range 0.1–0.5 sec (2–10 Hz) for all three components is at least 0.2g or the maximum value of PSV (5%-damped pseudo-relative response-spectral velocity) in the period range 0.5–1 sec (1–2 Hz) for all three components is at least 15.24 cm/sec, and (2) the maximum value of the standardized CAV for all three components is at least 0.16 g-sec. The criterion involving PSV is omitted in order to test the sensitivity of the results to the spectral velocity check. We call this CAV component the maximum standardized CAV (CAV_S). CAV_S is undefined if any one of the three components of a recording is missing. Because of the strict criteria for determining whether a recording passes both the response spectrum and CAV checks, we were able to use only 1281 of the 3551 recordings from the full PEER-NGA database (36.1%) and only 903 of the 1561 recordings from the CB08 subset of this database (57.8%) for the analysis of CAV_S (Table 3.1). If the spectral velocity check is ignored, the number of available recordings further reduces to 1182 from the full PEER-NGA database (33.3%) and to 819 from the CB08 subset of this database (53.4%) (Table 3.1).

3.2.3 JMA Instrumental Seismic Intensity (I_{JMA})

I_{JMA} is uniquely defined in terms of all three components of a recording. As a result, I_{JMA} is undefined if any one of these three components is missing. Since most of the recordings in the database have all three components, we were able to use 3482 of the 3551 recordings (98.1%) from the full PEER-NGA database and 1540 of the 1561 recordings (99.7%) from the CB08 subset of this database in the analysis of I_{JMA} (Table 3.1). The number of useable recordings is reduced to the number of CAV_S values for relationships that involve both of these parameters (Table 3.1).

4 Relationship between CAV_S and I_{JMA}

The purpose of developing relationships between CAV_S and I_{JMA} is twofold: (1) to evaluate the value of I_{JMA} that corresponds to a CAV_S value of 0.16 g-sec, which is defined in USNRC Regulatory Guide 1.166 (U.S. Nuclear Regulatory Agency 1997) as the threshold needed to shut down a nuclear power plant when the OBE response spectrum has been exceeded and (2) to correlate CAV_S with the qualitative descriptions of damage to well-engineered buildings in the JMA seismic intensity scale.

4.1 MEDIAN MODEL

The median model for estimating CAV_S is given by the following equation:

$$\overline{\ln \mathrm{CAV_S}} = c_0 + c_1 \mathrm{I_{JMA}} \tag{4.1}$$

where CAV_S has units of g-sec. Analyses were performed for both the CB08 subset and the full version of the PEER-NGA database with and without the spectral velocity check (four analyses in all) using the random-effects regression algorithms of Abrahamson and Youngs (1992). The results of the analyses are listed in Table 4.1. Plots of the equations are shown in Figure 4.1. We also tested bi-linear and quadratic functional forms, but the additional coefficients were found to be insignificantly different from zero at the 90% confidence level and, therefore, they were not included in the relationship. Validation of the linear model is also visually demonstrated by the residual plot shown in Figure 4.1.

Table 4.1 Model parameters for the relationship between CAV_S and I_{JMA}.

Parameter	Database	Spectral Velocity Check	c_0	c_1	$\sigma_{\ln CAV_S}$	$\tau_{\ln CAV_S}$	σ_T	R^2
CAV_S	CB08	Yes	-5.256	0.951	0.391	0.109	0.406	0.836
CAV_S	CB08	No	-5.274	0.955	0.400	0.108	0.414	0.817
CAV_S	Full	Yes	-5.257	0.934	0.394	0.139	0.418	0.850
CAV_S	Full	No	-5.306	0.944	0.402	0.137	0.425	0.838

Note: CAV_S has units of g-sec.

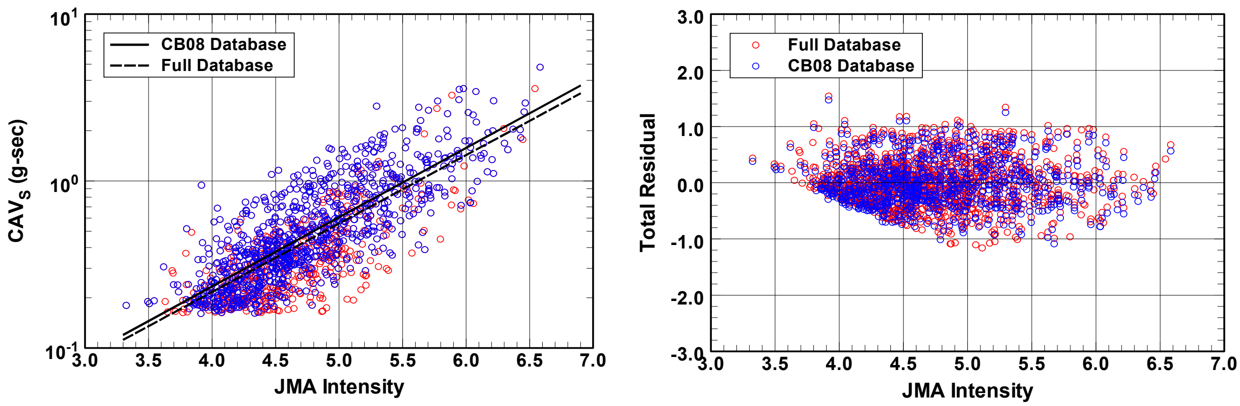

Fig. 4.1 Relationships between CAV_S and I_{JMA}: (left) median models; (right) total residuals. Median models that use data that pass the spectral velocity check are indistinguishable from those that use data that do not pass this check at the scale of the plot. Plotted data and residuals include those recordings that pass the spectral velocity check.

4.2 ALEATORY UNCERTAINTY MODEL

Consistent with the random-effects regression analysis used to derive the median model, the aleatory uncertainty model for CAV_S versus I_{JMA} is defined by the following equation (Campbell and Bozorgnia 2008):

$$(\ln CAV_S)_{ij} = (\overline{\ln CAV_S})_{ij} + \eta_i + \varepsilon_{ij} \tag{4.2}$$

where η_i is the interevent residual for event *i*; and $\overline{(\ln \mathrm{CAV_S})}_{ij}$, $(\ln \mathrm{CAV_S})_{ij}$, and ε_{ij} are the predicted median value, the observed value, and the intra-event residual for recording *j* of event *i*. The independent normally distributed variables η_i and ε_{ij} have zero means and estimated interevent, intra-event, and total standard deviations of $\tau = \tau_{\ln \mathrm{CAV_S}}$, $\sigma = \sigma_{\ln \mathrm{CAV_S}}$, and $\sigma_T = \sqrt{\sigma^2 + \tau^2}$, respectively (Table 4.1).

Figure 4.2 shows the distribution of the total residuals with respect to several physical parameters of the earthquake, including moment magnitude (**M**), rupture distance (R_{RUP}), 30-m shear-wave velocity (V_{S30}), median estimate of PGA on rock (A_{1100}), sediment or basin depth ($Z_{2.5}$), and rake angle (λ), for the CB08 subset of the PEER-NGA database that includes those data that pass the spectral velocity check. Biases in these residuals, especially with respect to magnitude and sediment depth, indicate that $\ln \mathrm{CAV_S}$ and $\mathrm{I_{JMA}}$ scale differently with respect to several of these physical parameters. Similar results were found for the full PEER-NGA database. One of the possible uses of these relationships is to evaluate $\mathrm{CAV_S}$ as a tentative trigger for an automatic or operator-assisted emergency shutdown of a nuclear reactor, also known as a SCRAM. In such a case, the physical parameters of an earthquake would not generally be known. Therefore, accounting for the correlation with respect to these physical parameters in Equation (4.1) is not considered to be meaningful.

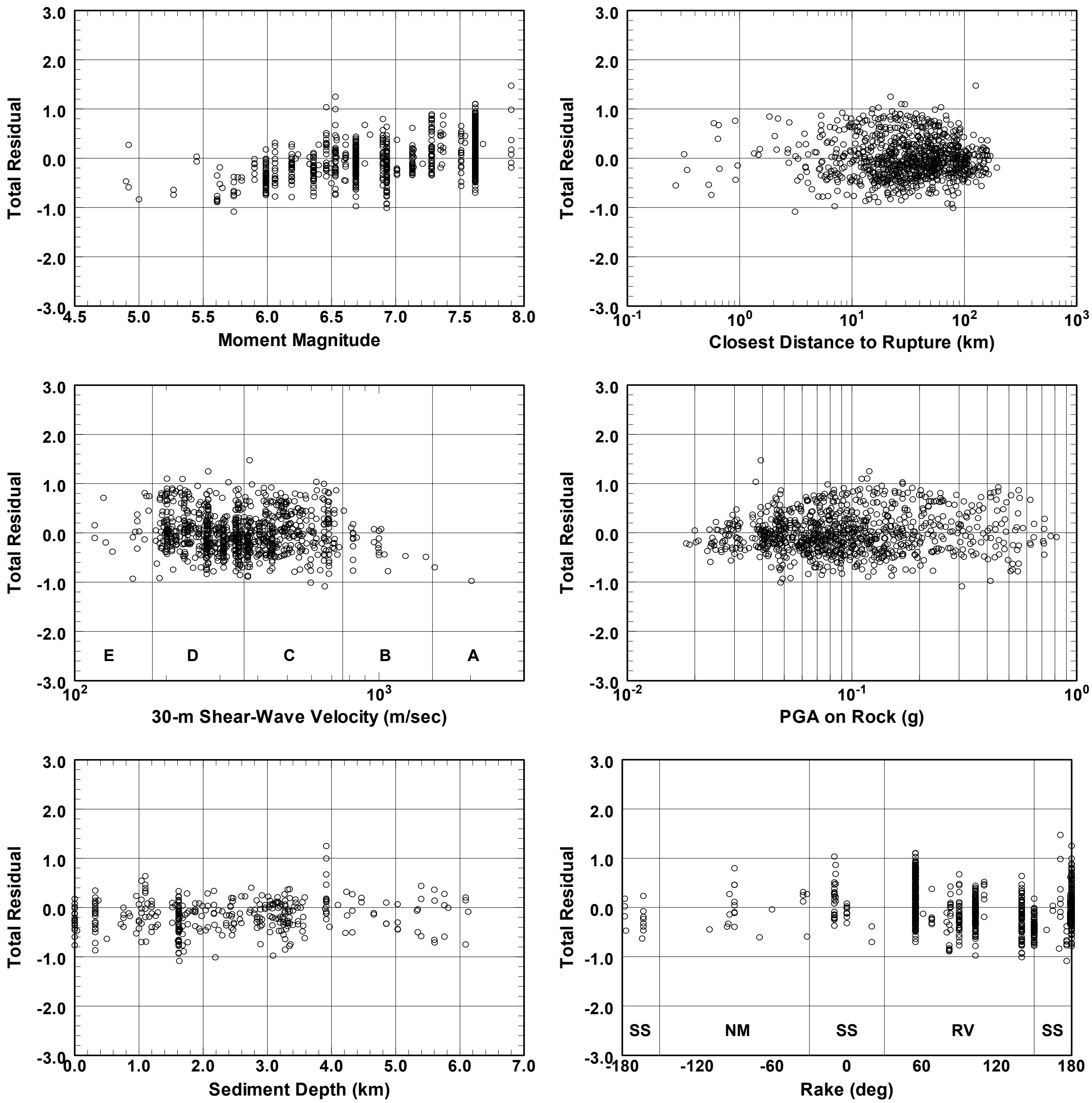

Fig. 4.2 Total residuals for the relationship between CAV_S and I_{JMA} showing their distribution with moment magnitude (M), rupture distance (R_{RUP}), median PGA on rock (A_{1100}), 30-m shear wave velocity (V_{S30}) binned by NEHRP site class, sediment depth ($Z_{2.5}$), and rake angle (λ) binned by fault mechanism (SS, strike slip; NM, normal; RV, reverse). Residuals are calculated with respect to the median model derived from the CB08 subset of the PEER-NGA database that includes those data that pass the spectral velocity check.

4.3 RELATIONSHIP TO QUALITATIVE DAMAGE DESCRIPTIONS

4.3.1 Qualitative Damage Descriptions in the JMA Intensity Scale

According to the descriptions of intensity levels associated with the JMA seismic intensity scale (Earthquake Research Committee 1998), the lowest intensity level where the onset of structural damage to well-engineered structures has been observed is 5 Lower (I_{JMA} 4.5–5.0). The effect of this intensity level on reinforced concrete buildings (a proxy for well-engineered structures) is described as "Occasionally, cracks formed in walls of less earthquake-resistant buildings." However, it is at an intensity level of 5 Upper (I_{JMA} 5.0–5.5) where structural damage to well-engineered structures with special earthquake-resistant design occurs, where the effect of this intensity level on reinforced concrete (RC) buildings is described as "… even highly earthquake-resistant buildings develop cracks." An updated version of the JMA intensity scale (Japan Meteorological Agency 2007) suggests that these damages occur at one intensity level higher, or 5 Upper for less earthquake-resistant buildings and 6 Lower (I_{JMA} 5.5–6.0) for highly earthquake-resistant buildings, where damage to RC buildings is described as "Cracks may form in walls, crossbeams and pillars."

4.3.2 Qualitative Damage Descriptions in the MMI Intensity Scale

To aid in the selection of an appropriate value for I_{JMA} that corresponds with the onset of structural damage to well-engineered structures, it is useful to correlate it to MMI, or more specifically, to an instrumental measure of MMI (I_{MMI}). One such correlation is given by Shabestari and Yamazaki (2001), who developed it from U.S. Geological Survey (USGS) assessments of MMI from the 1987 Whittier Narrows (**M** 6.0), the 1989 Loma Prieta (**M** 6.9), and the 1994 Northridge (**M** 6.7), California, earthquakes. Their relationship between I_{MMI} and the geometric average of I_{JMA} over specified values of MMI is given by the following equation:

$$I_{MMI} = 1.95\, I_{JMA} - 2.91 \qquad (4.3)$$

which has a standard deviation of 0.283 and an r-square value of 0.974. This relationship is considered to be valid for intensities in the range $\mathrm{IV} \le \mathrm{MMI} \le \mathrm{VIII}$. According to this equation, the median values of I_{MMI} that are consistent with the potential structural damage descriptions corresponding to I_{JMA} of 4.5, 5.0, and 5.5 are 5.87 ± 0.28 (MMI VI), 6.84 ± 0.28 (MMI VII), and 7.82 ± 0.28 (MMI VIII).

Another relationship between I_{MMI} and I_{JMA} was developed by Sokolov and Furumura (2008) from 598 recordings of nine earthquakes that occurred between 1999 and 2007. The recordings were obtained by the K-NET and KiK-net strong motion instruments deployed throughout Japan by the National Institute for Earth Science and Disaster Research (NIED) following the destructive Kobe, Japan, earthquake in 1995. The earthquakes ranged in magnitude from M_{JMA} 6.3 to 8.0. I_{MMI} was calculated using the Fourier amplitude spectra (FAS) method of Sokolov (2002). The relationship is given by the following equation:

$$I_{MMI} = 1.743\, I_{JMA} - 0.584 \tag{4.4}$$

which has a standard deviation of 0.384 and an r-square value of 0.984. It is considered to be valid for I_{MMI} 5.5 to 10.5 and I_{JMA} 3.5 to 6 Upper. According to this equation, the median values of I_{MMI} that are consistent with the description of potential structural damage corresponding to I_{JMA} of 4.5, 5.0, and 5.5 are 7.26 ± 0.38 (MMI VII), 8.13 ± 0.38 (MMI VIII), and 9.00 ± 0.38 (MMI IX).

The large difference between the estimates of I_{MMI} given by Equations (4.3) and (4.4) poses a problem in our ability to reliably assign a specific value if I_{MMI} to a potential structural damage threshold value of I_{JMA}. Some insight into this discrepancy is offered by Sokolov and Wald (2002). They performed a direct comparison of I_{MMI} from the 1999 (**M** 7.1) Hector Mine, California, and the 1999 (**M** 7.6) Chi-Chi, Taiwan, earthquakes between the FAS method of Sokolov (2002) and the peak amplitude method of Wald et al. (1999) and found that the latter method produced values that were approximately one intensity unit lower, more consistent with the estimates from Equation (4.3). Sokolov and Wald (2002) suggest that the FAS method, which is based on worldwide data and, therefore, averages different building codes and qualities of construction, provides the worst (pessimistic) assessment of I_{MMI}. The peak amplitude method, which reflects improved building practices, gives a more current optimistic view. These authors go on to say that the relationship of Wald et al. (1999) also provides lower intensity levels for the same peak motions than the relationship of Trifunac and Brady (1975), which was based on the older MMI assessments similar to those used by Sokolov (2002). They suggest that the shift may be related to improved building practices and the replacement or retrofit of weak structures over time in the United States. Thus, so far as the peak amplitude method is based primarily on data from recent earthquakes in California, the relationship characterizes existing building stock constructed in accordance with a stronger building code. Wald et al. (1999) also suggest that their relationship uses a more restricted intensity range than Trifunac and Brady (1975), which presumably removes the less reliable recordings.

One drawback of the MMI scale is that it does not give an adequate description of damage to well-engineered structures. This shortcoming has been corrected in the recent European macroseismic scale (EMS-98). The EMS-98 scale, which is similar to both the MMI and the Medvedev-Sponheuer-Kárník (MSK-64) scales, was specifically designed to describe damage to engineered structures (Grünthal 1998). Well-engineered structures fall into the EMS structure types defined as RC frames and walls with a moderate level of earthquake-resistant design (Vulnerability Class D) and steel structures and RC frames and walls with a high level of earthquake-resistant design (Vulnerability Class E). According to EMS-98, the onset of slight structural damage (Damage Grade 2) to Class D structures begins at intensity level VIII (I_{MMI} 7.5–8.5) and to Class E structures at intensity level IX (I_{MMI} 8.5–9.5). According to Equations (4.3) and (4.4), these intensity levels correspond to median I_{JMA} values of 4.6–5.3 and 5.2–5.9, respectively. Damage Grade 2 is described as "Cracks in columns and beams of frames and in structural walls." No structural damage is expected to Class D structures at intensity level VII or to Class E structures at intensity level VIII.

The descriptions of damage in the EMS-98 (MMI) intensity scale and its correlation with I_{JMA} would seem to confirm the relative assessment of damage to similar types of buildings described in the revision of the JMA intensity scale (Japan Meteorological Agency 2007). RC buildings of a less or moderate level of earthquake-resistant design begin to form cracks at I_{JMA} 5.0 or I_{MMI} 7.5 and those with a high level of earthquake-resistant design begin to form cracks at I_{JMA} 5.5 or I_{MMI} 8.5. The relationships of Shabestari and Yamazaki (2001) and Sokolov and Furumura (2008) estimate I_{MMI} values that bracket those inferred from the EMS-98 scale for the same values of I_{JMA}. For I_{JMA} values of 4.5, 5.0, and 5.5, these two relationships give average estimates of I_{MMI} of 6.56 ± 0.33, 7.49 ± 0.33, and 8.41 ± 0.33, within one standard deviation of those inferred from similar descriptions of damage in the EMS-98 scale that correspond to I_{MMI} values of 6.5, 7.5, and 8.5. It should be noted that EPRI (1988) selected MMI VII (I_{MMI} 6.5–7.5) as the intensity level representing the possible onset of structural damage to engineered (not necessarily well-engineered) industrial facilities, which lead EPRI (1991) to select 0.16 g-sec as the value of standardized CAV to associate with this MMI level.

4.3.3 Correlation of CAV_S with Qualitative Damage Descriptions in the JMA and MMI Intensity Scales

Table 4.2 lists the estimates of CAV_S from Equation (4.1) and Table 4.1 that are related to the potential values of I_{JMA} and I_{MMI} that correspond to the onset of structural damage to well-engineered structures as described in the JMA, MMI, MSK-64, and EMS-98 intensity scales. Also listed in this table are the probabilities that these estimates of CAV_S are less than the USNRC proposed threshold of 0.16 g-sec that is used as one of the criterion for plant shutdown after an earthquake. These latter probabilities are an indication of the likelihood that CAV_S will be less than that required to trigger the USNRC shutdown criteria given the potential damage indicated by the specified values of I_{JMA} and I_{MMI}. According to Table 4.2, even the most conservative value for the potential structural damage thresholds of I_{JMA} and I_{MMI}, combined with the more conservative relationship between CAV_S and I_{JMA} developed without those data that exceed the spectral velocity check, leads to relatively small nonexceedance probabilities, $P_{ne}(0.16) = P(CAV_S < 0.16 \mid I_{JMA})$, of 1.9% for the CB08 subset and 3.4% for the full version of the PEER-NGA database. The nonexceedance probabilities for the larger, less conservative values of I_{JMA} and I_{MMI} are all less than 0.2%.

Table 4.2 Statistical correlation between CAV_S and instrumental seismic intensity.

I_{JMA}	I_{MMI}	Database	Spectral Velocity Check	Median CAV_S	$\sigma_{\ln CAV_S}$	$P_{ne}(0.16)$	CAV_S		
							P_{ne}=5%	P_{ne}=2.5%	P_{ne}=1%
4.5	6.5	CB08	Yes	0.377	0.406	1.75×10^{-2}	0.193	0.170	0.146
4.5	6.5	CB08	No	0.377	0.414	1.93×10^{-2}	0.191	0.167	0.144
5.0	7.5	CB08	Yes	0.606	0.406	5.19×10^{-4}	0.311	0.273	0.236
5.0	7.5	CB08	No	0.607	0.414	6.38×10^{-4}	0.307	0.270	0.232
5.5	8.5	CB08	Yes	0.975	0.406	4.27×10^{-6}	0.500	0.440	0.379
5.5	8.5	CB08	No	0.979	0.414	6.08×10^{-6}	0.495	0.435	0.374
4.5	6.5	Full	Yes	0.349	0.418	3.13×10^{-2}	0.175	0.154	0.132
4.5	6.5	Full	No	0.347	0.425	3.42×10^{-2}	0.173	0.151	0.129
5.0	7.5	Full	Yes	0.556	0.418	1.44×10^{-3}	0.280	0.245	0.210
5.0	7.5	Full	No	0.557	0.425	1.68×10^{-3}	0.277	0.242	0.207
5.5	8.5	Full	Yes	0.887	0.418	2.09×10^{-5}	0.446	0.391	0.335
5.5	8.5	Full	No	0.892	0.425	2.63×10^{-5}	0.443	0.388	0.332

Note: P_{ne} is probability of nonexceedance; $P_{ne}(0.16) = P(CAV_S < 0.16 \mid I_{JMA})$; CAV_S has units of g-sec.

EPRI (1988) and EPRI (1991) selected the minimum value of CAV and standardized CAV of those recordings with an assessed site intensity of MMI VII as the proposed trigger threshold for shutting down a nuclear power plant when the OBE response spectrum is exceeded. A more objective approach of making this selection would be to perform a statistical analysis as we have done in Table 4.2. This table lists the values of CAV_S that are associated with nonexceedance probabilities (P_{ne}) of 5%, 2.5%, and 1%. This statistical analysis indicates that the 0.16 g-sec threshold for standardized CAV recommended by EPRI (1991) and used by the USNRC (U.S. Nuclear Regulatory Commission 1997) corresponds to a nonexceedance probability between 1% and 2.5% for a JMA instrumental seismic intensity corresponding to I_{JMA} 4.5 (I_{MMI} 6.5). For a JMA instrumental seismic intensity corresponding to I_{JMA} 5.0 (I_{MMI} 7.5), Table 4.2 indicates that the value of CAV_S with a probability of nonexceedance of 1% would be approximately 0.21–0.24 g-sec. This value increases to around 0.28–0.31 g-sec, or almost twice the value recommended by EPRI (1991) and the U.S. Nuclear Regulatory Commission (1997), for a nonexceedance probability of 5%.

5 Ground Motion Prediction Equations

We adopted the same functional forms that we used to define our NGA-West GMPEs (Campbell and Bozorgnia 2007, 2008) to develop GMPEs for CAV_{GM} and I_{JMA}. However, the number of CAV_S values in the CB08 subset of the PEER-NGA database (Table 3.1) is too small to use directly in the development of a GMPE for this parameter. Instead, we developed a relationship between CAV_S from CAV_{GM} and used the predicted median value of CAV_{GM} from its GMPE to estimate CAV_S. We found that a more simplified functional form could be used for the relationship between CAV_S and CAV_{GM} because of the similar dependence of these two parameters on many of the predictor variables.

The functional forms were selected according to (1) their sound seismological basis; (2) their unbiased residuals; (3) their ability to be extrapolated to values of magnitude, distance, and other predictor variables that are important for use in engineering and seismology; and (4) their simplicity, although this latter consideration was not an overriding factor. The third criterion was the most difficult to achieve because the data did not always allow the functional forms of some predictor variables to be developed empirically. In such cases, theoretical constraints were used to define the functional forms based on supporting studies sponsored by the NGA-West project (Power et al. 2008). Specific details regarding how these general selection criteria were applied is given in Campbell and Bozorgnia (2007, 2008). Model coefficients were determined using the random-effects regression algorithms of Abrahamson and Youngs (1992).

5.1 PREDICTION EQUATIONS FOR CAV$_{GM}$ AND I$_{JMA}$

5.1.1 Median Model

The median estimates of CAV$_{GM}$ and I$_{JMA}$ are given by the following general equation (Campbell and Bozorgnia 2008):

$$\overline{Y} = f_{mag} + f_{dis} + f_{flt} + f_{hng} + f_{site} + f_{sed} \tag{5.1}$$

where the magnitude term is given by the expression:

$$f_{mag} = \begin{cases} c_0 + c_1\mathbf{M}; & \mathbf{M} \le 5.5 \\ c_0 + c_1\mathbf{M} + c_2(\mathbf{M} - 5.5); & 5.5 < \mathbf{M} \le 6.5 \\ c_0 + c_1\mathbf{M} + c_2(\mathbf{M} - 5.5) + c_3(\mathbf{M} - 6.5); & \mathbf{M} > 6.5 \end{cases} \tag{5.2}$$

the distance term is given by the expression:

$$f_{dis} = (c_4 + c_5\mathbf{M})\ln\left(\sqrt{R_{RUP}^2 + c_6^2}\right) \tag{5.3}$$

the style-of-faulting (fault mechanism) term is given by the expressions:

$$f_{flt} = c_7 F_{RV} f_{flt,Z} + c_8 F_{NM} \tag{5.4}$$

$$f_{flt,Z} = \begin{cases} Z_{TOR}; & Z_{TOR} < 1 \\ 1; & Z_{TOR} \ge 1 \end{cases} \tag{5.5}$$

the hanging-wall term is given by the expressions:

$$f_{hng} = c_9 f_{hng,R} f_{hng,M} f_{hng,Z} f_{hng,\delta} \tag{5.6}$$

$$f_{hng,R} = \begin{cases} 1; & R_{JB} = 0 \\ \left[\max\left(R_{RUP}, \sqrt{R_{JB}^2 + 1}\right) - R_{JB}\right] \Big/ \max\left(R_{RUP}, \sqrt{R_{JB}^2 + 1}\right); & R_{JB} > 0, Z_{TOR} < 1 \\ (R_{RUP} - R_{JB}) / R_{RUP}; & R_{JB} > 0, Z_{TOR} \ge 1 \end{cases} \tag{5.7}$$

$$f_{hng,M} = \begin{cases} 0; & \mathbf{M} \le 6.0 \\ 2(\mathbf{M} - 6.0); & 6.0 < \mathbf{M} < 6.5 \\ 1; & \mathbf{M} \ge 6.5 \end{cases} \tag{5.8}$$

$$f_{hng,Z} = \begin{cases} 0; & Z_{TOR} \geq 20 \\ (20 - Z_{TOR})/20; & 0 \leq Z_{TOR} < 20 \end{cases} \tag{5.9}$$

$$f_{hng,\delta} = \begin{cases} 1; & |\delta| \leq 70 \\ (90 - |\delta|)/20; & |\delta| > 70 \end{cases} \tag{5.10}$$

the shallow site response term is given by the expression:

$$f_{site} = \begin{cases} c_{10} \ln\left(\dfrac{V_{S30}}{k_1}\right) + k_2 \left\{ \ln\left[A_{1100} + c\left(\dfrac{V_{S30}}{k_1}\right)^n \right] - \ln\left[A_{1100} + c\right] \right\}; & V_{S30} < k_1 \\ (c_{10} + k_2 n) \ln\left(\dfrac{V_{S30}}{k_1}\right); & k_1 \leq V_{S30} < 1100 \\ (c_{10} + k_2 n) \ln\left(\dfrac{1100}{k_1}\right); & V_{S30} \geq 1100 \end{cases} \tag{5.11}$$

and the basin response term is given by the expression:

$$f_{sed} = \begin{cases} c_{11}(Z_{2.5} - 1); & Z_{2.5} < 1 \\ 0; & 1 \leq Z_{2.5} \leq 3 \\ c_{12} k_3 e^{-0.75}\left[1 - e^{-0.25(Z_{2.5} - 3)}\right]; & Z_{2.5} > 3 \end{cases} \tag{5.12}$$

In the above equations, $\overline{Y}$ is the median estimate of CAV_{GM} (g-sec) or I_{JMA}, designated $\overline{\ln \text{CAV}_{\text{GM}}}$ and $\overline{\text{I}_{\text{JMA}}}$; **M** is moment magnitude; R_{RUP} is the closest distance to the coseismic rupture plane (km); R_{JB} is the closest distance to the surface projection of the coseismic rupture plane (km); F_{RV} is an indicator variable representing reverse and reverse-oblique faulting ($F_{RV} = 1$ for $30° < \lambda < 150°$, $F_{RV} = 0$ otherwise, and λ is rake angle defined as the average angle of slip measured in the plane of rupture between the strike direction and the slip vector); F_{NM} is an indicator variable representing normal and normal-oblique faulting ($F_{NM} = 1$ for $-150° < \lambda < -30°$ and $F_{NM} = 0$ otherwise); Z_{TOR} is the depth to the top of the coseismic rupture plane (km); $|\delta| \leq 90°$ is the absolute value of the angle of dip of the rupture plane measured from a horizontal plane; V_{S30} is the time-averaged shear-wave velocity in the top 30 m of the site (m/sec); A_{1100} is the median estimate of PGA on a rock outcrop with $V_{S30} = 1100$ m/sec (Campbell and Bozorgnia 2008) (g); and $Z_{2.5}$ is the depth to the 2.5 km/sec shear-wave velocity horizon, typically referred to as basin or sediment depth (km). The empirical coefficients c_i, k_1, and k_2 and the theoretical coefficients c, n, and k_3 are listed in Table 5.1. For comparison, this table also includes the model coefficients for PGA, PGV, PGD, and PSA from Campbell and Bozorgnia (2008).

The statistical robustness of $\mathrm{CAV_{GM}}$ allowed us to statistically fit the theoretically constrained coefficients k_1 and k_2 in the original NGA-West relationship, which had not been possible with many of the peak ground motion and response-spectral parameters. A hypothesis test determined that the theoretically derived value of k_1 of 400 obtained for PGV and PSA for $T \geq 1$ sec was not significantly different at the 99% confidence level from the statistically derived value of 397 and was, therefore, adopted in place of the statistically derived value. The value of k_3 was fixed at the value for PGV and one-second PSA to serve as a reference value in order to facilitate the comparison of the coefficient c_{12} to the values found in the relationships for peak and response-spectral parameters.

5.1.2 Aleatory Uncertainty Model

The aleatory uncertainty models for $\mathrm{CAV_{GM}}$ and $\mathrm{I_{JMA}}$ are defined by the following random-effects equation (Campbell and Bozorgnia 2008):

$$Y_{ij} = \overline{Y}_{ij} + \eta_i + \varepsilon_{ij} \tag{5.13}$$

where η_i is the inter-event residual for event *i* and $\overline{Y}_{ij}$, Y_{ij}, and ε_{ij} are the predicted median value, the observed value, and the intra-event residual for recording *j* of event *i*. The independent normally distributed variables η_i and ε_{ij} have zero means and estimated inter-event, intra-event, and total standard deviations (designated τ, σ, and σ_T, respectively) given by the following equations:

$$\tau = \tau_{\ln Y} \tag{5.14}$$

$$\sigma = \sqrt{\sigma^2_{\ln Y_B} + \sigma^2_{\ln AF} + \alpha^2\sigma^2_{\ln A_B} + 2\alpha\rho\sigma_{\ln Y_B}\sigma_{\ln A_B}} \tag{5.15}$$

$$\sigma_T = \sqrt{\sigma^2 + \tau^2} \tag{5.16}$$

where $\tau_{\ln Y}$ is the standard deviation of the inter-event residuals; $\sigma_{\ln Y}$ is the standard deviation of the intra-event residuals; $\sigma_{\ln Y_B} = (\sigma^2_{\ln Y} - \sigma^2_{\ln AF})^{1/2}$ is the estimated intra-event standard deviation of $\ln \mathrm{CAV}_{\mathrm{GM}}$ or $\mathrm{I}_{\mathrm{JMA}}$ at the base of the site profile; $\sigma_{\ln AF}$ is the estimated standard deviation of the logarithm of the site amplification factor f_{site} assuming linear site response; $\sigma_{\ln A_B} = (\sigma^2_{\ln \mathrm{PGA}} - \sigma^2_{\ln AF})^{1/2}$ is the estimated standard deviation of $\ln \mathrm{PGA}$ at the base of the site profile (Campbell and Bozorgnia 2008); ρ is the correlation coefficient between the intra-event residuals of the ground motion parameter of interest and PGA; and α is the linearized functional relationship between f_{site} and $\ln A_{1100}$, which is estimated from the partial derivative $\partial f_{site} / \partial \ln A_{1100}$ (Abrahamson and Silva 2008) according to the following expression:

$$\alpha = \begin{cases} k_2 A_{1100} \left\{ \left[A_{1100} + c\left(V_{S30}/k_1\right)^n \right]^{-1} - \left(A_{1100} + c\right)^{-1} \right\} & V_{S30} < k_1 \\ 0 & V_{S30} \geq k_1 \end{cases} \tag{5.17}$$

The model coefficients k_1, k_2, c and n are listed in Table 5.1. The standard deviations $\tau_{\ln Y}$, $\sigma_{\ln Y}$, σ_T, and $\sigma_{\ln AF}$ and the correlation coefficient ρ are listed in Table 5.2. For comparison, this table also includes the standard deviations and correlation coefficients for PGA, PGV, PGD, and PSA from Campbell and Bozorgnia (2008).

Table 5.1 Model coefficients for the GMPEs of peak ground motion and response-spectral parameters, CAV_{GM}, and I_{JMA}.

T (s)	c_0	c_1	c_2	c_3	c_4	c_5	c_6	c_7	c_8	c_9	c_{10}	c_{11}	c_{12}	k_1	k_2	k_3
0.010	-1.715	0.500	-0.530	-0.262	-2.118	0.170	5.60	0.280	-0.120	0.490	1.058	0.040	0.610	865	-1.186	1.839
0.020	-1.680	0.500	-0.530	-0.262	-2.123	0.170	5.60	0.280	-0.120	0.490	1.102	0.040	0.610	865	-1.219	1.840
0.030	-1.552	0.500	-0.530	-0.262	-2.145	0.170	5.60	0.280	-0.120	0.490	1.174	0.040	0.610	908	-1.273	1.841
0.050	-1.209	0.500	-0.530	-0.267	-2.199	0.170	5.74	0.280	-0.120	0.490	1.272	0.040	0.610	1054	-1.346	1.843
0.075	-0.657	0.500	-0.530	-0.302	-2.277	0.170	7.09	0.280	-0.120	0.490	1.438	0.040	0.610	1086	-1.471	1.845
0.10	-0.314	0.500	-0.530	-0.324	-2.318	0.170	8.05	0.280	-0.099	0.490	1.604	0.040	0.610	1032	-1.624	1.847
0.15	-0.133	0.500	-0.530	-0.339	-2.309	0.170	8.79	0.280	-0.048	0.490	1.928	0.040	0.610	878	-1.931	1.852
0.20	-0.486	0.500	-0.446	-0.398	-2.220	0.170	7.60	0.280	-0.012	0.490	2.194	0.040	0.610	748	-2.188	1.856
0.25	-0.890	0.500	-0.362	-0.458	-2.146	0.170	6.58	0.280	0.000	0.490	2.351	0.040	0.700	654	-2.381	1.861
0.30	-1.171	0.500	-0.294	-0.511	-2.095	0.170	6.04	0.280	0.000	0.490	2.460	0.040	0.750	587	-2.518	1.865
0.40	-1.466	0.500	-0.186	-0.592	-2.066	0.170	5.30	0.280	0.000	0.490	2.587	0.040	0.850	503	-2.657	1.874
0.50	-2.569	0.656	-0.304	-0.536	-2.041	0.170	4.73	0.280	0.000	0.490	2.544	0.040	0.883	457	-2.669	1.883
0.75	-4.844	0.972	-0.578	-0.406	-2.000	0.170	4.00	0.280	0.000	0.490	2.133	0.077	1.000	410	-2.401	1.906
1.0	-6.406	1.196	-0.772	-0.314	-2.000	0.170	4.00	0.255	0.000	0.490	1.571	0.150	1.000	400	-1.955	1.929
1.5	-8.692	1.513	-1.046	-0.185	-2.000	0.170	4.00	0.161	0.000	0.490	0.406	0.253	1.000	400	-1.025	1.974
2.0	-9.701	1.600	-0.978	-0.236	-2.000	0.170	4.00	0.094	0.000	0.371	-0.456	0.300	1.000	400	-0.299	2.019
3.0	-10.556	1.600	-0.638	-0.491	-2.000	0.170	4.00	0.000	0.000	0.154	-0.820	0.300	1.000	400	0.000	2.110
4.0	-11.212	1.600	-0.316	-0.770	-2.000	0.170	4.00	0.000	0.000	0.000	-0.820	0.300	1.000	400	0.000	2.200
5.0	-11.684	1.600	-0.070	-0.986	-2.000	0.170	4.00	0.000	0.000	0.000	-0.820	0.300	1.000	400	0.000	2.291
7.5	-12.505	1.600	-0.070	-0.656	-2.000	0.170	4.00	0.000	0.000	0.000	-0.820	0.300	1.000	400	0.000	2.517
10.0	-13.087	1.600	-0.070	-0.422	-2.000	0.170	4.00	0.000	0.000	0.000	-0.820	0.300	1.000	400	0.000	2.744
PGA	-1.715	0.500	-0.530	-0.262	-2.118	0.170	5.60	0.280	-0.120	0.490	1.058	0.040	0.610	865	-1.186	1.839
PGV	0.954	0.696	-0.309	-0.019	-2.016	0.170	4.00	0.245	0.000	0.358	1.694	0.092	1.000	400	-1.955	1.929
PGD	-5.270	1.600	-0.070	0.000	-2.000	0.170	4.00	0.000	0.000	0.000	-0.820	0.300	1.000	400	0.000	2.744
I_{JMA}	4.928	0.325	-0.091	-0.467	-1.845	0.170	3.40	0.347	-0.116	0.463	2.101	0.059	0.510	324	-2.105	1.929
CAV_{GM}	-4.354	0.942	-0.178	-0.346	-1.309	0.087	7.24	0.111	-0.108	0.362	2.549	0.090	0.662	400	-2.690	1.929

Note: $c = 1.88$ and $n = 1.18$; PGA and PSA have units of g; PGV and PGD have units of cm/sec and cm, respectively; CAV_{GM} has units of g-sec.

Table 5.2 Model standard deviations and correlation coefficients for the GMPEs of peak ground motion and response-spectral parameters, CAV_{GM}, and I_{JMA}.

T (s)	Standard Deviation for $V_{S30} \geq k_1$					ρ	
	$\sigma_{\ln Y}$	$\tau_{\ln Y}$	σ_C	σ_T	σ_{Arb}	PGA	CAV_S
0.010	0.478	0.219	0.166	0.526	0.551	1.000	0.205
0.020	0.480	0.219	0.166	0.528	0.553	0.999	0.205
0.030	0.489	0.235	0.165	0.543	0.567	0.989	0.205
0.050	0.510	0.258	0.162	0.572	0.594	0.963	0.205
0.075	0.520	0.292	0.158	0.596	0.617	0.922	0.191
0.10	0.531	0.286	0.170	0.603	0.627	0.898	0.176
0.15	0.532	0.280	0.180	0.601	0.628	0.890	0.173
0.20	0.534	0.249	0.186	0.589	0.618	0.871	0.168
0.25	0.534	0.240	0.191	0.585	0.616	0.852	0.137
0.30	0.544	0.215	0.198	0.585	0.618	0.831	0.115
0.40	0.541	0.217	0.206	0.583	0.618	0.785	0.105
0.50	0.550	0.214	0.208	0.590	0.626	0.735	0.090
0.75	0.568	0.227	0.221	0.612	0.650	0.628	0.073
1.0	0.568	0.255	0.225	0.623	0.662	0.534	0.058
1.5	0.564	0.296	0.222	0.637	0.675	0.411	0.045
2.0	0.571	0.296	0.226	0.643	0.682	0.331	0.045
3.0	0.558	0.326	0.229	0.646	0.686	0.289	0.045
4.0	0.576	0.297	0.237	0.648	0.690	0.261	0.045
5.0	0.601	0.359	0.237	0.700	0.739	0.200	0.045
7.5	0.628	0.428	0.271	0.760	0.807	0.174	0.045
10.0	0.667	0.485	0.290	0.825	0.874	0.174	0.045
PGA	0.478	0.219	0.166	0.526	0.551	1.000	0.205
PGV	0.484	0.203	0.190	0.525	0.558	0.691	0.072
PGD	0.667	0.485	0.290	0.825	0.874	0.174	0.045
I_{JMA}	0.396	0.157	–	0.426	–	0.824	0.040
CAV_{GM}	0.371	0.196	0.089	0.420	0.429	0.735	-0.009

Note: $\sigma_{\ln AF} = 0.3$; see text for calculation of standard deviations for $V_{S30} < k_1$.

Equation (5.14) recognizes that τ is approximately equal to the standard deviation of the inter-event residuals $\tau_{\ln Y}$, which is consistent with the common understanding that inter-event terms are not significantly affected by soil nonlinearity (e.g., Kwok and Stewart 2006; J. Stewart, personal comm. 2007). Even if we were to assume that τ was subject to soil nonlinearity effects as suggested by Abrahamson and Silva (2008), it would have only a relatively small effect on the total standard deviation because of the dominance of the intra-event standard deviation in Equation (5.16). The more complicated relationship for σ takes into account the soil nonlinearity effects embodied in Equation (5.11), which predicts that as the value of A_{1100} increases, the corresponding value of f_{site} decreases for soils with $V_{S30} < k_1$ m/sec. This nonlinearity impacts the intra-event standard deviation by reducing the variability in the site amplification factor at high values of A_{1100} as expressed in the first-order second-moment approximation of σ given by Equation (5.15). This approximation, a modified version of the propagation of uncertainty theorem, was first introduced by Bazzurro and Cornell (2004b) for the case where PSA is used as the reference rock ground motion and later extended to the case where PGA is used as the reference rock ground motion by Stewart and Goulet (2006).

The development of the aleatory uncertainty model assumes that $\sigma_{\ln Y}$ and $\sigma_{\ln \mathrm{PGA}}$ represent the aleatory uncertainty associated with linear site response. This assumption reflects the dominance of such recordings in the database. Another key element in this formulation is the selection of an appropriate value for $\sigma_{\ln AF}$. Although this value can be impacted by many factors, site response studies using both empirical methods (e.g., Baturay and Stewart 2003) and theoretical methods (e.g., Silva et al. 1999, 2000; Bazzurro and Cornell 2004a, 2005) have suggested that a period-independent value corresponding to $\sigma_{\ln AF} \approx 0.3$ is reasonable for deep soil sites once 3-D basin response has been removed as is the case in our model. This uncertainty is expected to decrease as sites become harder (Goulet and Stewart, 2009; Silva et al. 1999, 2000), but since such sites do not respond nonlinearly, σ becomes insensitive to $\sigma_{\ln AF}$ for these sites. Further justification of the dependence of the intra-event standard deviation on site classification and V_{S30} is given in Campbell and Bozorgnia (2008).

For some applications, engineers need an estimate of the aleatory uncertainty of the arbitrary horizontal component of ground motion (Baker and Cornell 2006). The standard deviation of this component can be calculated from the following equation:

$$\sigma_{Arb} = \sqrt{\sigma_T^2 + \sigma_C^2} \tag{5.18}$$

where σ_C is the intra-component standard deviation given by the expression (Boore 2005):

$$\sigma_C^2 = \frac{1}{4N} \sum_{j=1}^{N} (\ln y_{1j} - \ln y_{2j})^2 \tag{5.19}$$

where y_{ij} is the value of the ground motion parameter for component i of recording j and N is the total number of recordings. The standard deviations σ_C and σ_{Arb} for ground motions subject to linear site response (i.e., for $V_{S30} \geq k_1$ or small values of A_{1100}) are listed in Table 5.2. Because I_{JMA} is calculated from all three ground motion components, it does not have an arbitrary horizontal component and σ_{Arb} is undefined.

5.1.3 Model Evaluation

The distribution of the total residuals with respect to **M**, R_{RUP}, V_{S30}, A_{1100}, $Z_{2.5}$, and λ are given in Figures 5.1 and 5.2 for CAV_{GM} and I_{JMA}, respectively. These plots confirm that there are no significant trends between the residuals and the predictor variables included in the regression analysis. Similar results (not shown) were found for δ, Z_{TOP}, and f_{hng}. Median estimates with respect to R_{RUP}, **M**, fault mechanism (F_{RV} and F_{NM} for both footwall and hanging-wall sites), NEHRP site class (BSSC 2994), and $Z_{2.5}$ are given in Figures 5.3 and 5.4 for CAV_{GM} and I_{JMA}, respectively. In all cases, NEHRP site classes B, C, D, and E were evaluated for V_{S30} values of 1070, 525, 255, and 150 m/sec, respectively, corresponding to the median (logarithmic average) value of V_{S30} for each site class.

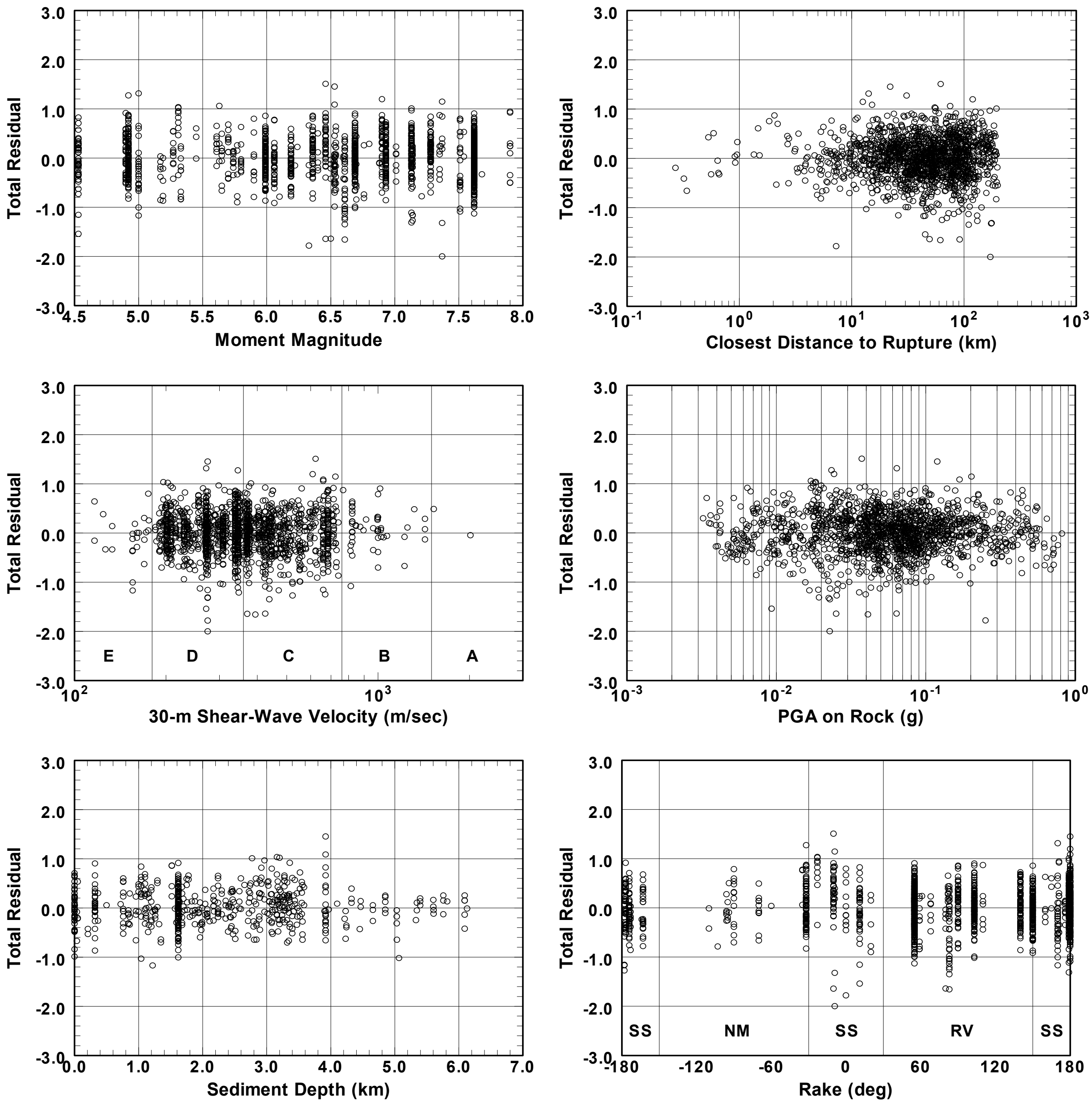

Fig. 5.1 Total residuals for the GMPE of CAV_{GM}. See caption to Fig. 4.2 for a description of the plots.

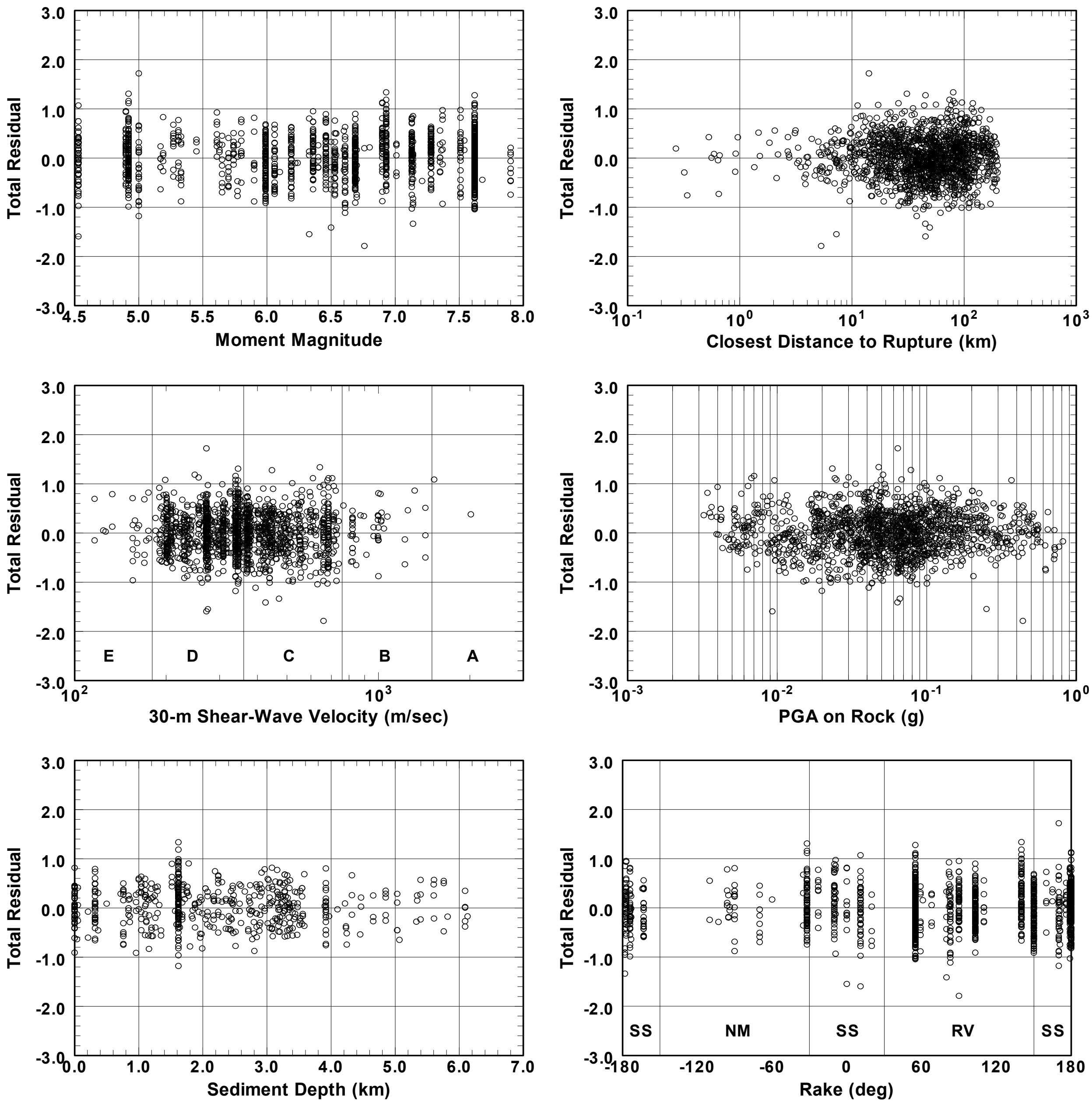

Fig. 5.2 Total residuals for the GMPE of I_{JMA}. See caption to Fig. 4.2 for a description of the plots.

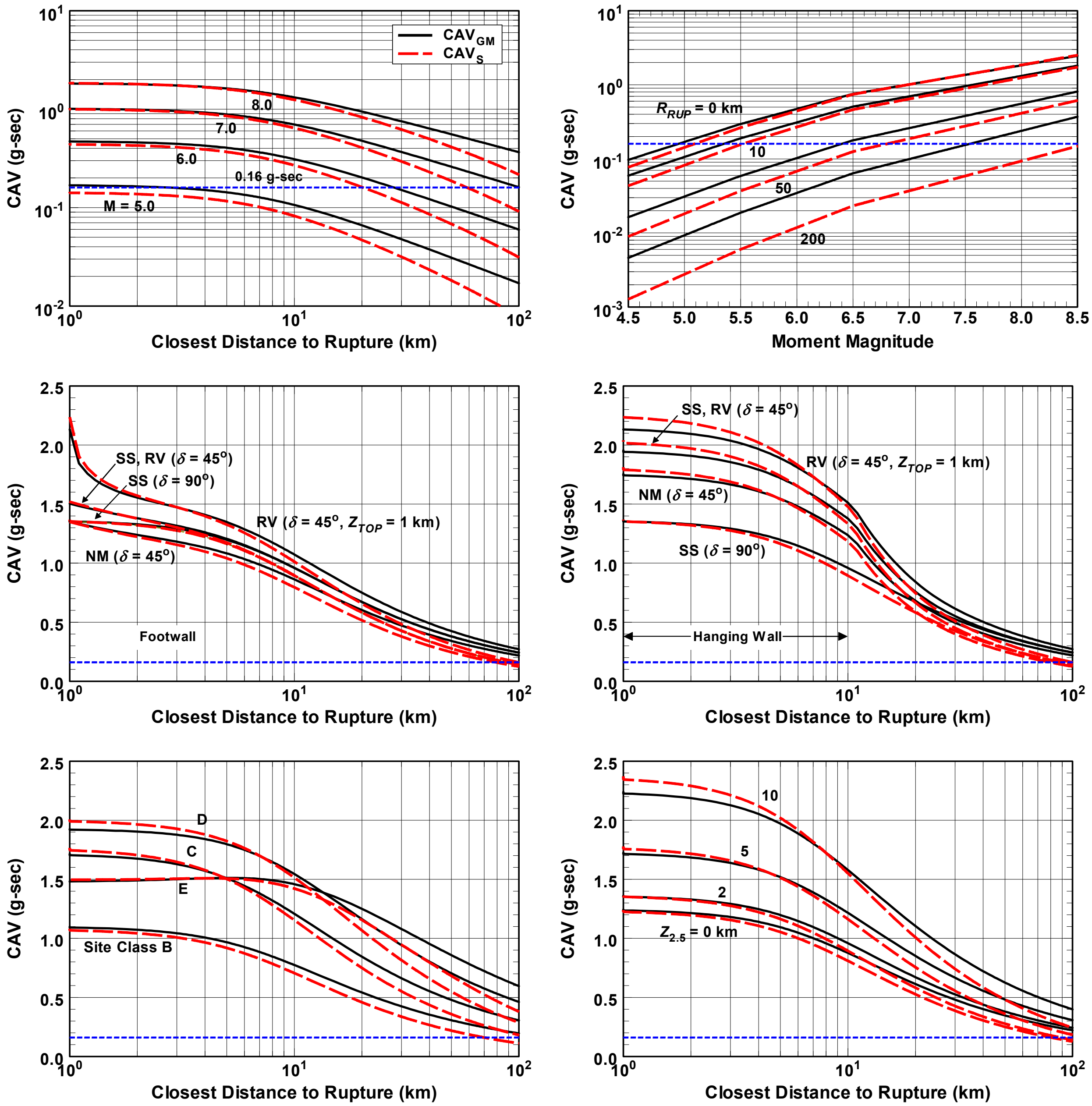

Fig. 5.3 Predicted median estimates of CAV$_{GM}$ and CAV$_S$ with respect to rupture distance (R_{RUP}), moment magnitude (M), fault mechanism for footwall sites (SS, strike slip; RV, reverse; NM, normal), fault mechanism for hanging-wall sites, NEHRP site class, and sediment depth ($Z_{2.5}$). Unless otherwise noted, CAV$_{GM}$ and CAV$_S$ are evaluated for $M = 7.5$, vertical ($\delta = 90°$) strike-slip faulting, $Z_{TOP} = 0$, NEHRP site class BC ($V_{S30} = 760$ m/sec), and $Z_{2.5} = 2$ km. CAV$_S$ is calculated from the relationship derived from the full version of the PEER-NGA database that includes those data that pass the spectral velocity check.

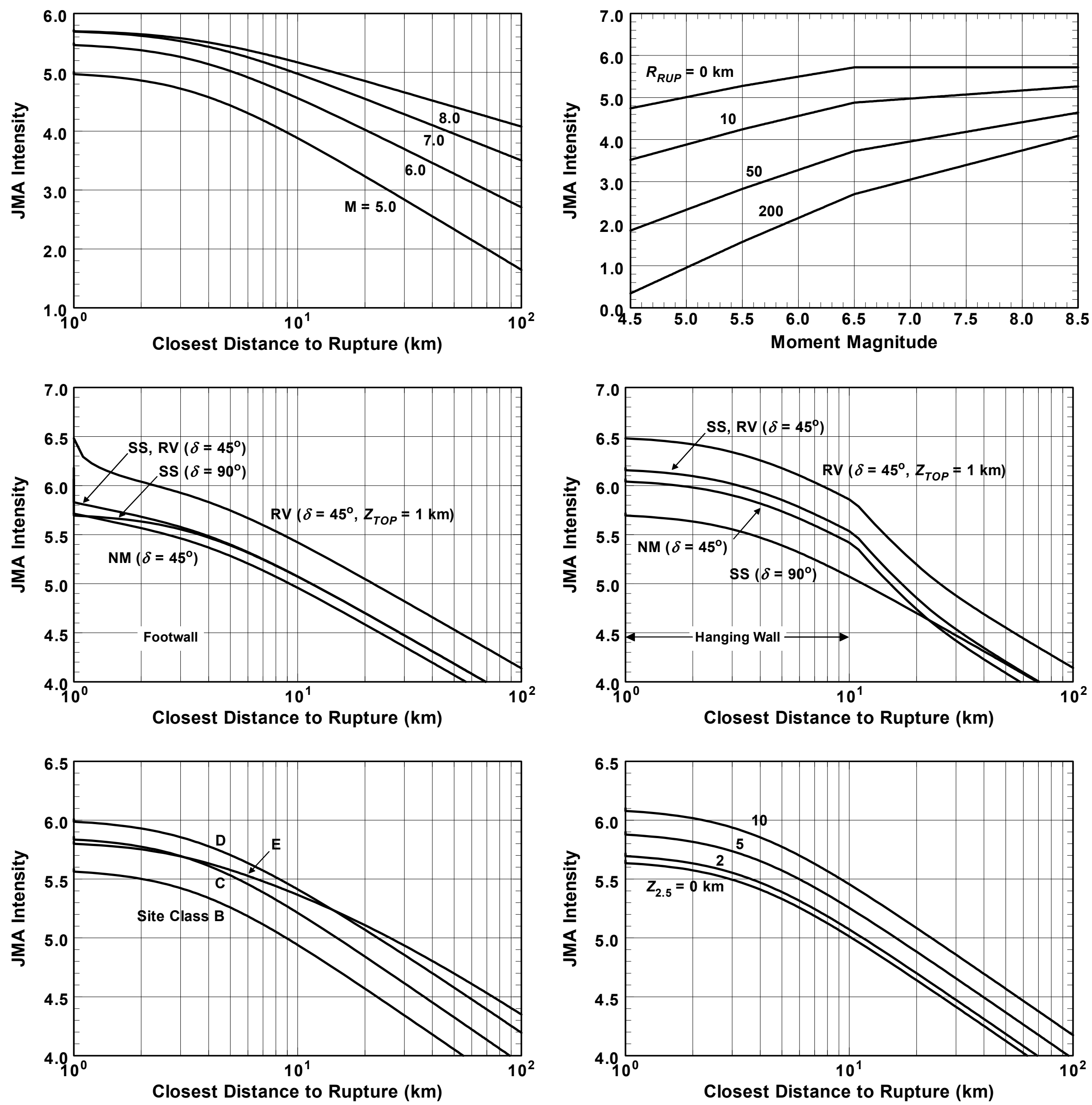

Fig. 5.4 Predicted median estimates of I_{JMA}. See caption to Fig. 5.3 for a description of the plots.

Figures 5.5 and 5.6 demonstrate the dependence of the predicted CAV_{GM} site amplification and I_{JMA} site increment terms on the median estimate of rock PGA and sediment depth. The plots with respect to rock PGA demonstrate the affect of soil nonlinearity on shallow site response for NEHRP site classes D and E. Figures 5.7 and 5.8 show the dependence of the standard deviations of $\ln \mathrm{CAV}_{GM}$ and I_{JMA} on the median estimate of rock PGA, which shows the affect of soil nonlinearity on ground motion variability for NEHRP site classes D and E.

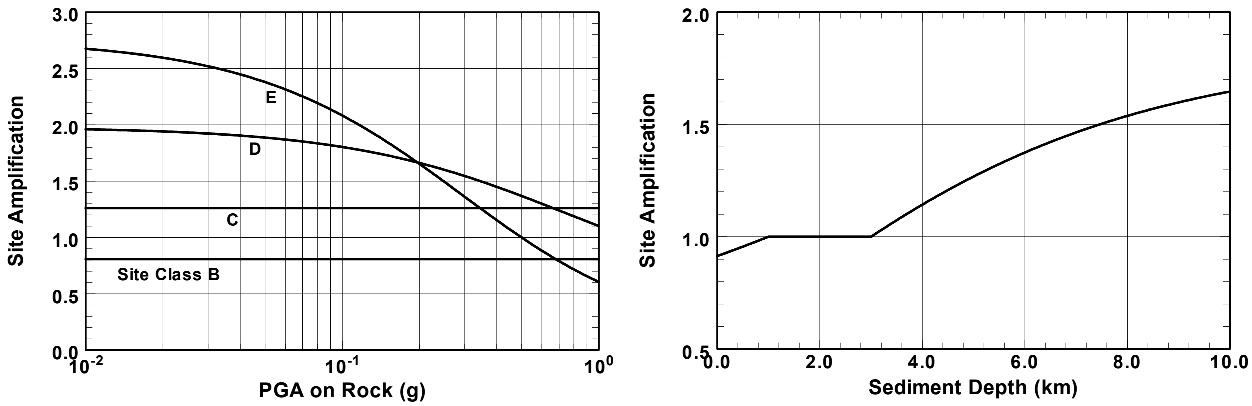

Fig. 5.5 Predicted site effects for $\mathrm{CAV_{GM}}$ and $\mathrm{CAV_S}$: (left) amplification factors for NEHRP site classes B, C, D and E (see text for associated values of V_{S30}); (right) amplification factors for sediment depths ($Z_{2.5}$) ranging between 0 and 10 km. $\mathrm{CAV_S}$ is calculated from the relationship derived from the full version of the PEER-NGA database that includes those data that pass the spectral velocity check.

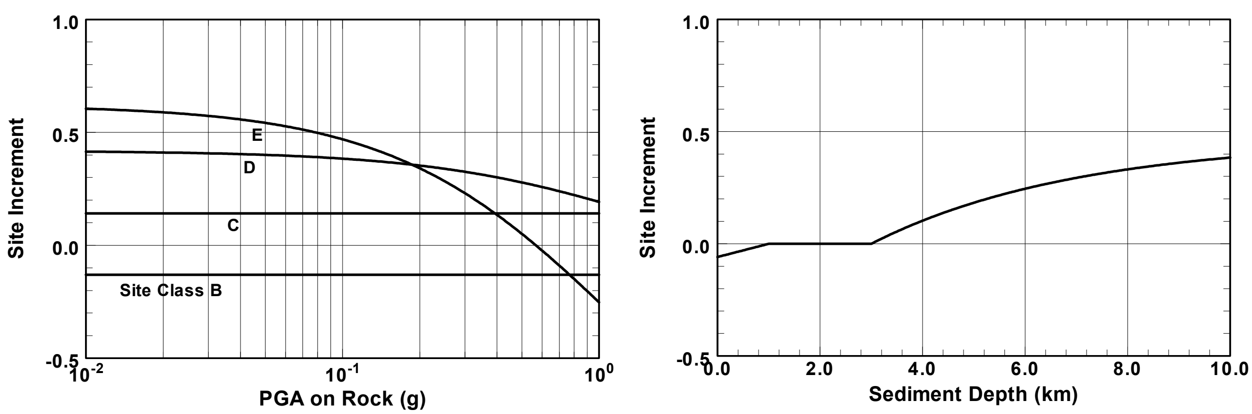

Fig. 5.6 Predicted site effects for I_{JMA}. See caption to Fig. 5.5 for a description of the plots, except that site effects are given in terms of intensity increments rather than amplification factors.

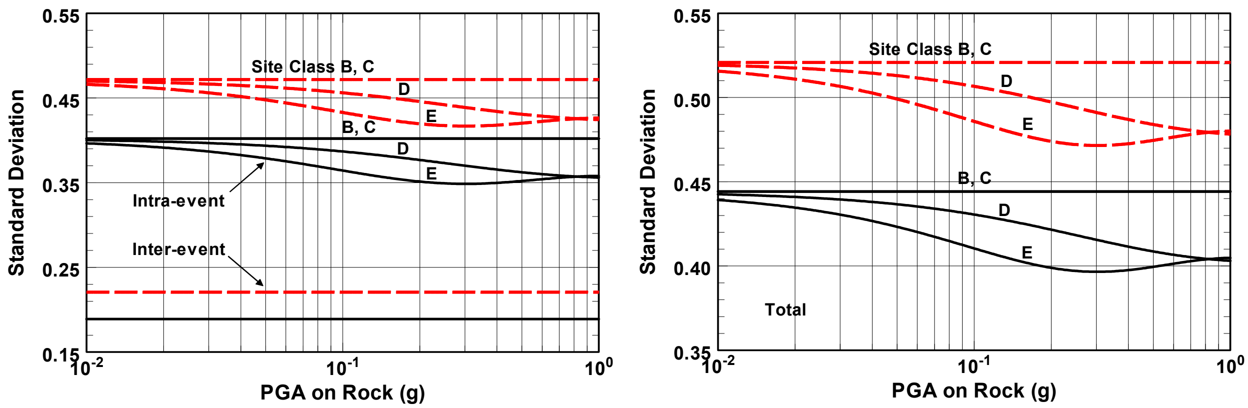

Fig. 5.7 Standard deviations of $\ln \mathrm{CAV}_{\mathrm{GM}}$ and $\ln \mathrm{CAV}_{\mathrm{S}}$ showing their dependence on nonlinear site response for NEHRP site classes B, C, D and E (see text for associated values of V_{S30}): (left) inter-event and intra-event standard deviations; (right) total standard deviations. Standard deviations of $\ln \mathrm{CAV}_{\mathrm{S}}$ are calculated from the relationship derived from the full version of the PEER-NGA database that includes those data that pass the spectral velocity check.

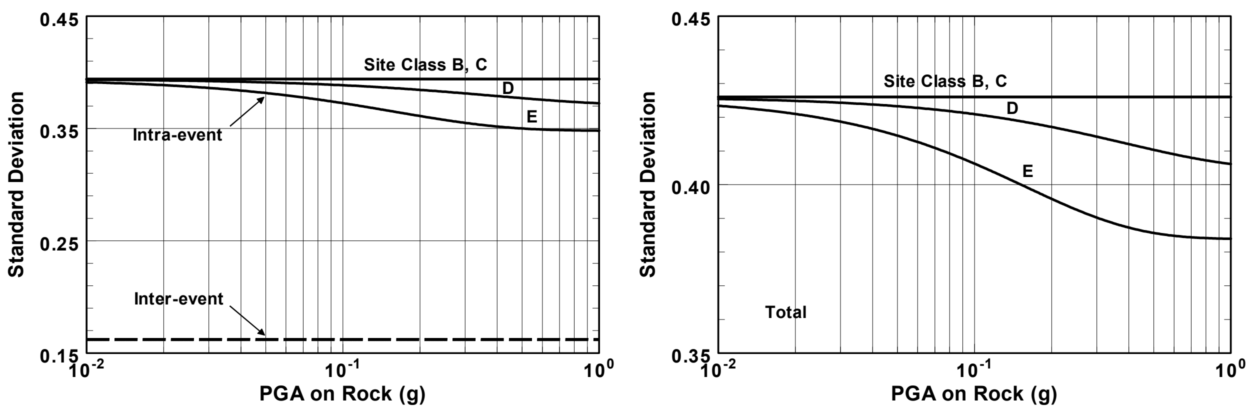

Fig. 5.8 Standard deviations of $\mathrm{I}_{\mathrm{JMA}}$ showing their dependence on nonlinear site response for NEHRP site classes B, C, D and E (see text for associated values of V_{S30}): (left) inter-event and intra-event standard deviations; (right) total standard deviations.

5.2 PREDICTION EQUATION FOR CAV$_S$

5.2.1 Median Model

The median estimate of CAV$_S$ is given by the following general equation:

$$\overline{\ln \mathrm{CAV_S}} = c_0 + c_1 \ln \mathrm{CAV_{GM}} + f_{mag} + f_{dis} \tag{5.20}$$

where the magnitude term is given by the expression:

$$f_{mag} = \begin{cases} 0; & \mathbf{M} \le 6.5 \\ c_2(\mathbf{M} - 6.5); & \mathbf{M} > 6.5 \end{cases} \tag{5.21}$$

and the distance term is given by the expression:

$$f_{dis} = c_3 R_{RUP} \tag{5.22}$$

In the above equations, CAV$_{GM}$ is the horizontal geometric mean component of CAV (g-sec), **M** is moment magnitude, and R_{RUP} is the closest distance to the coseismic rupture plane (km). The model coefficients c_i and the r-square values R^2 are listed in Table 5.3. When CAV$_{GM}$ is unknown and must be estimated, the value of $\ln \mathrm{CAV_{GM}}$ in Equation (5.20) should be replaced with its predicted median value, $\overline{\ln \mathrm{CAV_{GM}}}$, from Equation (5.1).

Table 5.3 Model coefficients and standard deviations for the GMPEs of CAV$_S$.

Database	Spectral Velocity Check	c_0	c_1	c_2	c_3	σ	τ	σ_T	R^2
When CAV$_{GM}$ is known (all V_{S30})									
CB08	Yes	0.0691	1.151	-0.173	-0.00265	0.130	0.101	0.165	0.973
CB08	No	0.0666	1.137	-0.138	-0.00304	0.108	0.104	0.150	0.976
Full	Yes	0.0072	1.115	-0.067	-0.00330	0.147	0.115	0.187	0.970
Full	No	0.0152	1.105	-0.044	-0.00369	0.131	0.115	0.174	0.973
When CAV$_{GM}$ is predicted ($V_{S30} \ge k_1$)									
CB08	Yes	0.0691	1.151	-0.173	-0.00265	0.446	0.247	0.510	0.973
CB08	No	0.0666	1.137	-0.138	-0.00304	0.435	0.246	0.500	0.976
Full	Yes	0.0072	1.115	-0.067	-0.00330	0.439	0.247	0.504	0.970
Full	No	0.0152	1.105	-0.044	-0.00369	0.430	0.245	0.495	0.973

Note: CAV$_S$ has units of g-sec; see text for calculation of standard deviations for $V_{S30} < k_1$.

5.2.2 Aleatory Uncertainty Model

The aleatory uncertainty model for $\mathrm{CAV_S}$ is similar to that for $\mathrm{CAV_{GM}}$ and I_{JMA} described in Section 5.1.2. One difference is that the intra-event standard deviation σ is not subject to nonlinear site effects, such that $\tau = \tau_{\ln \mathrm{CAV_S}}$ and $\sigma = \sigma_{\ln \mathrm{CAV_S}}$. As before, σ_T is calculated from Equation (5.16). Since the shear-wave velocity V_{S30} is not a parameter in the GMPE, soil nonlinearity effects are included through the intra-event variability of $\mathrm{CAV_{GM}}$.

When $\mathrm{CAV_S}$ is calculated from $\overline{\ln \mathrm{CAV_{GM}}}$, the uncertainty in $\mathrm{CAV_{GM}}$ must be included in the calculation of the standard deviation of $\ln \mathrm{CAV_S}$ using the first-order second-moment approximation of the propagation of uncertainty theorem given by the following equations:

$$\tau = \sqrt{\tau_{\ln \mathrm{CAV_S}}^2 + \alpha_1^2 \tau(\mathrm{CAV_{GM}})^2} \tag{5.23}$$

$$\sigma = \sqrt{\sigma_{\ln \mathrm{CAV_S}}^2 + \alpha_1^2 \sigma(\mathrm{CAV_{GM}})^2} \tag{5.24}$$

where the values of $\tau(\mathrm{CAV_{GM}})$ and $\sigma(\mathrm{CAV_{GM}})$ inside the radicals are calculated from Equations (5.14) and (5.15) and α_1 is the linearized functional relationship between $\overline{\ln \mathrm{CAV_S}}$ and $\ln \mathrm{CAV_{GM}}$ estimated from the following partial derivative of Equation (5.20):

$$\alpha_1 = \frac{\partial \overline{\ln \mathrm{CAV_S}}}{\partial \ln \mathrm{CAV_{GM}}} = c_1 \tag{5.25}$$

The term involving ρ in Equation (5.15) is not included in the expressions for τ and σ because the residuals of $\ln \mathrm{CAV_S}$ and $\ln \mathrm{CAV_{GM}}$ were found to be uncorrelated (i.e., $\rho \approx 0$). The model coefficient c_1 and the standard deviations τ, σ, and σ_T are listed in Table 5.3. Because $\mathrm{CAV_S}$ is defined as the maximum of the three ground motion components, it does not have an arbitrary horizontal component and σ_{Arb} is undefined.

5.2.3 Model Evaluation

The distribution of the total residuals with respect to $\mathrm{CAV_{GM}}$ is shown in Figure 5.9 for the $\mathrm{CAV_S}$ relationships that were derived from the CB08 subset and the full version of the PEER-NGA database. Both databases include those data that pass the spectral velocity check. The lack of any biases or trends in these residuals confirms the adequacy of the linear relationship between $\ln \mathrm{CAV_S}$ and $\ln \mathrm{CAV_{GM}}$. This figure clearly shows the increased variability associated with the less reliable full PEER-NGA database, especially at low values of $\mathrm{CAV_{GM}}$. The distribution of the total residuals with respect to **M**, R_{RUP}, V_{S30}, A_{1100}, $Z_{2.5}$, and λ for the relationship that was derived from the CB08 subset of the PEER-NGA database that includes those data that pass the spectral velocity check is given in Figure 5.10. These plots confirm that there are not only no significant biases or trends between the residuals and the two predictor variables that were included in the relationship, **M** and R_{RUP}, but that there are no significant trends between the residuals and those variables that were not included in the relationship. This implies that $\mathrm{CAV_S}$ and $\mathrm{CAV_{GM}}$ scale similarly with respect to these additional variables. Similar results (not shown) were found for δ, Z_{TOP}, and f_{hng}. The only noticeable bias in the residuals is at small PGA values, where $\mathrm{CAV_S}$ approaches its absolute limit of 0.16 g-sec. This bias is seen only for rock PGA values less than 0.03g.

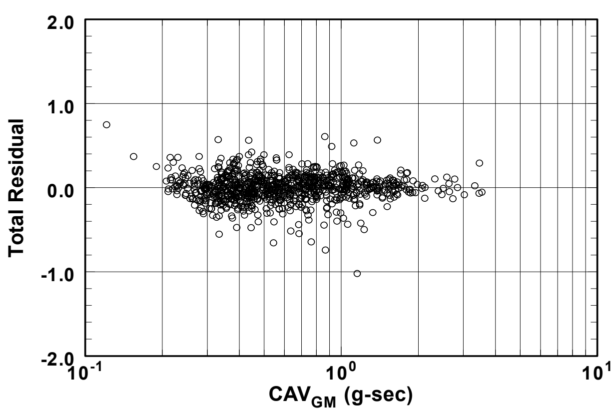

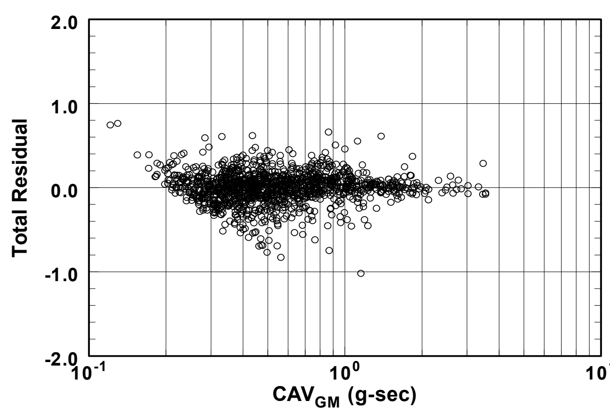

Fig. 5.9 Total residuals for the relationship between $\mathrm{CAV_S}$ and $\mathrm{CAV_{GM}}$ plotted as a function of $\mathrm{CAV_{GM}}$: (left) relationship derived from the CB08 subset of the PEER-NGA database; (right) relationship derived from the full version of the PEER-NGA database. Both databases include those data that pass the spectral velocity check.

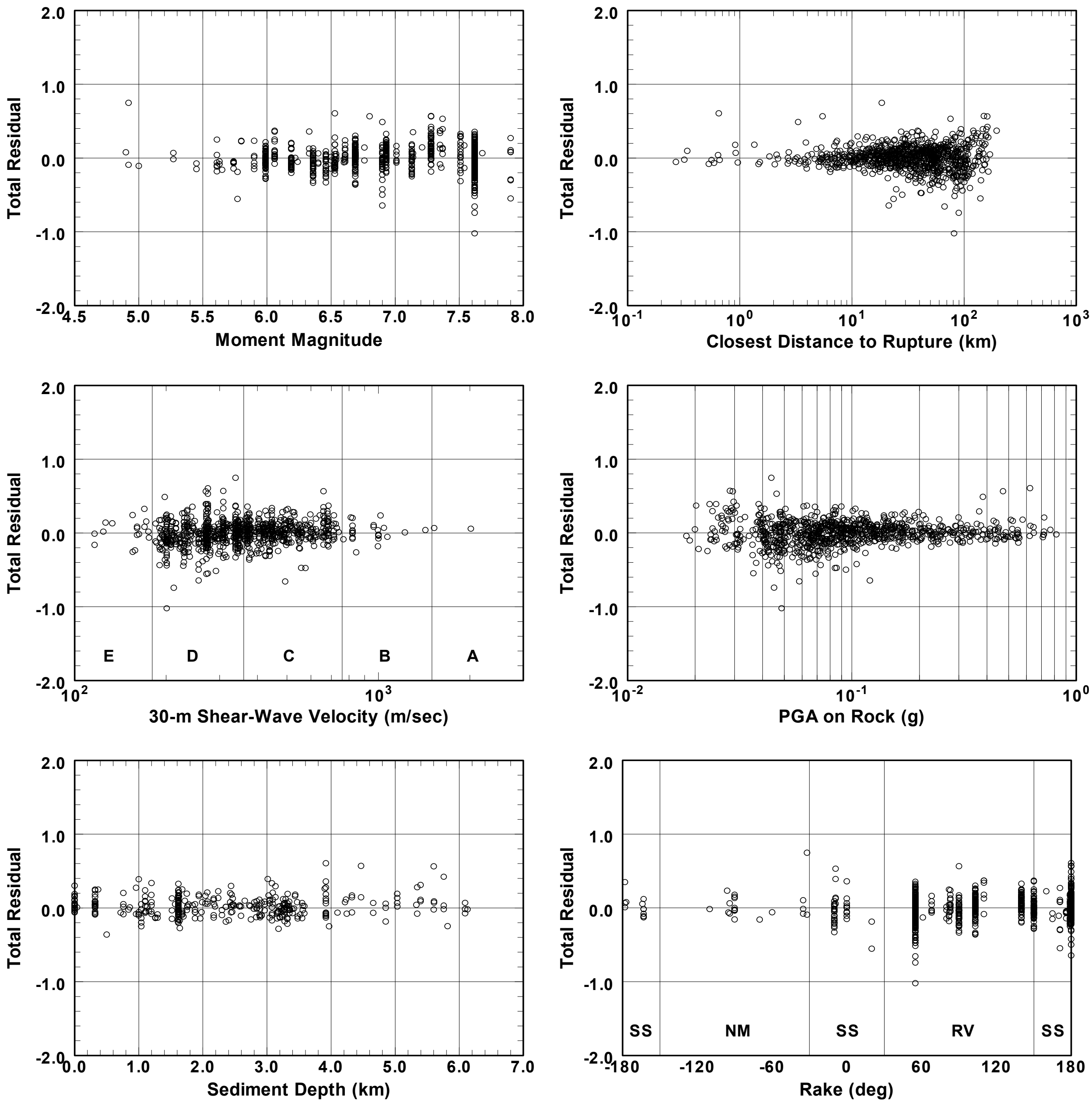

Fig. 5.10 Total residuals for the relationship between CAV_S and CAV_{GM} derived from the CB08 subset of the PEER-NGA database that includes those data that pass the spectral velocity check. See caption to Fig. 4.2 for a description of the plots.

Figure 5.11 shows the distribution of the total residuals with respect to **M**, R_{RUP}, V_{S30}, A_{1100}, $Z_{2.5}$, and λ for the relationship that was derived from the full version of the PEER-NGA database that includes those data that pass the spectral velocity check. This figure confirms the conclusions from Figure 5.10 and shows the increased variability associated with the less reliable full database. Similar results (not shown) were found for δ, Z_{TOP}, and f_{hng}. There appears to be a slight bias in the residuals with respect to sediment depth, but since this bias was not found for the CB08 subset (Fig. 5.9) and since there were only a few additional recordings in the full database with known values of $Z_{2.5}$, we decided to exclude $Z_{2.5}$ as a predictor variable in this relationship.

Figure 5.3 compares the median prediction of $\mathrm{CAV_S}$ with the median prediction of $\mathrm{CAV_{GM}}$ after combining the prediction equations for $\mathrm{CAV_S}$ and $\mathrm{CAV_{GM}}$ to create a single GMPE. $\mathrm{CAV_S}$ was calculated using the full version of the PEER-NGA database that includes those data that pass the spectral velocity check.

Figure 5.5 shows the dependence of the predicted site amplification of $\mathrm{CAV_S}$ (from the GMPE) on the median estimate of rock PGA and sediment depth. This dependence is the same as that for $\mathrm{CAV_{GM}}$. The plots with respect to rock PGA demonstrate the affect of soil nonlinearity on shallow site response for NEHRP site classes D and E. Figure 5.7 compares the dependence of the standard deviations of $\ln \mathrm{CAV_S}$ (from the GMPE) and $\ln \mathrm{CAV_{GM}}$ on the median estimate of rock PGA. The standard deviations of $\ln \mathrm{CAV_S}$ were calculated from Equations (5.23) and (5.24) using values of $\tau_{\ln \mathrm{CAV_S}}$ and $\sigma_{\ln \mathrm{CAV_S}}$ derived from the full version of the PEER-NGA database that includes those data that pass the spectral velocity check.

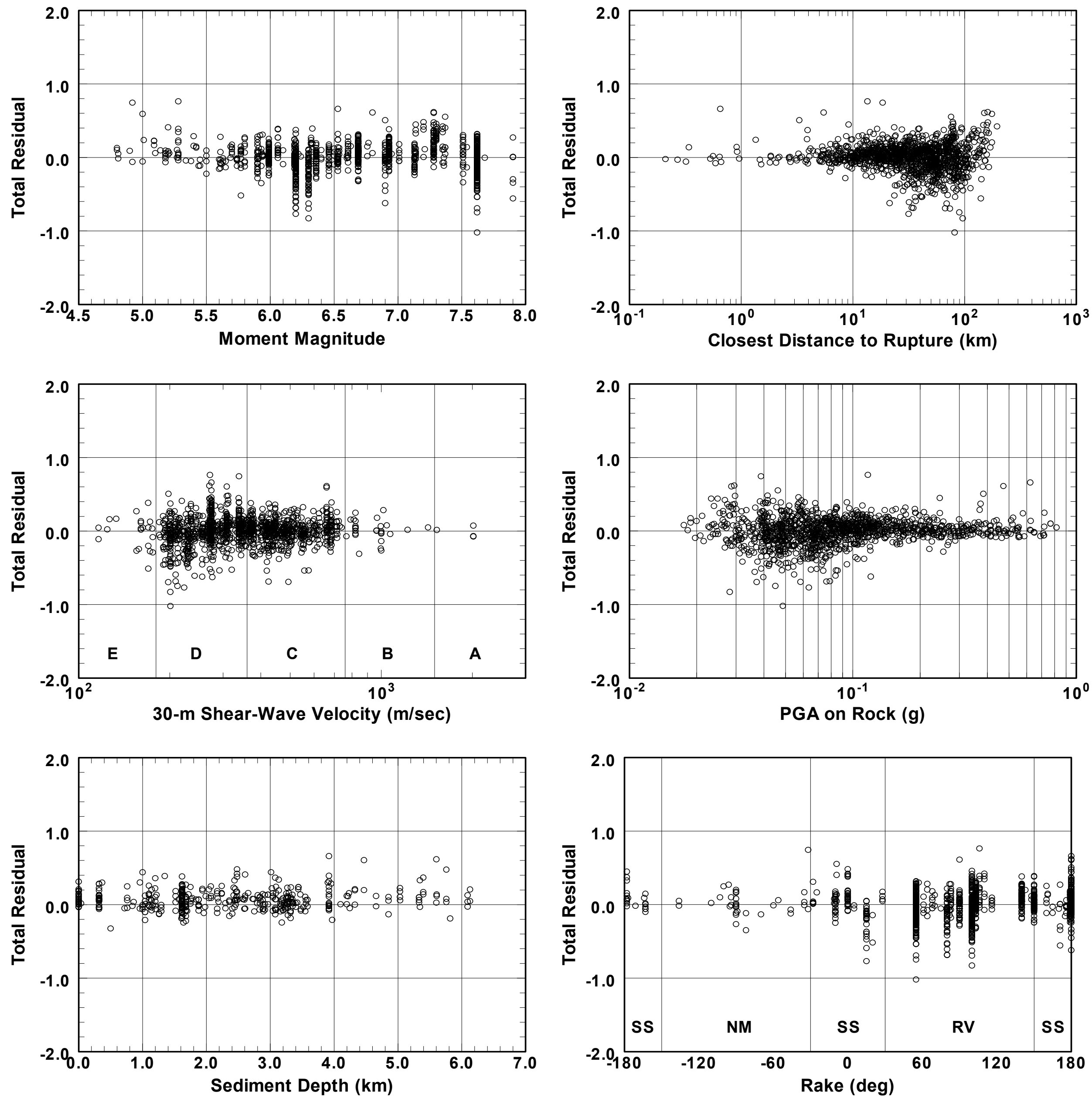

Fig. 5.11 Total residuals for the relationship between CAV_S and CAV_{GM} derived from the full version of the PEER-NGA database that includes those data that pass the spectral velocity check. See caption to Fig. 4.2 for a description of the plots.

6 Use of CAV Filter in Probabilistic Seismic Hazard Analysis

6.1 HAZARD INTEGRAL WITH CAV FILTER

It is standard practice to use a lower-bound moment magnitude in the probabilistic seismic hazard analysis (PSHA) of nuclear facilities (EPRI 1989) and civil structures (Petersen et al 2008). However, this lower-bound magnitude cut-off is unrealistically sharp and can lead to the over-representation of small-magnitude non-damaging earthquakes in the PSHA in regions where the hazard is dominated by source zones rather than individual faults. This is particularly a problem in regions of low seismicity where the hazard at a site is dominated by nearby small earthquakes. To help overcome this problem, EPRI (2006) and Watson-Lamprey and Abrahamson (2007) proposed the use of a lower-bound (minimum) CAV in addition to a lower-bound magnitude in the PSHA. This is based on the recommendation of EPRI (1988) that CAV can be used to quantify the potential for small earthquakes to cause structural damage to industrial facilities. In other words, CAV can be used as a means of screening out non-damaging earthquakes that have magnitudes larger than the assumed lower bound.

A lower-bound magnitude is included in the PSHA by setting m_{min} as the lower limit of integration over magnitude in the following generalized hazard integral (modified from McGuire 2004; EPRI 2006; Watson-Lamprey and Abrahamson 2007):

$$\nu(Y > y) = \sum_{i=1}^{N_s} N_i(m \geq m_{min}) \int_{m_{min}}^{m_{\max}} \int_{r_{min}}^{r_{\max}} f_i(m) f_i(r \mid m) P_i(Y > y \mid m, r)\, dr\, dm \qquad (6.1)$$

where $\nu(Y > y)$ is the total frequency that the ground motion parameter Y exceeds the value y in a specified period of time (usually one year); m is magnitude; r is distance; $N_i(m \geq m_{min})$ is the rate of occurrence of earthquakes with $m \geq m_{min}$ on source *i*; N_s is the total number of seismic sources; $f(m)$ and $f(r \mid m)$ are probability density functions describing the distributions of magnitude ($m_{min} \leq m \leq m_{max}$) and distance ($r_{min} \leq r \leq r_{max}$); and $P(Y > y \mid m, r)$ is the probability that Y is greater than y given m and r. Assuming $\ln Y$ is normally distributed, as has been demonstrated by many investigators (e.g., Campbell 1981), this latter probability is given by the following integral of the normal probability density function (PDF):

$$P(X > x) = \int_{x}^{\infty} f_X(x)\, dx \tag{6.2}$$

where

$$f_X(x) = \frac{1}{\sigma_X \sqrt{2\pi}} \exp\left[-\frac{1}{2} \left(\frac{x - \overline{x}}{\sigma_X} \right)^2 \right] \tag{6.3}$$

and $X = \ln Y$, $x = \ln y$, and $\overline{x} = \overline{\ln y}$ and $\sigma_X = \sigma_{\ln Y}$ are the predicted median value and standard deviation of $\ln Y$ given *m* and *r*, respectively (e.g., from a GMPE).

The CAV filter is included in the PSHA by replacing the exceedance probability $P(Y > y \mid m, r)$ in the integrand of Equation (6.1) with the joint exceedance probability $P(Y > y, \mathrm{CAV_S} > \mathrm{CAV}_{min} \mid m, r)$. This requires that we account for the correlation between the exceedance probabilities of *Y* and $\mathrm{CAV_S}$ (EPRI 2006; Watson-Lamprey and Abrahamson 2007). At first, it might not be apparent why these two probability distributions might be correlated. After all, both parameters are dependent on magnitude and distance as well as other predictor variables. Thus, it would appear that their dependence is already being accommodated through the inclusion of these variables. However, *Y* and $\mathrm{CAV_S}$ are not single valued; rather, they are defined by a lognormal distribution with a given median and logarithmic standard deviation. Therefore, even if the predictor variables are known, there is still a large range of possible values for each of these parameters. Because *Y* and $\mathrm{CAV_S}$ are calculated from the same ground motion recordings, we might expect that a higher-than-average value of *Y* should correspond to a higher-than-average value of $\mathrm{CAV_S}$. Conversely, we might expect that a lower-than-average value of *Y* should correspond to a lower-than-average value of $\mathrm{CAV_S}$. In other words, we might expect the variability in *Y* to be positively correlated with the variability in $\mathrm{CAV_S}$.

We evaluated the potential correlation between the variability of *Y* and $\mathrm{CAV_S}$ by calculating the correlation coefficients ρ between the residuals of $\ln Y$ and $\ln \mathrm{CAV_S}$ from their respective prediction equations and testing whether these correlation coefficients are significantly different from zero at the 95% confidence level. This could be done only for the CB08 subset of the PEER-NGA database for which we have residuals for PGA, PGV, and PSA from Campbell and Bozorgnia (2008). We found that the calculated correlation coefficients decreased from about $\rho = 0.2$ for PGA and PSA with $T \leq 0.05$ sec to $\rho < 0.05$ for PSA with $T \geq 1.5$ sec (Table 5.2). The hypothesis tests indicated that the correlation coefficients are statistically significant for PGA, PGV, and PSA for $T \leq 0.75$ sec.

Under the assumption that the joint probability distribution of two variables is normal if their marginal distributions are normal, their joint exceedance probability is given by the following double integral of the joint normal PDF (e.g., Benjamin and Cornell 1970):

$$P(X_1 > x_1, X_2 > x_2) = \int_{x_1}^{\infty}\int_{x_2}^{\infty} f_{X_1,X_2}(x_1, x_2)\, dx_1\, dx_2 \tag{6.4}$$

where

$$f_{X_1,X_2}(x_1, x_2) = \frac{1}{2\pi\sigma_{X_1}\sigma_{X_2}\sqrt{1-\rho^2}} \exp\left\{-\frac{1}{2(1-\rho^2)}\left[\left(\frac{x_1-\bar{x}_1}{\sigma_{X_1}}\right)^2 - 2\rho\left(\frac{(x_1-\bar{x}_1)(x_2-\bar{x}_2)}{\sigma_{X_1}\sigma_{X_2}}\right) + \left(\frac{x_2-\bar{x}_2}{\sigma_{X_2}}\right)^2\right]\right\} \tag{6.5}$$

Following the vector-valued hazard approach proposed by Bazzurro and Cornell (2002), it is convenient to factor the above PDF into its marginal and conditional distributions (e.g., Benjamin and Cornell 1970), resulting in the alternative form:

$$P(X_1 > x_1, X_2 > x_2) = \int_{x_1}^{\infty}\int_{x_2}^{\infty} f_{X_1}(x_1) f_{X_2|X_1}(x_2, x_1)\, dx_1\, dx_2 \tag{6.6}$$

where $f_{X_1}(x_1)$ is the marginal PDF of x_1 from Equation (6.3) and the conditional PDF is defined by the modified normal PDF:

$$f_{X_2|X_1}(x_2, x_1) = \frac{1}{\sigma'_{X_2}\sqrt{2\pi}} \exp\left[-\frac{1}{2}\left(\frac{x_2-\bar{x}_2{}'}{\sigma'_{X_2}}\right)^2\right] \tag{6.7}$$

where

$$\bar{x}_2' = \bar{x}_2 + \rho \frac{\sigma_{X_2}}{\sigma_{X_1}} (x_1 - \bar{x}_1) \tag{6.8}$$

$$\sigma'_{X_2} = \sigma_{X_2} \sqrt{1-\rho^2} \tag{6.9}$$

In the marginal and conditional form of the joint normal PDF, all of the parameters of the distribution are defined in terms of the marginal means and standard deviations of the two variables. In terms of Y and $\mathrm{CAV_S}$, this means that the joint exceedance probability given by Equations 6.6–6.9 can be evaluated by letting $X_1 = \ln Y$, $x_1 = \ln y$, $\bar{x}_1 = \overline{\ln Y}$, $\sigma_{X_1} = \sigma_T(Y)$, $X_2 = \ln \mathrm{CAV_S}$, $x_2 = \ln \mathrm{CAV}_{min}$, $\bar{x}_2 = \overline{\ln \mathrm{CAV_S}}$, and $\sigma_{X_2} = \sigma_T(\mathrm{CAV_S})$, where $\overline{\ln Y}$ is the predicted median value of Y for the ground motion parameter of interest (e.g., from Equation (5.1) and Table 5.1), $\overline{\ln \mathrm{CAV_S}}$ is the predicted median value of $\mathrm{CAV_S}$ (from Equation (5.20) and Table 5.3), $\sigma_T(Y)$ is the total standard deviation of $\ln Y$ for the ground motion parameter of interest (from Table 5.2), $\sigma_T(\mathrm{CAV_S})$ is the total standard deviation of $\ln \mathrm{CAV_S}$ when $\mathrm{CAV_{GM}}$ is predicted (Table 5.3), and ρ is the correlation coefficient between the total variability of Y and $\mathrm{CAV_S}$ (Table 5.2).

It is easily shown that if the two variables are uncorrelated (i.e., $\rho \approx 0$), Equation (6.7) simplifies to the marginal PDF of x_2 and the integrand in Equation (6.6) simplifies to the product of the marginal PDFs of x_1 and x_2. In terms of Y and $\mathrm{CAV_S}$, this means that the joint exceedance probability simplifies to the following product of marginal exceedance probabilities:

$$P(Y > y, \mathrm{CAV_S} > \mathrm{CAV}_{min} \mid m, r) = P(Y > y \mid m, r) P(\mathrm{CAV_S} > \mathrm{CAV}_{min} \mid m, r) \tag{6.10}$$

Taking into account the joint exceedance probability of Y and $\mathrm{CAV_S}$, the vector-valued hazard integral becomes

$$\nu(Y > y, \mathrm{CAV_S} > \mathrm{CAV}_{min}) = \sum_{i=1}^{N_S} N_i(m \geq m_{min}) \int_{m_{min}}^{m_{\max}} \int_{r_{min}}^{r_{\max}} f_i(m) f_i(r \mid m) P_i(Y > y, \mathrm{CAV_S} > \mathrm{CAV}_{min} \mid m, r)\, dr\, dm \tag{6.11}$$

where $P(Y > y, \mathrm{CAV_S} > \mathrm{CAV}_{min} \mid m, r)$ is given by either Equation (6.10), if the variability of Y and $\mathrm{CAV_S}$ is statistically independent (uncorrelated), or Equation (6.6), if it is not. The assumed bivariate normal distribution used to define the joint probability distribution can also be evaluated using bivariate normal probability tables (e.g., National Bureau of Standards 1956; Owen 1956, and references therein) or analytical approximations (e.g., Mee and Owen 1982;

Cox and Wermuth 1991). However, it should be noted that these latter approximations become less accurate at small exceedance probabilities.

Although the hazard integral approach of applying the CAV filter is preferred, EPRI (2006) demonstrates how the CAV filter can be applied in an approximate manner to the deaggregation results of a standard PSHA (e.g., McGuire 2004), when the hazard software does not include a CAV filter. In this case, the total vector-valued hazard can be estimated from the following summation:

$$\nu(Y > y \,|\, \mathrm{CAV_S} > \mathrm{CAV}_{min}) = \sum_{i=1}^{N_m}\sum_{j=1}^{N_r} \nu(Y > y \,|\, m_i, r_j, \mathrm{CAV}_{min}) \tag{6.12}$$

where

$$\nu(Y > y \,|\, m_i, r_j, \mathrm{CAV}_{min}) = \nu(Y > y) D(Y > y \,|\, m_i, r_j) P(Y > y, \mathrm{CAV_S} > \mathrm{CAV}_{min} \,|\, m_i, r_j) \tag{6.13}$$

and N_m is the number of magnitude bins, N_r is the number of distance bins (often defined in terms of $\ln r$ rather than *r*), $\nu(Y > y)$ is the exceedance frequency of *Y* from the standard PSHA given by Equation (6.1), $P(Y > y, \mathrm{CAV_S} > \mathrm{CAV}_{min} \,|\, m_i, r_j)$ is the joint exceedance probability of *Y* and $\mathrm{CAV_S}$ given by either Equation (6.6) or Equation (6.10), and $D(Y > y \,|\, m_i, r_j)$ is the hazard deaggregation of *Y*, i.e., the fraction of the exceedance frequency of *Y* that is associated with events of magnitude m_i and distance r_j (e.g., McGuire 2004).

Based on the requirements in USNRC Regulatory Guide 1.166 (U.S. Nuclear Regulatory Commission 1997), EPRI (2006) and Watson-Lamprey and Abrahamson (2007) recommended 0.16 g-sec as the lower-bound (minimum) value of standardized CAV to use in a PSHA. This value has subsequently been accepted by the USNRC for use in PSHA studies for nuclear power plants in the central and eastern United States. However, the above equations can be used with any minimum value of standardized CAV.

EPRI (2006) and Watson-Lamprey and Abrahamson (2007) included both a magnitude filter and a CAV filter in their hazard integral. For consistency with these studies, we have also left the magnitude filter in Equation (6.11). One might argue that once the CAV filter is included in this integral there is no need for a magnitude filter. However, as we show in the next section, there is still a significant contribution to the probability that $\mathrm{CAV_S}$ exceeds 0.16 g-sec for earthquakes with $\mathbf{M} < 4.6$ ($m_{bLg} < 5$) in low seismicity regions. EPRI (1989) concluded that even large values of PGA from earthquakes with $\mathbf{M} < 5$ will not cause structural damage to well-engineered structures. Therefore, it is still important to use a magnitude filter in addition to a CAV filter in order to eliminate all non-damaging earthquakes. In this case, the CAV filter is used to remove non-damaging earthquakes with magnitudes greater than the minimum magnitude from contributing to the calculated ground motion exceedance frequencies. This will not only make the hazard results more meaningful, but also the deaggregation results by shifting the mode and mean hazard away from smaller non-damaging earthquakes to larger damaging events.

6.2 EXAMPLE HAZARD ANALYSIS WITH CAV FILTER

We demonstrate the impact of including a CAV filter in the hazard integral with an example PSHA for the central and eastern United States (CEUS) presented by EPRI (2006) and Watson-Lamprey and Abrahamson (2007). The hazard is computed for a CEUS rock site that is located away from the Charleston and New Madrid regions using the USGS smoothed seismicity sources (Frankel et al. 2002) and the Toro et al. (1997) GMPE.

Figure 5.12 shows the hazard curves for the 0.05 sec (20 Hz) PSA with and without including the CAV filter. Removing the events with a standardized CAV less than 0.16 g-sec flattens the hazard curve at small ground motion levels. The hazard curve at high ground motion levels is not impacted, since these levels are associated with a standardized CAV that is greater than 0.16 g-sec. Figure 6.1 shows the same impact on the uniform hazard spectrum (UHS) for a mean annual exceedance probability of 10^{-4}. At this hazard level, the UHS is reduced by about 10–25% due to the CAV filter. For sites close to the Charleston and New Madrid regions, the effect of the CAV filter on the low-frequency part of the UHS will be smaller, since the ground motions that form these larger magnitude earthquakes will have larger standardized CAV values.

Figure 6.2 shows the results of a hazard deaggregation of the 0.05 sec (20 Hz) PSA for a mean exceedance probability of 10^{-4} with and without the CAV filter. The CAV filter removes the contribution from smaller magnitudes, shifting the peak in the deaggregation to larger magnitudes and distances. For the PSHA using a fixed lower-bound magnitude of **M** 4.6 but no CAV filter, there is a significant contribution from **M** 4.6–5.0 earthquakes, but the contribution from these events are reduced significantly, although not totally eliminated, by the CAV filter.

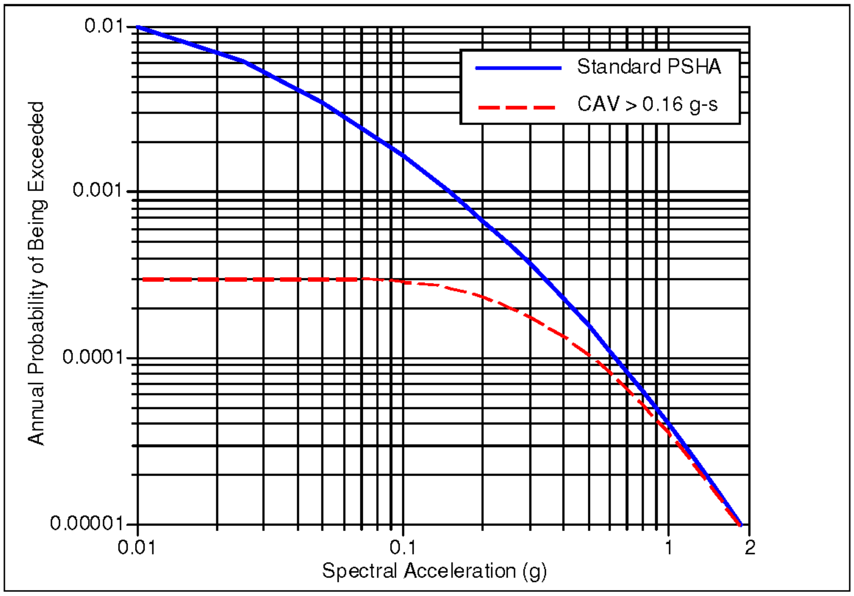

Fig. 6.1 Example hazard curves for 5%-damped 0.05 sec (20 Hz) PSA for a site in the CEUS showing the impact of including (red curve) and excluding (blue curve) a CAV filter that screens out events with standardized CAV greater than 0.16 g-sec. After EPRI (2006) and Watson-Lamprey and Abrahamson 2007).

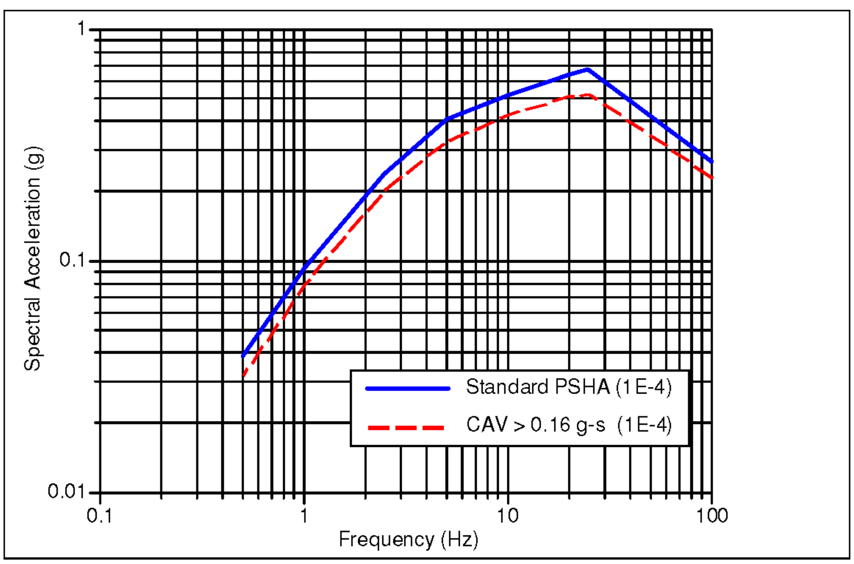

Fig. 6.2 Example uniform hazard spectra with a mean annual exceedance probability of 10^{-4} for 5%-damped PSA at a site in the CEUS showing the impact of including a CAV filter that screens out events with standardized CAV greater than 0.16 g-sec. After EPRI (2006) and Watson-Lamprey and Abrahamson 2007).

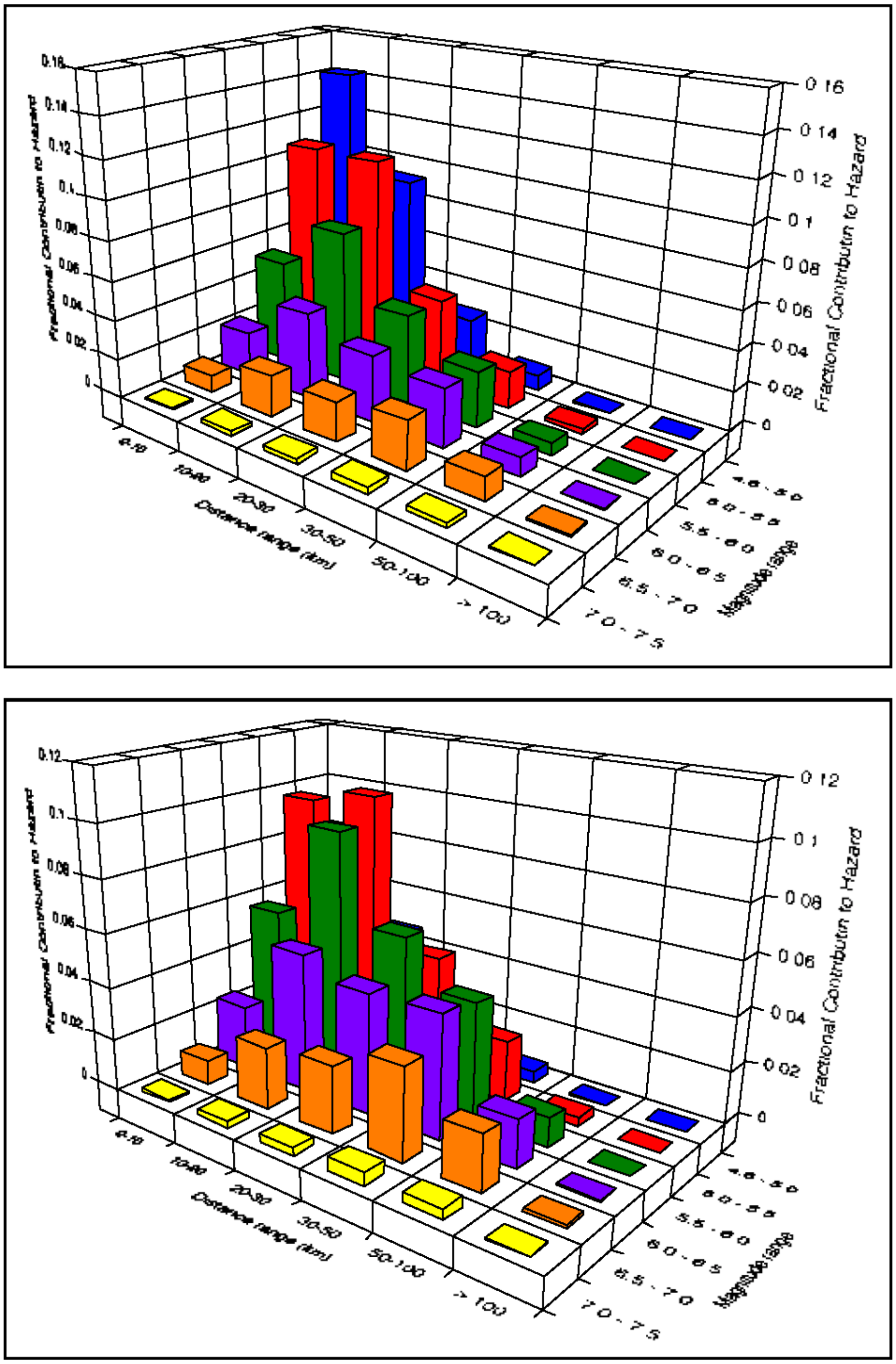

Fig. 6.3 Example hazard deaggregation analysis for 5%-damped 0.05 sec (20 Hz) PSA with a mean annual exceedance probability of 10^{-4} at a site in the CEUS showing the impact of excluding (top histogram) and including (bottom histogram) a CAV filter that screens out events with standardized CAV greater than 0.16 g-sec. After EPRI (2006) and Watson-Lamprey and Abrahamson 2007).

7 Discussion

7.1 COMPARISON WITH EXISTING RELATIONSHIPS

There are only a few GMPEs for CAV and I_{JMA} that we can use to compare with ours (see Chapter 1 for a list of these relationships). For purposes of these comparisons, we evaluated our GMPE for vertical strike-slip faulting and a sediment depth of $Z_{2.5} = 2$ km. We evaluated shallow site conditions by setting the value of V_{S30} in our GMPE to be as consistent as possible with one of the site categories in the GMPE we were evaluating. None of the relationships used in the comparisons include V_{S30} or $Z_{2.5}$ as a predictor variable and some did not distinguish between different fault mechanisms. In other cases, magnitude and distance were defined using different metrics. Although we attempted to evaluate the relationships in a manner similar to ours, we did not attempt to correct for differences in parameter definitions in making the comparisons.

7.1.1 Relationships for CAV_S and Standardized CAV

We are not aware of any published GMPE that uses our specific definition of CAV_S. There are, however, two published relationships for standardized CAV that we can use to compare with ours. Recall that the only difference between these two parameters is that CAV_S includes the response spectrum check, whereas, standardized CAV does not. The most relevant relationship is the GMPE developed by EPRI (2006) because of its use of the PEER-NGA strong motion database. For purposes of comparison, we use EPRI's Equation (2-9) to estimate standardized CAV from PGA and our GMPE (Campbell and Bozorgnia 2008) to estimate PGA. Both relationships were evaluated for the set of parameter values listed in the caption to Figure 5.3.

The comparison in Figure 7.1 shows that there is good agreement between these relationships above the imposed CAV threshold value of 0.16 g-sec even though the EPRI relationship used both horizontal components in its development rather than the maximum of the horizontal and vertical components as stipulated in Regulatory Guide 1.166 (U.S. Nuclear Regulatory Commission 1997). The relationships developed in this study are not valid below the CAV_S threshold of 0.16 g-sec, so any comparison below this value is irrelevant.

The second relationship is the GMPE developed by Kostov (2005) using the European strong motion database. Like EPRI's, this relationship used both horizontal components. It defines magnitude in terms of surface-wave magnitude rather than moment magnitude, and distance in terms of epicentral distance rather than closest distance to coseismic rupture. Furthermore, it does not contain terms to account for the effects of fault mechanism and site conditions. For comparison with the Kostov relationship, we evaluated our GMPE for NEHRP site class C ($V_{S30} = 525$ m/sec), which we assume to be generally consistent with the predominant site type represented by the Kostov relationship. We used an average hypocentral depth of 8 km to evaluate this relationship and a variable depth-to-top of rupture (Z_{TOR}) of 10 km for **M** 5.0, 5 km for **M** 6.0, and 0 for **M** 7.0 in our relationship. The comparison in Figure 7.1 shows that, although the two relationships have similar magnitude scaling, there is generally poor agreement between the two relationships in terms of amplitude and attenuation.

7.1.2 Relationships for CAV and CAV_{GM}

There is only one published GMPE for the average horizontal component of CAV that we can use to compare with our relationship for CAV_{GM}. This GMPE was developed using Greek recordings of the European strong motion database (Danciu and Tselentis 2007). It uses epicentral distance and the arithmetic average of the two horizontal ground motion components, whereas, we use closest distance to coseismic rupture and the geometric mean of the two horizontal components. They determined an average hypocentral depth of 14 km from the regression analysis. We evaluated their GMPE for their site category C ($V_{S30} = 360 - 665$ m/sec) and our relationship for local site conditions and depth-to-top of rupture as described in the previous section. The comparison in Figure 7.1 shows relatively good agreement between the two relationships at small magnitudes, but a lack of magnitude saturation causes the Danciu and

Tselentis relationship to predict much higher values of CAV close in to large magnitude earthquakes where data are lacking in the Greek database.

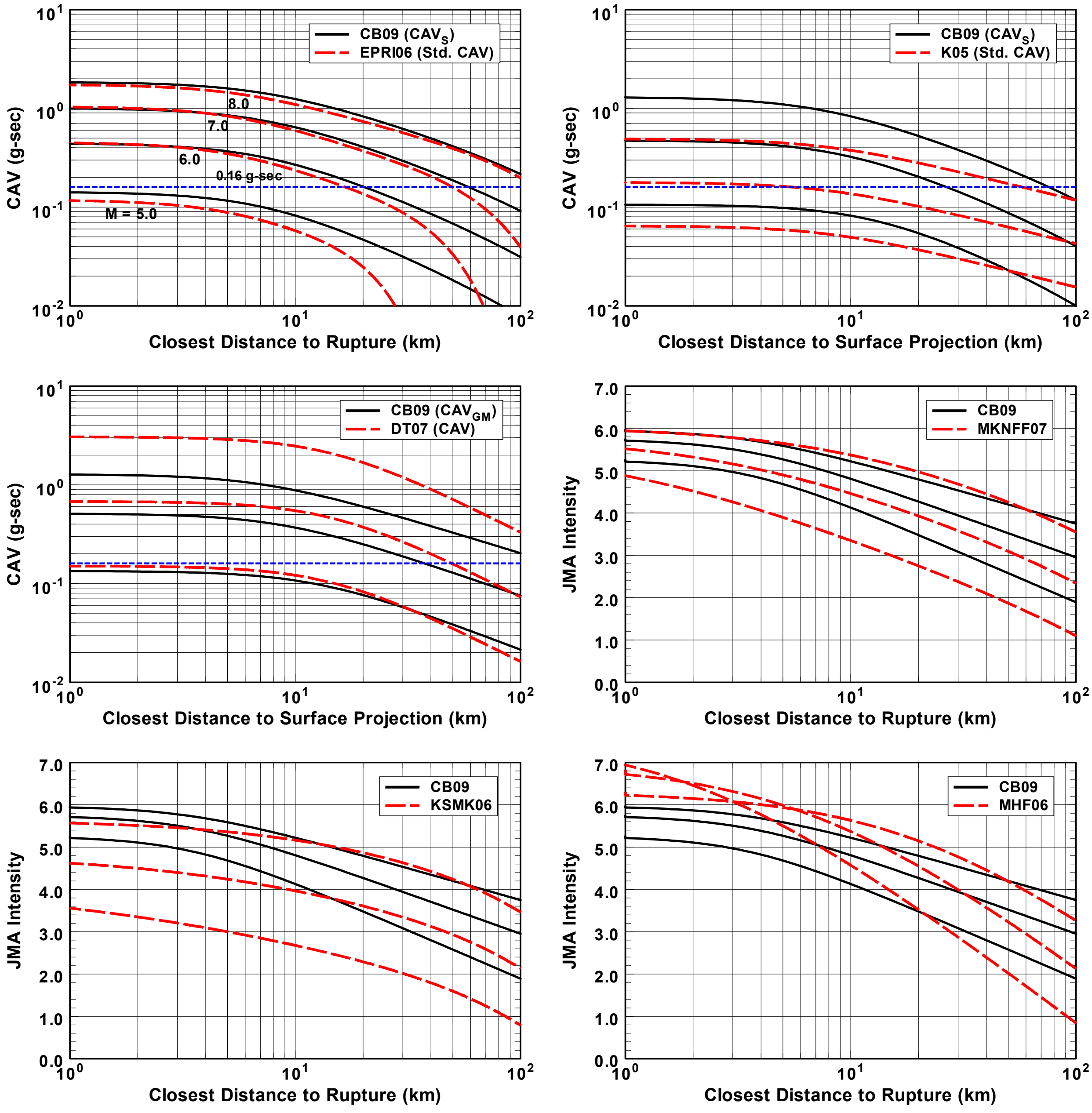

Fig. 7.1 GMPEs for CAV_S, CAV_{GM}, and I_{JMA} developed in this study [CB09] compared with those of: (top left) standardized CAV by EPRI (2006) [EPRI06]; (top right) standardized CAV by Kostov (2005) [K05]; (middle left) CAV by Danciu and Tselentis (2007) [DT07]; (middle right) I_{JMA} by Morikawa et al. (2007) [MKNFF07]; (lower left) I_{JMA} by Kataoka et al. (2006) [KSMK06]; (lower right) I_{JMA} by Matsuzaki et al. (2006) [MHF06].

7.1.3 Relationships for I_{JMA}

We used three Japanese GMPEs for I_{JMA} published in the Japanese literature to compare with our relationship for I_{JMA}. A fourth relationship (Shabestari and Yamazaki 1998) was not used because, unlike the others, it did not attempt to take into account near-source effects in its development. None of the relationships distinguish between different focal mechanisms as our relationship does; however, like ours, they all use rupture distance as the distance metric. We evaluated our GMPE and that of Morikawa et al. (2007) for $V_{S30} = 400$ m/sec. This is consistent with the engineering bedrock category of Kataoka et al. (2006) and the Soil Type 2 category of Matsuzaki et al. (2006), for which Zhao et al. (2006) determined a V_{S30} in the range of 300–600 m/sec. The relationship of Matsuzaki et al. uses JMA magnitude as the magnitude scale, whereas we use moment magnitude, and they include hypocentral depth as a predictor variable in order to distinguish between earthquakes of different tectonic environments (i.e., shallow crustal and shallow-to-intermediate depth subduction earthquakes). We use a focal depth of 5 km to evaluate this relationship in an attempt to constrain the prediction to shallow crustal earthquakes. The relationships of Kataoka et al. and Morikawa et al. both use moment magnitude as the magnitude scale. The former relationship used only shallow crustal earthquakes, or what are referred to as inland earthquakes. The latter relationship limits focal depths to 30 km, but includes both crustal and shallow subduction earthquakes.

The comparison in Figure 7.1 shows that the closest agreement between the three Japanese relationships and ours is with the Kataoka et al. (2006) GMPE, which isolates shallow crustal earthquakes in Japan and uses moment magnitude as the magnitude scale. This relationship exhibits similar magnitude scaling as ours; however, it predicts much stronger attenuation at the smaller magnitudes. The other two Japanese relationships predict greater magnitude scaling than ours regardless of whether JMA or moment magnitude is used as the magnitude scale. However, unlike Kataoka et al., their attenuation characteristics are more similar to ours. The best agreement in both amplitude and attenuation amongst all of the relationships is at magnitude 7.0.

7.2 EVALUATION OF ALEATORY UNCERTAINTY

One of the more significant results of this study is the statistical robustness of CAV_{GM}, which is better than any of the peak ground motion and peak linear-elastic and inelastic response-spectral parameters that we have evaluated thus far (Campbell and Bozorgnia 2008; Bozorgnia et al. 2006, 2010a, 2010b). Danciu and Tselentis (2007) found a similar result. Prior to this study, the smallest standard deviations that we had found were for PGA, PGV, and PSA for $T \leq 0.02$ sec (Table 5.2). A comparison of the standard deviations of $\ln \mathrm{CAV}_{\mathrm{GM}}$ and $\ln \mathrm{PGA}$ in Table 5.2 yields reductions of 11% in the inter-event standard deviation ($\tau_{\ln Y}$), 22% in the intra-event standard deviation ($\sigma_{\ln Y}$), 20% in the total standard deviation (σ_T), 46% in the intra-component standard deviation (σ_C), and 22% in the arbitrary horizontal component standard deviation (σ_{Arb}). The largest reduction is found for the intra-component standard deviation. In the terminology of performance-based seismic hazard, these results indicate that CAV has a high level of predictability (Shome and Cornell 1999).

The standard deviations of $\ln \mathrm{CAV}_{\mathrm{S}}$ when CAV_{GM} is predicted are similar to those of the predicted values of PGA, PGV, and short-period PSA (Table 5.2). We can also compare the aleatory uncertainty in CAV_S from our relationship with that of the GMPE for standardized CAV from EPRI (2006). The total standard deviation for the predicted natural logarithm of standardized CAV from their relationship is 0.46 when PGA is known. This value is 2.5 to 3 times higher than our standard deviations of 0.150–0.187 for $\ln \mathrm{CAV}_{\mathrm{S}}$ when CAV_{GM} is known (Table 5.3). The total standard deviation for $\ln \mathrm{PGA}$ is also larger than that of $\ln \mathrm{CAV}_{\mathrm{GM}}$ (Table 5.2), which adds to this difference. In order to compare the total aleatory uncertainty in standardized CAV and CAV_S after accounting for the uncertainty in PGA and CAV_{GM}, we need to take into account the uncertainty in the prediction of these later parameters.

EPRI (2006) did not derive a relationship for estimating the total standard deviation of standardized CAV that includes the uncertainty in PGA. Therefore, we developed this relationship ourselves in order to compare their total standard deviation to ours. The first-order second-moment approximation of the propagation of uncertainty theorem as applied to their Equation 2-9 yields the following equation for the total aleatory uncertainty:

$$\sigma_T = \sqrt{\sigma^2_{\ln \mathrm{CAV|PGA}} + \alpha_1^2 \sigma^2_{\ln \mathrm{PGA}} + \alpha_1 \rho \sigma_{\ln \mathrm{CAV|PGA}} \sigma_{\ln \mathrm{PGA}}} \tag{7.1}$$

where CAV represents standardized CAV, ρ is the correlation coefficient of the variability (residuals) between $\ln \mathrm{CAV}$ and $\ln \mathrm{PGA}$, and α_1 is the linearized functional relationship between $\overline{\ln \mathrm{CAV}}$ and $\overline{\ln \mathrm{PGA}}$, which is estimated from the partial derivative:

$$\alpha_1 = \frac{\partial \overline{\ln \mathrm{CAV}}}{\partial \overline{\ln \mathrm{PGA}}} = d_2 - \frac{d_3}{(\ln \mathrm{PGA} + d_4)^2} \tag{7.2}$$

where $d_2 = 0.509$, $d_3 = -2.11$, and $d_4 = 4.25$ (EPRI 2006).

EPRI (2006) did not provide an estimate of ρ. However, we assume that it is similar to the correlation coefficient of the variability between $\ln \mathrm{PGA}$ and $\ln \mathrm{CAV_S}$ found in this study ($\rho = 0.20$). Using this correlation coefficient and the total standard deviation of the arbitrary horizontal component of $\ln \mathrm{PGA}$ in Table 5.2 (0.551), consistent with EPRI's regression analysis, we were able to calculate σ_T for $\ln \mathrm{CAV}$ from Equations (7.1) and (7.2). These values are listed in Table 7.1, where they are compared to the estimates of σ_T for $\ln \mathrm{CAV_S}$ when $\mathrm{CAV_{GM}}$ is predicted given in Table 5.3. Although our σ_T values are similar to those for PGA, PGV, and short-period PSA (Table 5.2), Table 7.1 shows that the estimated EPRI σ_T values for NEHRP BC site conditions are larger than ours by about 20% for $\mathrm{PGA} > 0.6$ g to more 100% for $\mathrm{PGA} < 0.1$ g. In the terminology of performance-based seismic hazard, our estimates have a higher level of predictability (Shome and Cornell 1999). These differences can have a significant impact on the calculated hazard. For example, Bommer and Abrahamson (2006) demonstrate that a difference of 40% between two logarithmic standard deviations can lead to ground motion differences of 39%, 48%, and 65% at annual exceedance frequencies of 10^{-2}, 10^{-3}, and 10^{-4}, respectively.

Table 7.1 Comparison of total standard deviations between CAV_S in this study and standardized CAV in EPRI (2006).

PGA (g)	σ_T (this study)	σ_T (EPRI 2006)	Difference
0.05	0.495 – 0.510	1.160	127 – 134%
0.10	0.495 – 0.510	0.781	53 – 58%
0.20	0.495 – 0.510	0.673	32 – 36%
0.40	0.495 – 0.510	0.629	23 – 27%
0.60	0.495 – 0.510	0.614	20 – 24%
0.80	0.495 – 0.510	0.607	19 – 23%
1.00	0.495 – 0.510	0.602	18 – 22%

Note: $\sigma_{\ln \mathrm{CAV}} = 0.46$, $\sigma_T(\ln \mathrm{CAV}_{GM}) = 0.420$, $\sigma_T(\ln \mathrm{PGA}) = 0.551$, $\rho = 0.2$, NEHRP BC site conditions.

7.3 IMPACT OF DATABASE SELECTION

The relationship between CAV_S and CAV_{GM} given by Equation (5.20) depends on the database that was used in the regression analysis (Table 5.3). The relationship with the lowest standard deviation and the highest r-square value uses the CB08 subset of the PEER-NGA database and does not invoke the spectral velocity check recommended by the USNRC (U.S. Nuclear Regulatory Commission 1997) for determining whether the OBE has been exceeded. This makes sense, since the CB08 subset was selected from the full PEER-NGA database using criteria that was intended to increase its reliability (Campbell and Bozorgnia 2007, 2008) and not invoking the spectral velocity check removes more small-amplitude ground motions that lead to higher variability in CAV_S. Conversely, the relationship with the highest standard deviation and the lowest r-square value uses the full PEER-NGA database and invokes the spectral velocity check. The original recommendation by EPRI (1988) did not include the spectral velocity check. This check was added by the USNRC during the development of Regulatory Guide 1.166.

All four relationships have relatively low standard deviations and high r-square values, which makes the decision as to which one to use more philosophical than statistical. Considering only data reliability as a decision metric, we would prefer the relationship derived from the CB08 subset of the PEER-NGA database. However, use of the full database potentially provides a relationship that is more robust and, therefore, might be more transferable to other regions. If the objective is to screen out non-damaging, small-magnitude, high-amplitude ground motions from triggering a SCRAM of a nuclear power plant, we would prefer the relationships that do not invoke the spectral velocity check. As we demonstrated in Section 3.2.2, the spectral velocity check would allow large magnitude, low-amplitude ground motions to meet the USNRC criteria for exceeding an OBE when the value of standardized CAV is greater than or equal to 0.16 g-sec, even though these ground motions night not otherwise be damaging. If the objective is to apply the USNRC criteria exactly, then the spectral velocity check must be invoked. Engineers familiar with the vulnerability and fragility of nuclear structures ultimately should decide which relationship to use after considering all of the other conservatisms involved in determining whether a particular ground motion is potentially damaging to a specific structure or class of structures.

7.4 CORRELATION WITH QUALITATIVE ASSESSMENTS OF DAMAGE

We provide data and analyses in Section 4.3 that might be useful in establishing appropriate levels of JMA seismic intensity, MMI, and CAV_S that relate to the onset of structural damage to well-engineered structures. This assessment suggests that structural damage to highly earthquake-resistant RC buildings might initiate at a JMA intensity of 6 Lower (I_{JMA} 5.5) and a MMI, MSK-64, and EMS-98 intensity of IX (I_{MMI} 8.5). This latter intensity level approximately corresponds to I_{JMA} 5.85 ± 0.15 according to the relationship of Shabestari and Yamazaki (2001), which is somewhat higher than the potential structural damage threshold suggested by the JMA intensity scale. No structural damage to highly earthquake-resistant RC buildings is expected to occur at a JMA intensity 5 Upper (I_{JMA} 5.0) or a MMI, MSK-64, and EMS-98 intensity of VIII (I_{MMI} 7.5), but there could be structural damage to RC buildings with a more moderate level of earthquake-resistance design. EPRI (1988) recommended MMI VII (I_{MMI} 6.5) as an appropriate structural damage threshold intensity for engineered (although not necessarily well-engineered) industrial facilities.

The value of CAV_S that is associated with the potential structural damage threshold levels of seismic intensity discussed in the previous paragraph depends on which database is used and whether the spectral velocity check is invoked in deriving the relationship between CAV_S and CAV_{GM} (Table 4.2). It also depends on the value of nonexceedance probability (P_{ne}) that is considered to be acceptable. For I_{JMA} 5.0 and I_{MMI} 6.5, the statistical results in Table 4.2 indicate that the probability of nonexceedance for a CAV_S value of 0.16 g-sec ranges between 0.05% and 0.17%. For I_{JMA} 5.5, these probabilities decrease considerably, ranging between 0.0004% and 0.003%. Both sets of probabilities are relatively small. Increasing these nonexceedance probabilities to larger values (e.g., 1% to 5%) would allow the selection of a larger value of CAV_S to associate with a given intensity level. For a P_{ne} of 1%, CAV_S is estimated to be 0.207–0.236 g-sec for I_{JMA} 5.0 and 0.332–0.379 g-sec for I_{JMA} 5.5. For a less conservative P_{ne} of 5%, these values increase further to 0.277–0.311 g-sec for I_{JMA} 5.0 and 0.443–0.500 g-sec for I_{JMA} 5.5.

7.5 APPLICATION TO OTHER REGIONS

The GMPEs for CAV_{GM} and CAV_S given by Equations (5.1) and (5.20) were developed from the PEER-NGA strong motion database and, therefore, represent the attenuation properties of shallow crustal earthquakes in active tectonic regions throughout the world. In order to estimate these ground motion parameters in other types of tectonic environments, either new relationships will need to be developed or those developed in this study will need to be modified to better represent the attenuation properties of these environments. This can be done using the hybrid-empirical, stochastic simulation, and numerical modeling methods that have been used to develop GMPEs for the eastern United States (see Petersen et al. 2008 for a list of these relationships).

EPRI (2006) attempted to avoid this issue by making standardized CAV a function of PGA and allowing the regional differences in attenuation properties to be accounted for by using a regional GMPE for PGA. However, as discussed in Section 7.2, this approach leads to a substantially higher standard deviation for standardized CAV than the approach used to estimate CAV_S in our study, which can lead to a substantially higher estimate of seismic hazard. Therefore, if possible, it is beneficial to develop regional GMPEs for standardized CAV, CAV_{GM}, and CAV_S rather than depend on potentially less regionally independent relationships that rely on PGA.

8 Conclusions

Like the NGA-West relationships that precede them, the GMPEs for CAV_S, CAV_{GM}, and I_{JMA} presented in this report represent a significant advancement in the empirical prediction of ground motion for use in engineering and seismology. They incorporate such important features as magnitude saturation, magnitude-dependent attenuation, style of faulting, depth of rupture, hanging-wall effects, shallow linear and nonlinear site response, basin response, and amplitude-dependent (nonlinear) intra-event aleatory uncertainty.

We consider the relationships developed in this study to be appropriate for shallow continental crustal earthquakes in active tectonic regions. We believe that they are most reliable when predictor variables are limited to the following range of values: (1) $\mathbf{M} > 5.0$, (2) $\mathbf{M} < 8.5$ for strike-slip faulting, $\mathbf{M} < 8.0$ for reverse faulting, and $\mathbf{M} < 7.5$ for normal faulting; (3) $R_{RUP} < 100$ km for $\mathbf{M} < 7.0$ and $R_{RUP} < 200$ km for larger events; (4) $V_{S30} = 150-1500$ m/sec or, alternatively, NEHRP site classes B ($V_{S30} = 1070$ m/s), C ($V_{S30} = 525$ m/s), D ($V_{S30} = 255$ m/s) and E ($V_{S30} = 150$ m/s); (5) $Z_{2.5} < 10$ km; (6) $Z_{TOR} < 15$ km; and (7) $|\delta| = 15-90°$. The recommended upper magnitude limits represent an extrapolation of approximately 0.5 from the largest magnitude of each type of fault mechanism in our database. We believe that this extrapolation is justified given the magnitude scaling constraints imposed in the model. We also have extended the applicable range of some of the other predictor variables beyond the limits of the data when we believe that the relationships have been adequately constrained either empirically or theoretically (Campbell and Bozorgnia 2007, 2008).

A comparison of our CAV_S relationship with that for standardized CAV developed by EPRI (2006) indicates that the median prediction from this latter relationship is consistent with ours for CAV values greater than 0.16 g-sec, the current threshold used to trigger the shutdown of a nuclear power plant in the United States when the OBE response spectrum is exceeded (U.S.

Nuclear Regulatory Commission 1997). However, the standard deviation associated with the EPRI relationship is substantially larger than ours after taking into account the added uncertainty in the statistical estimation of CAV_{GM} and PGA. Our CAV_{GM} relationship has less aleatory uncertainty than any of the peak ground motion and elastic and inelastic response-spectral parameters that we have analyzed thus far, suggesting that it has a higher level of predictability (Shome and Cornell (1999). Our CAV_S relationship has aleatory uncertainty among the smallest of those parameters we have analyzed thus far.

A comparison of our CAV_S relationship with that for standardized CAV developed by Kostov (2005) and a comparison of our CAV_{GM} relationship with that for CAV developed by Danciu and Tselentis (2007) shows that these relationships predict magnitude scaling effects for moment magnitudes greater than approximately 6.0–6.5 that are inconsistent with our relationships. Although some of this discrepancy can be explained by differences in the definitions of CAV or the predictor variables, most of it is likely due to there being an insufficient number of recordings in the near-source region of large magnitude earthquakes in order to constrain the magnitude scaling in this region. Interestingly, a comparison of our I_{JMA} relationship with those developed from Japanese data show relatively good agreement at large magnitudes and relatively poor agreement at small magnitudes.

The data, interpretations, and relationships provided in this report have been used to correlate CAV_S with qualitative measures of ground shaking intensity and structural damage as described in the JMA, MMI, MSK-64, and EMS-98 intensity scales. Although these intensity scales present only a qualitative description of the damage to general classes of buildings of different earthquake-resistant design, they are useful in understanding the general relationship between CAV_S and the physical damage that might be expected to occur to a structure during an earthquake.

REFERENCES

Abrahamson, N. A., and Youngs, R. R., 1992. A stable algorithm for regression analyses using the random effects model, Bull. Seismol. Soc. Am. 82, 505–510.

Abrahamson, N., and Silva, W., 2008. Summary of the Abrahamson & Silva NGA ground motion relations, Earthq. Spectra 24, 67–97.

Baker, J. W., and Cornell, C. A., 2006. Which spectral acceleration are you using?, Earthq. Spectra 22, 293–312.

Baturay, M. B., and Stewart, J. P., 2003. Uncertainty and bias in ground motion estimates from ground response analyses, Bull. Seismol. Soc. Am. 93, 2025–2042.

Bazzurro, P., and Cornell, C. A., 2002. Vector-valued probabilistic seismic hazard analysis, in Proc., 7th National Conference on Earthquake Engineering, Boston, Paper No. 447, 10 pp.

Bazzurro, P., and Cornell, C. A., 2004a. Ground motion amplification in nonlinear soil sites with uncertain properties, Bull. Seismol. Soc. Am. 94, 2090–2109.

Bazzurro, P., and Cornell, C. A., 2004b. Nonlinear soil-site effects in probabilistic seismic-hazard analysis, Bull. Seismol. Soc. Am. 94, 2110–2123.

Bazzurro, P., and Cornell, C. A., 2005. Erratum: ground motion amplification in nonlinear soil sites with uncertain properties, Bull. Seismol. Soc. Am. 95, 2027.

Benjamin, J. R., and Cornell, C. A., 1970. Probability, Statistics, and Decision for Civil Engineers, McGraw-Hill, New York.

Beyer, K., and Bommer, J. J., 2006. Relationships between median values and between aleatory variabilities for different definitions of the horizontal component of motion, Bull. Seismol. Soc. Am. 96, 1512–1522.

Bommer, J. J., and Abrahamson, N. A., 2006. Why do modern probabilistic seismic-hazard analyses often lead to increased hazard estimates?, Bull. Seismol. Soc. Am. 96, 1967–1977.

Boore, D. M., 2005. Erratum: equations for estimating horizontal response spectra and peak acceleration from western North American earthquakes: a summary of recent work, Seismol. Res. Lett. 76, 368–369.

Boore, D. M., Watson-Lamprey, J., and Abrahamson, N., 2006. Orientation-independent measures of ground motion, Bull. Seismol. Soc. Am. 96, 1502–1511.

Bozorgnia, Y., Hachem, M. M., and Campbell, K. W., 2006. Attenuation of inelastic and damage spectra, in Proc., 8th National Conference on Earthquake Engineering, San Francisco, Paper No. 1127, 10 pp.

Bozorgnia, Y., Hachem, M. M., and Campbell, K. W., 2010a. Ground motion prediction equation ("attenuation relationship") for inelastic response spectra, Earthq. Spectra 26, 1–23.

Bozorgnia, Y., Hachem, M. M., and Campbell, K. W., 2010b. Deterministic and probabilistic predictions of yield strength and inelastic displacement spectra, Earthq. Spectra 26, 25–40.

Building Seismic Safety Council (BSSC) (2004). NEHRP Recommended Provisions for Seismic Regulations for New Buildings and Other Structures (FEMA 450), 2003 edition, National Institute of Building Sciences, Washington, D.C.

Cabañas, L., Benito, B., and Herráiz, M., 1997. An approach to the measurement of the potential structural damage of earthquake ground motions, Earthq. Eng. Struct. Dyn. 26, 79–92.

Campbell, K. W., 1981. Near-source attenuation of peak horizontal acceleration, Bull. Seismol. Soc. Am. 71, 2039–2070.

Campbell, K. W., and Bozorgnia, Y., 2006. Next generation attenuation (NGA) empirical ground motion models: can they be used in Europe?, in Proc., 1st European Conference on Earthquake Engineering and Seismology, Geneva, Switzerland, Paper No. 458, 10 pp.

Campbell, K. W., and Bozorgnia, Y., 2007. Campbell-Bozorgnia NGA Ground Motion Relations for the Geometric Mean Horizontal Component of Peak and Spectral Ground Motion Parameters, PEER Report No. 2007/02, Pacific Earthquake Engineering Research Center, University of California, Berkeley, 238 pp.

Campbell, K. W., and Bozorgnia, Y., 2008. NGA ground motion model for the geometric mean horizontal component of PGA, PGV, PGD and 5% damped linear elastic response spectra for periods ranging from 0.01 to 10 s, Earthq. Spectra 24, 139–171.

Chiou, B., Darragh, R., Gregor, N., and Silva, W., 2008. NGA project strong motion database, Earthq. Spectra 24, 23–44.

Cox, D. R., and Wermuth, N., 1991. A simple approximation for bivariate and trivariate normal integrals, Int. Statist. Rev. 59, 263–269.

Danciu, L., and Tselentis, G., 2007. Engineering ground motion parameters attenuation relationships for Greece, Bull. Seismol. Soc. Am. 97, 162–183.

Davenport, P. N., 2001. Seismic intensities derived from strong motion instruments in New Zealand, in Proc., Technical Conference of the New Zealand Society for Earthquake Engineering (NZSEE 2001), Wairakei, New Zealand, Paper No. 4.03.01, 7 pp.

Davenport, P. N., 2003. Instrumental measures of earthquake intensity in New Zealand, in Proc., 7th Pacific Conference on Earthquake Engineering, Christchurch, New Zealand, Paper No. 071, 5 pp.

Dong, H., Yamazaki, F., Shimizu, Y., and Sasaki, H., 1996. Correlation of instrumental seismic intensity with ground motion measures, Proc., 51st Annual Meeting of the Japan Society of Earthquake Engineering, vol. B, 458–459 (in Japanese).

Earthquake Research Committee, 1998. Seismic Activity in Japan, Headquarters for Earthquake Research Promotion, Prime Minister's Office, Government of Japan, Tokyo, 222 pp.

Electrical Power Research Institute (EPRI), 2006. Program on Technology Innovation: Use of Cumulative Absolute Velocity (CAV) in Determining Effects of Small Magnitude Earthquakes on Seismic Hazard Analyses, Report No. 1014099, EPRI, Palo Alto, California, and U.S. Department of Energy, Germantown, Maryland.

Electrical Power Research Institute (EPRI), 1991. Standardization of the Cumulative Absolute Velocity, Report No. EPRI TR-100082-T2, EPRI, Palo Alto, California.

Electrical Power Research Institute (EPRI), 1989. Proceedings: Engineering Characterization of Small-Magnitude Earthquakes, Report No. EPRI NP-6389, EPRI, Palo Alto, California.

Electrical Power Research Institute (EPRI), 1988. A Criterion for Determining Exceedance of the Operating Basis Earthquake, Report No. EPRI NP-5930, EPRI, Palo Alto, California.

Frankel, A. D., Petersen, M. D., Muller, C. S., Haller, K. M., Wheeler, R. L., Leyendecker, E. V., Wesson, R. L., Harmsen, S. C., Cramer, C. H., Perkins, D. M., and Rukstales, K. S., 2002. Documentation for the 2002 update of the national seismic hazard maps, U.S. Geol. Survey Open-File Report 02-420.

Fujimoto, K., and Midorikawa, S., 2005. Empirical method for estimating J.M.A. instrumental seismic intensity from ground motion parameters using strong motion records during recent major earthquakes, J. Social Safety Sci. 7, 241–246 (in Japanese).

Goulet, C. A., and Stewart, J. P., 2009. Site effects and seismic hazard: impact of site response versus Vs30 models on hazard curves, Abstract, Seismol. Res. Lett. 80, 364.

Grünthal, G. (ed.), 1998. European Macroseismic Scale 1998, in Cahiers du Centre Européen de Géodynamique et de Séismologie, vol. 15, Centre Européen de Géodynamique et de Séismologie, Luxembourg, 99 pp.

Japan Meteorological Agency, 1996. Note on the JMA seismic intensity, Gyosei, 46–224 (in Japanese).

Japan Meteorological Agency, 2007. Tables Explaining the JMA Seismic Intensity Scale, http://www.jma.go.jp/jma/en/Activities/earthquake.html#S_I, last accessed July 2009.

Karim, K. R., and Yamazaki, F., 2002. Correlation of JMA instrumental seismic intensity with strong motion parameters, Earthq. Eng. Struct. Dyn. 31, 1191–1212.

Kataoka, S., Satoh, T., Matsumoto, S., and Kusakabe, T., 2006. Attenuation relationships of ground motion intensity using short period level as a variable, J. Struct. Earthq. Eng., JSCE 62, 740–757 (in Japanese).

Koliopoulos, P. K., Margaris, B. N., and Klimis, N. S., 1998. Duration and energy characteristics of Greek strong motion records, J. Earthq. Eng. 2, 390–417.

Kostov, M., 2005. Site specific estimation of cumulative absolute velocity, in Proc., 18th International Conference on Structural Mechanics in Reactor Technology (SMiRT 18), Beijing, China, 3041–3050.

Kramer, S. L., and Mitchell, R. A., 2006. Ground motion intensity measures for liquefaction hazard evaluation, Earthq. Spectra 22, 413–438.

Kwok, A. O., and Stewart, J. P., 2006. Evaluation of the effectiveness of theoretical 1D amplification factors for earthquake ground motion prediction, Bull. Seismol. Soc. Am. 96, 1422–1436.

Lin, P.-S., 2007, A Comparison Study of Earthquake Strong-Ground Motions in California and in Taiwan, PEER Report No. 2006/12, Pacific Earthquake Engineering Research Center, University of California, Berkeley.

Martinez-Rueda, J. E., Moutsokapas, G., and Tsantali, E., 2008. Predictive equations to estimate Arias intensity and cumulative absolute velocity as a function of Housner intensity, in Proc., Seismic Engineering Conference Commemorating the 1908 Messina and Reggio Calabria Earthquake, Messina, Italy, 309–306.

Matsuzaki, S., Hisada Y., and Fukushima, Y., 2006. Attenuation relation of JMA seismic intensity applicable to near source region, J. Struct. Const. Eng., AIJ 604, 201–208 (in Japanese).

McGuire, R. K., 2004. Seismic Risk and Risk Analysis, EERI Publication No. MNO-10, Earthquake Engineering Research Institute, Oakland, California.

Mee, R. W., and Owen, D. B., 1982. A Simple Approximation for Bivariate Normal Probabilities, Technical Report No. 169, Department of Statistics, Southern Methodist University, Dallas, Texas, 11 pp.

Midorikawa, S., Fujimoto, K., and Muramatsu, I., 1999. Correlation of new J.M.A. instrumental seismic intensity with former J.M.A. seismic intensity and ground motion parameters, J. Social Safety Sci. 1, 51–56 (in Japanese).

Morikawa, N., Kanno, T., Narita, A., Fujiwara, H., and Fukushima, Y., 2007. An attenuation relation of seismic intensity based on strong motion records, in Programme and Abstracts, Fall Meeting of the Seismological Society of Japan, Abstract No. B31-05 (in Japanese).

National Bureau of Standards, 1956. Tables of Bivariate Normal Distribution Function and Related Functions, U.S. Government Printing Office, Washington, D.C.

Owen, D. B. (1956). Tables for computing bivariate normal probabilities, Ann. Math. Statist. 27, 1075–1090.

Peruš, I., and Fajfar, P., 2009. How reliable are the ground motion prediction equations?, in Proc., 20th International Conference on Structural Mechanics in Reactor Technology (SMiRT 20), Espoo, Finland, Paper No. 1662, 9 pp.

Petersen, M., Frankel, A., Harmsen, S., Mueller, C., Haller, K., Wheeler, R., Wesson, R., Zeng, Y., Boyd, O., Perkins, D., Luco, N., Field, E., Wills, C., and Rukstales, K., 2008. Documentation for the 2008 update of the United States national seismic hazard maps, U.S. Geol. Survey Open-File Report 2008-1128.

Power, M., Chiou, B., Abrahamson, N., Bozorgnia, Y., Shantz, T., and Roblee, C., 2008. An overview of the NGA project, Earthq. Spectra 24, 3–21.

Scasserra, G., Stewart, J. P., Bazzurro, P., Lanzo, G., and Mollaioli, F., 2009. Comparison of NGA ground motion prediction equations to Italian data, Bull. Seismol. Soc. Am. 99, 2961–2978.

Shabestari, K. T., and Yamazaki, F., 2001. A proposal of instrumental seismic intensity scale compatible with MMI evaluated from three-component acceleration records, Earthq. Spectra 17, 711–723.

Shabestari, K. T., and Yamazaki, F., 1998. Attenuation relationship of JMA seismic intensity using recent JMA records, in Proc., 10th Japan Earthquake Engineering Symposium, Yokohama, Japan, vol. 1, 529–534.

Shoja-Taheri, J., Naserieh, S., and Ghofrani, H., 2010, A test of the applicability of NGA models to the strong ground motion data in the Iranian Plateau, J. Earthq Eng. 14, 278–292.

Shome, N., and Cornell, C. A., 1999. Probabilistic Seismic Demand Analysis of Nonlinear Structures, Report. No. RMS-35, Reliability of Marine Structures Program, Department of Civil and Environmental Engineering, Stanford University, California.

Silva, W. J., Li, S., Darragh, R. B., and Gregor, N., 1999. Surface Geology Based Strong Motion Amplification Factors for the San Francisco Bay and Los Angeles Areas, Report to Pacific Earthquake Engineering Research Center, University of California, Berkeley.

Silva, W. J., Darragh, R. B., Gregor, N., Martin, G., Abrahamson, N. A., and Kircher, C., 2000. Reassessment of Site Coefficients and Near-Fault Factors for Building Code Provisions, Final Technical Report, U.S. Geol. Survey Award No. 98HQGR1010.

Sokolov, V. Y., 2002. Seismic intensity and Fourier acceleration spectra: revised relationship, Earthq. Spectra 18, 161–187.

Sokolov, V., and Furumura, T., 2008. Comparative analysis of two methods for instrumental intensity estimations using the database accumulated during recent large earthquakes in Japan, Earthq. Spectra 24, 513–532.

Sokolov, V., and Wald, D. J., 2002. Instrumental intensity distribution for the Hector Mine, California, and the Chi-Chi, Taiwan, earthquakes: comparison of two methods, Bull. Seismol. Soc. Am. 92, 2145–2162.

Stafford, P. J., Strasser, F. O., and Bommer, J. J., 2008. An evaluation of the applicability of the NGA models to ground motion prediction in the Euro-Mediterranean region, Bull. Earthq. Eng. 6, 149–177.

Stewart, J. P., and Goulet, C. A., 2006. Comment on "Nonlinear soil-site effects in probabilistic seismic-hazard analysis" by Paolo Bazzurro and C. Allin Cornell, Bull. Seismol. Soc. Am. 96, 745–747.

Sugawara, M., Kobayashi, Y., and Mashimo, M., 1999. The study of the relation between the measured seismic intensity and the other indexes, in Summaries of Technical Papers of Annual Meeting, Architectural Institute of Japan, vol. B-2, 175–176 (in Japanese).

Tong, H., and Yamazaki, F., 1996. Relationship between ground motion indices and new JMA seismic intensity, Seisan-Kenkyu 48, 65–68 (in Japanese).

Toro, G. R., Abrahamson, N. A., and Schneider, J. F., 1997. Model of strong ground motions from earthquakes in central and eastern North America: best estimates and uncertainties, Seismol. Res. Lett. 68, 58–73.

Travasarou, T., Bray, J. D., and Abrahamson, N. A., 2003. Empirical attenuation relationship for Arias intensity, Earthq. Eng. Struct. Dyn. 32, 1133–1155.

Trifunac, M. D., and Brady, A. G., 1975. On the correlation of seismic intensity scales with the peaks of recorded strong ground motion, Bull. Seismol. Soc. Am. 65, 139–162.

Tselentis, G., and Danciu, L., 2008. Empirical relationships between modified Mercalli intensity and engineering ground motion parameters in Greece, Bull. Seismol. Soc. Am. 98, 1863–1875.

U.S. Nuclear Regulatory Commission, 1997. Pre-earthquake Planning and Immediate Nuclear Power Plant Operator Postearthquake Actions, Regulatory Guide 1.166, Washington, D.C., 8 pp.

Wald, D. J., Quitoriano, V., Heaton, T. H., and Kanamori, H., 1999. Relationships between peak ground acceleration, peak ground velocity and modified Mercalli intensity in California. Earthq. Spectra 15, 557–564.

Watson-Lamprey, J. A., and Abrahamson, N. A., 2007. Use of minimum CAV in seismic hazard analyses, in Proc., 9th Canadian Conference on Earthquake Engineering, Ottawa, 352–358.

Watson-Lamprey, J. A., and Boore, D. M., 2007. Beyond SaGMRotI: conversion to Sa_{Arb}, Sa_{SN}, and Sa_{MaxRot}, Bull. Seismol. Soc. Am. 97, 1511–1524.

Yamazaki, F., 1996. Earthquake monitoring and real-time damage assessment systems in Japan: developments and future directions, Proc., 6th U.S.–Japan Workshop on Earthquake Resistant Design of Lifeline Facilities and Countermeasures Against Soil Liquefaction, Technical Report NCEER-960012, National Center for Earthquake Engineering Research, Buffalo, New York, 727–740.

Yamazaki, F., Noda, S., and Meguro, K., 1998. Developments of early earthquake damage assessment systems in Japan, Proc., 7th International Conference on Structural Safety and Reliability, Kyoto, Japan, 1553–1580.

Zhao, J. X., Zhang, J., Akihiro, A., Ohno, Y., Oouchi, T., Takahashi, T., Ogawa, H., Irikura, K., Thio, H. K., Somerville, P. G., Fukushima, Y., and Fukushima, Y., 2006. Attenuation relations of strong ground motion in Japan using site classification based on predominant period, Bull. Seismol. Soc. Am. 96, 898–913.

PEER REPORTS

PEER reports are available individually or by yearly subscription. PEER reports can be ordered at http://peer.berkeley.edu/publications/peer_reports.html or by contacting the Pacific Earthquake Engineering Research Center, 1301 South 46th Street, Richmond, CA 94804-4698. Tel.: (510) 665-3448; Fax: (510) 665-3456; Email: peer_editor@berkeley.edu

PEER 2009/03 *The Integration of Experimental and Simulation Data in the Study of Reinforced Concrete Bridge Systems Including Soil-Foundation-Structure Interaction.* Matthew Dryden and Gregory L. Fenves. November 2009.

PEER 2009/02 *Improving Earthquake Mitigation through Innovations and Applications in Seismic Science, Engineering, Communication, and Response. Proceedings of a U.S.-Iran Seismic Workshop.* October 2009.

PEER 2009/01 *Evaluation of Ground Motion Selection and Modification Methods: Predicting Median Interstory Drift Response of Buildings.* Curt B. Haselton, Ed. June 2009.

PEER 2008/10 *Technical Manual for Strata.* Albert R. Kottke and Ellen M. Rathje. February 2009.

PEER 2008/09 *NGA Model for Average Horizontal Component of Peak Ground Motion and Response Spectra.* Brian S.-J. Chiou and Robert R. Youngs. November 2008.

PEER 2008/08 *Toward Earthquake-Resistant Design of Concentrically Braced Steel Structures.* Patxi Uriz and Stephen A. Mahin. November 2008.

PEER 2008/07 *Using OpenSees for Performance-Based Evaluation of Bridges on Liquefiable Soils.* Stephen L. Kramer, Pedro Arduino, and HyungSuk Shin. November 2008.

PEER 2008/06 *Shaking Table Tests and Numerical Investigation of Self-Centering Reinforced Concrete Bridge Columns.* Hyung IL Jeong, Junichi Sakai, and Stephen A. Mahin. September 2008.

PEER 2008/05 *Performance-Based Earthquake Engineering Design Evaluation Procedure for Bridge Foundations Undergoing Liquefaction-Induced Lateral Ground Displacement.* Christian A. Ledezma and Jonathan D. Bray. August 2008.

PEER 2008/04 *Benchmarking of Nonlinear Geotechnical Ground Response Analysis Procedures.* Jonathan P. Stewart, Annie On-Lei Kwok, Yousseff M. A. Hashash, Neven Matasovic, Robert Pyke, Zhiliang Wang, and Zhaohui Yang. August 2008.

PEER 2008/03 *Guidelines for Nonlinear Analysis of Bridge Structures in California.* Ady Aviram, Kevin R. Mackie, and Božidar Stojadinović. August 2008.

PEER 2008/02 *Treatment of Uncertainties in Seismic-Risk Analysis of Transportation Systems.* Evangelos Stergiou and Anne S. Kiremidjian. July 2008.

PEER 2008/01 *Seismic Performance Objectives for Tall Buildings.* William T. Holmes, Charles Kircher, William Petak, and Nabih Youssef. August 2008.

PEER 2007/12 *An Assessment to Benchmark the Seismic Performance of a Code-Conforming Reinforced Concrete Moment-Frame Building.* Curt Haselton, Christine A. Goulet, Judith Mitrani-Reiser, James L. Beck, Gregory G. Deierlein, Keith A. Porter, Jonathan P. Stewart, and Ertugrul Taciroglu. August 2008.

PEER 2007/11 *Bar Buckling in Reinforced Concrete Bridge Columns.* Wayne A. Brown, Dawn E. Lehman, and John F. Stanton. February 2008.

PEER 2007/10 *Computational Modeling of Progressive Collapse in Reinforced Concrete Frame Structures.* Mohamed M. Talaat and Khalid M. Mosalam. May 2008.

PEER 2007/09 *Integrated Probabilistic Performance-Based Evaluation of Benchmark Reinforced Concrete Bridges.* Kevin R. Mackie, John-Michael Wong, and Božidar Stojadinović. January 2008.

PEER 2007/08 *Assessing Seismic Collapse Safety of Modern Reinforced Concrete Moment-Frame Buildings.* Curt B. Haselton and Gregory G. Deierlein. February 2008.

PEER 2007/07 *Performance Modeling Strategies for Modern Reinforced Concrete Bridge Columns.* Michael P. Berry and Marc O. Eberhard. April 2008.

PEER 2007/06 *Development of Improved Procedures for Seismic Design of Buried and Partially Buried Structures.* Linda Al Atik and Nicholas Sitar. June 2007.

PEER 2007/05 *Uncertainty and Correlation in Seismic Risk Assessment of Transportation Systems.* Renee G. Lee and Anne S. Kiremidjian. July 2007.

PEER 2007/04 *Numerical Models for Analysis and Performance-Based Design of Shallow Foundations Subjected to Seismic Loading.* Sivapalan Gajan, Tara C. Hutchinson, Bruce L. Kutter, Prishati Raychowdhury, José A. Ugalde, and Jonathan P. Stewart. May 2008.

PEER 2007/03 *Beam-Column Element Model Calibrated for Predicting Flexural Response Leading to Global Collapse of RC Frame Buildings.* Curt B. Haselton, Abbie B. Liel, Sarah Taylor Lange, and Gregory G. Deierlein. May 2008.

PEER 2007/02 *Campbell-Bozorgnia NGA Ground Motion Relations for the Geometric Mean Horizontal Component of Peak and Spectral Ground Motion Parameters.* Kenneth W. Campbell and Yousef Bozorgnia. May 2007.

PEER 2007/01 *Boore-Atkinson NGA Ground Motion Relations for the Geometric Mean Horizontal Component of Peak and Spectral Ground Motion Parameters.* David M. Boore and Gail M. Atkinson. May. May 2007.

PEER 2006/12 *Societal Implications of Performance-Based Earthquake Engineering.* Peter J. May. May 2007.

PEER 2006/11 *Probabilistic Seismic Demand Analysis Using Advanced Ground Motion Intensity Measures, Attenuation Relationships, and Near-Fault Effects.* Polsak Tothong and C. Allin Cornell. March 2007.

PEER 2006/10 *Application of the PEER PBEE Methodology to the I-880 Viaduct.* Sashi Kunnath. February 2007.

PEER 2006/09 *Quantifying Economic Losses from Travel Forgone Following a Large Metropolitan Earthquake.* James Moore, Sungbin Cho, Yue Yue Fan, and Stuart Werner. November 2006.

PEER 2006/08 *Vector-Valued Ground Motion Intensity Measures for Probabilistic Seismic Demand Analysis*. Jack W. Baker and C. Allin Cornell. October 2006.

PEER 2006/07 *Analytical Modeling of Reinforced Concrete Walls for Predicting Flexural and Coupled–Shear-Flexural Responses*. Kutay Orakcal, Leonardo M. Massone, and John W. Wallace. October 2006.

PEER 2006/06 *Nonlinear Analysis of a Soil-Drilled Pier System under Static and Dynamic Axial Loading.* Gang Wang and Nicholas Sitar. November 2006.

PEER 2006/05 *Advanced Seismic Assessment Guidelines.* Paolo Bazzurro, C. Allin Cornell, Charles Menun, Maziar Motahari, and Nicolas Luco. September 2006.

PEER 2006/04 *Probabilistic Seismic Evaluation of Reinforced Concrete Structural Components and Systems.* Tae Hyung Lee and Khalid M. Mosalam. August 2006.

PEER 2006/03 *Performance of Lifelines Subjected to Lateral Spreading.* Scott A. Ashford and Teerawut Juirnarongrit. July 2006.

PEER 2006/02 *Pacific Earthquake Engineering Research Center Highway Demonstration Project.* Anne Kiremidjian, James Moore, Yue Yue Fan, Nesrin Basoz, Ozgur Yazali, and Meredith Williams. April 2006.

PEER 2006/01 *Bracing Berkeley. A Guide to Seismic Safety on the UC Berkeley Campus.* Mary C. Comerio, Stephen Tobriner, and Ariane Fehrenkamp. January 2006.

PEER 2005/16 *Seismic Response and Reliability of Electrical Substation Equipment and Systems.* Junho Song, Armen Der Kiureghian, and Jerome L. Sackman. April 2006.

PEER 2005/15 *CPT-Based Probabilistic Assessment of Seismic Soil Liquefaction Initiation.* R. E. S. Moss, R. B. Seed, R. E. Kayen, J. P. Stewart, and A. Der Kiureghian. April 2006.

PEER 2005/14 *Workshop on Modeling of Nonlinear Cyclic Load-Deformation Behavior of Shallow Foundations.* Bruce L. Kutter, Geoffrey Martin, Tara Hutchinson, Chad Harden, Sivapalan Gajan, and Justin Phalen. March 2006.

PEER 2005/13 *Stochastic Characterization and Decision Bases under Time-Dependent Aftershock Risk in Performance-Based Earthquake Engineering.* Gee Liek Yeo and C. Allin Cornell. July 2005.

PEER 2005/12 *PEER Testbed Study on a Laboratory Building: Exercising Seismic Performance Assessment.* Mary C. Comerio, editor. November 2005.

PEER 2005/11 *Van Nuys Hotel Building Testbed Report: Exercising Seismic Performance Assessment.* Helmut Krawinkler, editor. October 2005.

PEER 2005/10 *First NEES/E-Defense Workshop on Collapse Simulation of Reinforced Concrete Building Structures.* September 2005.

PEER 2005/09 *Test Applications of Advanced Seismic Assessment Guidelines.* Joe Maffei, Karl Telleen, Danya Mohr, William Holmes, and Yuki Nakayama. August 2006.

PEER 2005/08 *Damage Accumulation in Lightly Confined Reinforced Concrete Bridge Columns.* R. Tyler Ranf, Jared M. Nelson, Zach Price, Marc O. Eberhard, and John F. Stanton. April 2006.

PEER 2005/07 *Experimental and Analytical Studies on the Seismic Response of Freestanding and Anchored Laboratory Equipment.* Dimitrios Konstantinidis and Nicos Makris. January 2005.

PEER 2005/06 *Global Collapse of Frame Structures under Seismic Excitations*. Luis F. Ibarra and Helmut Krawinkler. September 2005.

PEER 2005//05 *Performance Characterization of Bench- and Shelf-Mounted Equipment.* Samit Ray Chaudhuri and Tara C. Hutchinson. May 2006.

PEER 2005/04 *Numerical Modeling of the Nonlinear Cyclic Response of Shallow Foundations.* Chad Harden, Tara Hutchinson, Geoffrey R. Martin, and Bruce L. Kutter. August 2005.

PEER 2005/03 *A Taxonomy of Building Components for Performance-Based Earthquake Engineering.* Keith A. Porter. September 2005.

PEER 2005/02 *Fragility Basis for California Highway Overpass Bridge Seismic Decision Making*. Kevin R. Mackie and Božidar Stojadinović. June 2005.

PEER 2005/01 *Empirical Characterization of Site Conditions on Strong Ground Motion.* Jonathan P. Stewart, Yoojoong Choi, and Robert W. Graves. June 2005.

PEER 2004/09 *Electrical Substation Equipment Interaction: Experimental Rigid Conductor Studies.* Christopher Stearns and André Filiatrault. February 2005.

PEER 2004/08 *Seismic Qualification and Fragility Testing of Line Break 550-kV Disconnect Switches.* Shakhzod M. Takhirov, Gregory L. Fenves, and Eric Fujisaki. January 2005.

PEER 2004/07 *Ground Motions for Earthquake Simulator Qualification of Electrical Substation Equipment.* Shakhzod M. Takhirov, Gregory L. Fenves, Eric Fujisaki, and Don Clyde. January 2005.

PEER 2004/06 *Performance-Based Regulation and Regulatory Regimes.* Peter J. May and Chris Koski. September 2004.

PEER 2004/05 *Performance-Based Seismic Design Concepts and Implementation: Proceedings of an International Workshop.* Peter Fajfar and Helmut Krawinkler, editors. September 2004.

PEER 2004/04 *Seismic Performance of an Instrumented Tilt-up Wall Building.* James C. Anderson and Vitelmo V. Bertero. July 2004.

PEER 2004/03 *Evaluation and Application of Concrete Tilt-up Assessment Methodologies.* Timothy Graf and James O. Malley. October 2004.

PEER 2004/02 *Analytical Investigations of New Methods for Reducing Residual Displacements of Reinforced Concrete Bridge Columns.* Junichi Sakai and Stephen A. Mahin. August 2004.

PEER 2004/01 *Seismic Performance of Masonry Buildings and Design Implications.* Kerri Anne Taeko Tokoro, James C. Anderson, and Vitelmo V. Bertero. February 2004.

PEER 2003/18 *Performance Models for Flexural Damage in Reinforced Concrete Columns.* Michael Berry and Marc Eberhard. August 2003.

PEER 2003/17 *Predicting Earthquake Damage in Older Reinforced Concrete Beam-Column Joints.* Catherine Pagni and Laura Lowes. October 2004.

PEER 2003/16 *Seismic Demands for Performance-Based Design of Bridges.* Kevin Mackie and Božidar Stojadinović. August 2003.

PEER 2003/15 *Seismic Demands for Nondeteriorating Frame Structures and Their Dependence on Ground Motions.* Ricardo Antonio Medina and Helmut Krawinkler. May 2004.

PEER 2003/14 *Finite Element Reliability and Sensitivity Methods for Performance-Based Earthquake Engineering.* Terje Haukaas and Armen Der Kiureghian. April 2004.

PEER 2003/13 *Effects of Connection Hysteretic Degradation on the Seismic Behavior of Steel Moment-Resisting Frames.* Janise E. Rodgers and Stephen A. Mahin. March 2004.

PEER 2003/12 *Implementation Manual for the Seismic Protection of Laboratory Contents: Format and Case Studies.* William T. Holmes and Mary C. Comerio. October 2003.

PEER 2003/11 *Fifth U.S.-Japan Workshop on Performance-Based Earthquake Engineering Methodology for Reinforced Concrete Building Structures.* February 2004.

PEER 2003/10 *A Beam-Column Joint Model for Simulating the Earthquake Response of Reinforced Concrete Frames.* Laura N. Lowes, Nilanjan Mitra, and Arash Altoontash. February 2004.

PEER 2003/09 *Sequencing Repairs after an Earthquake: An Economic Approach.* Marco Casari and Simon J. Wilkie. April 2004.

PEER 2003/08 *A Technical Framework for Probability-Based Demand and Capacity Factor Design (DCFD) Seismic Formats.* Fatemeh Jalayer and C. Allin Cornell. November 2003.

PEER 2003/07 *Uncertainty Specification and Propagation for Loss Estimation Using FOSM Methods.* Jack W. Baker and C. Allin Cornell. September 2003.

PEER 2003/06 *Performance of Circular Reinforced Concrete Bridge Columns under Bidirectional Earthquake Loading*. Mahmoud M. Hachem, Stephen A. Mahin, and Jack P. Moehle. February 2003.

PEER 2003/05 *Response Assessment for Building-Specific Loss Estimation.* Eduardo Miranda and Shahram Taghavi. September 2003.

PEER 2003/04 *Experimental Assessment of Columns with Short Lap Splices Subjected to Cyclic Loads*. Murat Melek, John W. Wallace, and Joel Conte. April 2003.

PEER 2003/03 *Probabilistic Response Assessment for Building-Specific Loss Estimation.* Eduardo Miranda and Hesameddin Aslani. September 2003.

PEER 2003/02 *Software Framework for Collaborative Development of Nonlinear Dynamic Analysis Program.* Jun Peng and Kincho H. Law. September 2003.

PEER 2003/01 *Shake Table Tests and Analytical Studies on the Gravity Load Collapse of Reinforced Concrete Frames.* Kenneth John Elwood and Jack P. Moehle. November 2003.

PEER 2002/24 *Performance of Beam to Column Bridge Joints Subjected to a Large Velocity Pulse.* Natalie Gibson, André Filiatrault, and Scott A. Ashford. April 2002.

PEER 2002/23 *Effects of Large Velocity Pulses on Reinforced Concrete Bridge Columns.* Greg L. Orozco and Scott A. Ashford. April 2002.

PEER 2002/22 *Characterization of Large Velocity Pulses for Laboratory Testing.* Kenneth E. Cox and Scott A. Ashford. April 2002.

PEER 2002/21 *Fourth U.S.-Japan Workshop on Performance-Based Earthquake Engineering Methodology for Reinforced Concrete Building Structures*. December 2002.

PEER 2002/20 *Barriers to Adoption and Implementation of PBEE Innovations.* Peter J. May. August 2002.

PEER 2002/19 *Economic-Engineered Integrated Models for Earthquakes: Socioeconomic Impacts.* Peter Gordon, James E. Moore II, and Harry W. Richardson. July 2002.

PEER 2002/18 *Assessment of Reinforced Concrete Building Exterior Joints with Substandard Details.* Chris P. Pantelides, Jon Hansen, Justin Nadauld, and Lawrence D. Reaveley. May 2002.

PEER 2002/17 *Structural Characterization and Seismic Response Analysis of a Highway Overcrossing Equipped with Elastomeric Bearings and Fluid Dampers: A Case Study.* Nicos Makris and Jian Zhang. November 2002.

PEER 2002/16 *Estimation of Uncertainty in Geotechnical Properties for Performance-Based Earthquake Engineering.* Allen L. Jones, Steven L. Kramer, and Pedro Arduino. December 2002.

PEER 2002/15 *Seismic Behavior of Bridge Columns Subjected to Various Loading Patterns.* Asadollah Esmaeily-Gh. and Yan Xiao. December 2002.

PEER 2002/14 *Inelastic Seismic Response of Extended Pile Shaft Supported Bridge Structures.* T.C. Hutchinson, R.W. Boulanger, Y.H. Chai, and I.M. Idriss. December 2002.

PEER 2002/13 *Probabilistic Models and Fragility Estimates for Bridge Components and Systems.* Paolo Gardoni, Armen Der Kiureghian, and Khalid M. Mosalam. June 2002.

PEER 2002/12 *Effects of Fault Dip and Slip Rake on Near-Source Ground Motions: Why Chi-Chi Was a Relatively Mild M7.6 Earthquake.* Brad T. Aagaard, John F. Hall, and Thomas H. Heaton. December 2002.

PEER 2002/11 *Analytical and Experimental Study of Fiber-Reinforced Strip Isolators*. James M. Kelly and Shakhzod M. Takhirov. September 2002.

PEER 2002/10 *Centrifuge Modeling of Settlement and Lateral Spreading with Comparisons to Numerical Analyses***.** Sivapalan Gajan and Bruce L. Kutter. January 2003.

PEER 2002/09 *Documentation and Analysis of Field Case Histories of Seismic Compression during the 1994 Northridge, California, Earthquake.* Jonathan P. Stewart, Patrick M. Smith, Daniel H. Whang, and Jonathan D. Bray. October 2002.

PEER 2002/08 *Component Testing, Stability Analysis and Characterization of Buckling-Restrained Unbonded Braces™.* Cameron Black, Nicos Makris, and Ian Aiken. September 2002.

PEER 2002/07 *Seismic Performance of Pile-Wharf Connections.* Charles W. Roeder, Robert Graff, Jennifer Soderstrom, and Jun Han Yoo. December 2001.

PEER 2002/06 *The Use of Benefit-Cost Analysis for Evaluation of Performance-Based Earthquake Engineering Decisions.* Richard O. Zerbe and Anthony Falit-Baiamonte. September 2001.

PEER 2002/05 *Guidelines, Specifications, and Seismic Performance Characterization of Nonstructural Building Components and Equipment*. André Filiatrault, Constantin Christopoulos, and Christopher Stearns. September 2001.

PEER 2002/04 *Consortium of Organizations for Strong-Motion Observation Systems and the Pacific Earthquake Engineering Research Center Lifelines Program: Invited Workshop on Archiving and Web Dissemination of Geotechnical Data, 4–5 October 2001*. September 2002.

PEER 2002/03 *Investigation of Sensitivity of Building Loss Estimates to Major Uncertain Variables for the Van Nuys Testbed.* Keith A. Porter, James L. Beck, and Rustem V. Shaikhutdinov. August 2002.

PEER 2002/02 *The Third U.S.-Japan Workshop on Performance-Based Earthquake Engineering Methodology for Reinforced Concrete Building Structures*. July 2002.

PEER 2002/01 *Nonstructural Loss Estimation: The UC Berkeley Case Study.* Mary C. Comerio and John C. Stallmeyer. December 2001.

PEER 2001/16 *Statistics of SDF-System Estimate of Roof Displacement for Pushover Analysis of Buildings.* Anil K. Chopra, Rakesh K. Goel, and Chatpan Chintanapakdee. December 2001.

PEER 2001/15 *Damage to Bridges during the 2001 Nisqually Earthquake.* R. Tyler Ranf, Marc O. Eberhard, and Michael P. Berry. November 2001.

PEER 2001/14 *Rocking Response of Equipment Anchored to a Base Foundation.* Nicos Makris and Cameron J. Black. September 2001.

PEER 2001/13 *Modeling Soil Liquefaction Hazards for Performance-Based Earthquake Engineering.* Steven L. Kramer and Ahmed-W. Elgamal. February 2001.

PEER 2001/12 *Development of Geotechnical Capabilities in OpenSees.* Boris Jeremi . September 2001.

PEER 2001/11 *Analytical and Experimental Study of Fiber-Reinforced Elastomeric Isolators*. James M. Kelly and Shakhzod M. Takhirov. September 2001.

PEER 2001/10 *Amplification Factors for Spectral Acceleration in Active Regions.* Jonathan P. Stewart, Andrew H. Liu, Yoojoong Choi, and Mehmet B. Baturay. December 2001.

PEER 2001/09 *Ground Motion Evaluation Procedures for Performance-Based Design.* Jonathan P. Stewart, Shyh-Jeng Chiou, Jonathan D. Bray, Robert W. Graves, Paul G. Somerville, and Norman A. Abrahamson. September 2001.

PEER 2001/08 *Experimental and Computational Evaluation of Reinforced Concrete Bridge Beam-Column Connections for Seismic Performance*. Clay J. Naito, Jack P. Moehle, and Khalid M. Mosalam. November 2001.

PEER 2001/07 *The Rocking Spectrum and the Shortcomings of Design Guidelines.* Nicos Makris and Dimitrios Konstantinidis. August 2001.

PEER 2001/06 *Development of an Electrical Substation Equipment Performance Database for Evaluation of Equipment Fragilities*. Thalia Agnanos. April 1999.

PEER 2001/05 *Stiffness Analysis of Fiber-Reinforced Elastomeric Isolators.* Hsiang-Chuan Tsai and James M. Kelly. May 2001.

PEER 2001/04 *Organizational and Societal Considerations for Performance-Based Earthquake Engineering.* Peter J. May. April 2001.

PEER 2001/03 *A Modal Pushover Analysis Procedure to Estimate Seismic Demands for Buildings: Theory and Preliminary Evaluation.* Anil K. Chopra and Rakesh K. Goel. January 2001.

PEER 2001/02 *Seismic Response Analysis of Highway Overcrossings Including Soil-Structure Interaction.* Jian Zhang and Nicos Makris. March 2001.

PEER 2001/01 *Experimental Study of Large Seismic Steel Beam-to-Column Connections.* Egor P. Popov and Shakhzod M. Takhirov. November 2000.

PEER 2000/10 *The Second U.S.-Japan Workshop on Performance-Based Earthquake Engineering Methodology for Reinforced Concrete Building Structures.* March 2000.

PEER 2000/09 *Structural Engineering Reconnaissance of the August 17, 1999 Earthquake: Kocaeli (Izmit), Turkey.* Halil Sezen, Kenneth J. Elwood, Andrew S. Whittaker, Khalid Mosalam, John J. Wallace, and John F. Stanton. December 2000.

PEER 2000/08 *Behavior of Reinforced Concrete Bridge Columns Having Varying Aspect Ratios and Varying Lengths of Confinement.* Anthony J. Calderone, Dawn E. Lehman, and Jack P. Moehle. January 2001.

PEER 2000/07 *Cover-Plate and Flange-Plate Reinforced Steel Moment-Resisting Connections.* Taejin Kim, Andrew S. Whittaker, Amir S. Gilani, Vitelmo V. Bertero, and Shakhzod M. Takhirov. September 2000.

PEER 2000/06 *Seismic Evaluation and Analysis of 230-kV Disconnect Switches.* Amir S. J. Gilani, Andrew S. Whittaker, Gregory L. Fenves, Chun-Hao Chen, Henry Ho, and Eric Fujisaki. July 2000.

PEER 2000/05 *Performance-Based Evaluation of Exterior Reinforced Concrete Building Joints for Seismic Excitation.* Chandra Clyde, Chris P. Pantelides, and Lawrence D. Reaveley. July 2000.

PEER 2000/04 *An Evaluation of Seismic Energy Demand: An Attenuation Approach.* Chung-Che Chou and Chia-Ming Uang. July 1999.

PEER 2000/03 *Framing Earthquake Retrofitting Decisions: The Case of Hillside Homes in Los Angeles.* Detlof von Winterfeldt, Nels Roselund, and Alicia Kitsuse. March 2000.

PEER 2000/02 *U.S.-Japan Workshop on the Effects of Near-Field Earthquake Shaking.* Andrew Whittaker, ed. July 2000.

PEER 2000/01 *Further Studies on Seismic Interaction in Interconnected Electrical Substation Equipment.* Armen Der Kiureghian, Kee-Jeung Hong, and Jerome L. Sackman. November 1999.

PEER 1999/14 *Seismic Evaluation and Retrofit of 230-kV Porcelain Transformer Bushings*. Amir S. Gilani, Andrew S. Whittaker, Gregory L. Fenves, and Eric Fujisaki. December 1999.

PEER 1999/13 *Building Vulnerability Studies: Modeling and Evaluation of Tilt-up and Steel Reinforced Concrete Buildings.* John W. Wallace, Jonathan P. Stewart, and Andrew S. Whittaker, editors. December 1999.

PEER 1999/12 *Rehabilitation of Nonductile RC Frame Building Using Encasement Plates and Energy-Dissipating Devices.* Mehrdad Sasani, Vitelmo V. Bertero, James C. Anderson. December 1999.

PEER 1999/11 *Performance Evaluation Database for Concrete Bridge Components and Systems under Simulated Seismic Loads.* Yael D. Hose and Frieder Seible. November 1999.

PEER 1999/10 *U.S.-Japan Workshop on Performance-Based Earthquake Engineering Methodology for Reinforced Concrete Building Structures.* December 1999.

PEER 1999/09 *Performance Improvement of Long Period Building Structures Subjected to Severe Pulse-Type Ground Motions*. James C. Anderson, Vitelmo V. Bertero, and Raul Bertero. October 1999.

PEER 1999/08 *Envelopes for Seismic Response Vectors.* Charles Menun and Armen Der Kiureghian. July 1999.

PEER 1999/07 *Documentation of Strengths and Weaknesses of Current Computer Analysis Methods for Seismic Performance of Reinforced Concrete Members.* William F. Cofer. November 1999.

PEER 1999/06 *Rocking Response and Overturning of Anchored Equipment under Seismic Excitations.* Nicos Makris and Jian Zhang. November 1999.

PEER 1999/05 *Seismic Evaluation of 550 kV Porcelain Transformer Bushings.* Amir S. Gilani, Andrew S. Whittaker, Gregory L. Fenves, and Eric Fujisaki. October 1999.

PEER 1999/04 *Adoption and Enforcement of Earthquake Risk-Reduction Measures.* Peter J. May, Raymond J. Burby, T. Jens Feeley, and Robert Wood.

PEER 1999/03 *Task 3 Characterization of Site Response General Site Categories*. Adrian Rodriguez-Marek, Jonathan D. Bray, and Norman Abrahamson. February 1999.

PEER 1999/02 *Capacity-Demand-Diagram Methods for Estimating Seismic Deformation of Inelastic Structures: SDF Systems*. Anil K. Chopra and Rakesh Goel. April 1999.

PEER 1999/01 *Interaction in Interconnected Electrical Substation Equipment Subjected to Earthquake Ground Motions.* Armen Der Kiureghian, Jerome L. Sackman, and Kee-Jeung Hong. February 1999.

PEER 1998/08 *Behavior and Failure Analysis of a Multiple-Frame Highway Bridge in the 1994 Northridge Earthquake.* Gregory L. Fenves and Michael Ellery. December 1998.

PEER 1998/07 *Empirical Evaluation of Inertial Soil-Structure Interaction Effects.* Jonathan P. Stewart, Raymond B. Seed, and Gregory L. Fenves. November 1998.

PEER 1998/06 *Effect of Damping Mechanisms on the Response of Seismic Isolated Structures.* Nicos Makris and Shih-Po Chang. November 1998.

PEER 1998/05 *Rocking Response and Overturning of Equipment under Horizontal Pulse-Type Motions.* Nicos Makris and Yiannis Roussos. October 1998.

PEER 1998/04 *Pacific Earthquake Engineering Research Invitational Workshop Proceedings, May 14–15, 1998: Defining the Links between Planning, Policy Analysis, Economics and Earthquake Engineering.* Mary Comerio and Peter Gordon. September 1998.

PEER 1998/03 *Repair/Upgrade Procedures for Welded Beam to Column Connections.* James C. Anderson and Xiaojing Duan. May 1998.

PEER 1998/02 *Seismic Evaluation of 196 kV Porcelain Transformer Bushings.* Amir S. Gilani, Juan W. Chavez, Gregory L. Fenves, and Andrew S. Whittaker. May 1998.

PEER 1998/01 *Seismic Performance of Well-Confined Concrete Bridge Columns.* Dawn E. Lehman and Jack P. Moehle. December 2000.

ONLINE REPORTS

The following PEER reports are available by Internet only at http://peer.berkeley.edu/publications/peer_reports.html

PEER 2010/102 *Analysis of Cumulative Absolute Velocity (CAV) and JMA Instrumental Seismic Intensity (I_{JMA}) Using the PEER–NGA Strong Motion Database.* Kenneth W. Campbell and Yousef Bozorgnia. February 2010.

PEER 2009/109 *Simulation and Performance-Based Earthquake Engineering Assessment of Self-Centering Post-Tensioned Concrete Bridge Systems.* Won K. Lee and Sarah L. Billington. December 2009.

PEER 2009/108 *PEER Lifelines Geotechnical Virtual Data Center.* J. Carl Stepp, Daniel J. Ponti, Loren L. Turner, Jennifer N. Swift, Sean Devlin, Yang Zhu, Jean Benoit, and John Bobbitt. September 2009.

PEER 2009/107 *Experimental and Computational Evaluation of Current and Innovative In-Span Hinge Details in Reinforced Concrete Box-Girder Bridges: Part 2: Post-Test Analysis and Design Recommendations.* Matias A. Hube and Khalid M. Mosalam. December 2009.

PEER 2009/106 *Shear Strength Models of Exterior Beam-Column Joints without Transverse Reinforcement.* Sangjoon Park and Khalid M. Mosalam. November 2009.

PEER 2009/105 *Reduced Uncertainty of Ground Motion Prediction Equations through Bayesian Variance Analysis.* Robb Eric S. Moss. November 2009.

PEER 2009/104 *Advanced Implementation of Hybrid Simulation.* Andreas H. Schellenberg, Stephen A. Mahin, Gregory L. Fenves. November 2009.

PEER 2009/103 *Performance Evaluation of Innovative Steel Braced Frames.* T. Y. Yang, Jack P. Moehle, and Božidar Stojadinovic. August 2009.

PEER 2009/102 *Reinvestigation of Liquefaction and Nonliquefaction Case Histories from the 1976 Tangshan Earthquake.* Robb Eric Moss, Robert E. Kayen, Liyuan Tong, Songyu Liu, Guojun Cai, and Jiaer Wu. August 2009.

PEER 2009/101 *Report of the First Joint Planning Meeting for the Second Phase of NEES/E-Defense Collaborative Research on Earthquake Engineering.* Stephen A. Mahin et al. July 2009.

PEER 2008/104 *Experimental and Analytical Study of the Seismic Performance of Retaining Structures.* Linda Al Atik and Nicholas Sitar. January 2009.

PEER 2008/103 *Experimental and Computational Evaluation of Current and Innovative In-Span Hinge Details in Reinforced Concrete Box-Girder Bridges. Part 1: Experimental Findings and Pre-Test Analysis.* Matias A. Hube and Khalid M. Mosalam. January 2009.

PEER 2008/102 *Modeling of Unreinforced Masonry Infill Walls Considering In-Plane and Out-of-Plane Interaction.* Stephen Kadysiewski and Khalid M. Mosalam. January 2009.

PEER 2008/101 *Seismic Performance Objectives for Tall Buildings.* William T. Holmes, Charles Kircher, William Petak, and Nabih Youssef. August 2008.

PEER 2007/101 *Generalized Hybrid Simulation Framework for Structural Systems Subjected to Seismic Loading.* Tarek Elkhoraibi and Khalid M. Mosalam. July 2007.

PEER 2007/100 *Seismic Evaluation of Reinforced Concrete Buildings Including Effects of Masonry Infill Walls.* Alidad Hashemi and Khalid M. Mosalam. July 2007.